UNIVERSITY OF CALIFORNIA, SAN DIEGO

Studies of ambient noise in shallow water environments off Mexico and Alaska: characteristics, metrics and time-synchronization applications

A dissertation submitted in partial satisfaction of the

requirements for the degree Doctor of Philosophy

in

Oceanography

by

Melania Guerra

Committee in charge:

Aaron M. Thode, Chair
William A. Kuperman, Co-chair
Jay Barlow
Ann E. Bowles
Sarah L. Mesnick
Truong Q. Nguyen

2013

The dissertation of Melania Guerra is approved, and it is acceptable in the quality and form for publication on microfilm:

_____

_____

_____

_____

_____

Co-Chair

_____

Chair

University of California, San Diego

2013

TABLE OF CONTENTS

LIST OF FIGURES

LIST OF TABLES

LIST OF ACRONYMS AND ABBREVIATIONS

AIM	Acoustic Integration Model
~	approximately
DASAR	Directional Autonomous Seafloor Acoustic Recorder
dB	decibel
ESA	(U.S.) Endangered Species Act
FFT	Fast Fourier Transform
FIR	Finite Impulse Response
ft	feet
Gb	gigabytes
GIS	Geographic Information System
GPS	Global Positioning System
Hz	Hertz (cycles per second)
IHA	Incidental Harassment Authorization (under U.S. MMPA)
in^3	cubic inches
kHz	kilohertz
km	kilometer
km^2	square kilometer
km/h	kilometers per hour
LSI	Laguna San Ignacio
LSIESP	Laguna San Ignacio Ecosystem Science Project
µPa	micro Pascal
m	meters
MFP	Matched Field Processing
min	minutes
MLM	Minimum Level Metric
MMO	Marine Mammal Observer
MMPA	(U.S.) Marine Mammal Protection Act
M/V	Merchant Vessel
NCF	Noise Correlation Function
NMFS	(U.S.) National Marine Fisheries Service
NOAA	(U.S.) National Oceanic and Atmospheric Administration
PAM	Passive Acoustic Monitoring
PSD	Power Spectral Density
RM	Reverberation Metric
rms	root-mean-square
R/V	Research Vessel
s	seconds
SEL	Sound Exposure Level
SNR	Signal to Noise Ratio
SONAR	SOund Navigation And Ranging
SPL	Sound Pressure Level

TDGF	Time Domain Green's Function
TOAD	Time Of Arrival Difference
TTS	Temporary Threshold Shift
UABCS	Universidad Autónoma de Baja California Sur
V	Volt

ACKNOWLEDGMENTS

De vez en cuando hay que hacer
una pausa
contemplarse a sí mismo
sin la fruición cotidiana
examinar el pasado
rubro por rubro
etapa por etapa
baldosa por baldosa
y no llorarse las mentiras
sino cantarse las verdades.
Mario Benedetti

Although my name stands alone on the title of this document, a Ph.D. dissertation embodies what teamwork is all about. I owe gratitude to many people who have made my long Ph.D. journey possible. This is my best attempt at thanking all of you, mentors, teachers, gurus and overall favorite people in the world, who contributed logistical support, psychological encouragement, professional guidance, unconditional love or endless laughter to the life that hides behind these printed pages.

My academic path is strongly shaped by teachings and advice from my six Ph.D. committee members. First and foremost, I would like to express my deepest

appreciation to my advisor Aaron Thode. As his first mentee graduate student, we navigated many experiences together for each other's first time. Aaron taught me conceptual and practical lessons I will forever value, like how to question results and how to mathematically express theoretical ideas, how to reduce complexity to basic principles and how to properly tie nautical knots. While he vigilantly oversaw my progress, he also gave me the freedom to pursue various side projects without objection, allowing me to develop many complementary skills outside of the traditional coursework. His careful revisions of my writings and countless corrections to my scientific language are an asset that I now appreciate daily! Above all, thank you Aaron for not giving up on me and fighting to see me through to the end of this process.

To my committee members William Kuperman, Jay Barlow and Truong Q. Nguyen, many thanks for providing positive feedback and encouraging suggestions, which were always thought provoking and helpful in focusing my research. I was also amazingly fortunate to count on two other committee members, Ann E. Bowles and Sarah Mesnick, who poked me on the big-picture, life-beyond-the-thesis questions and to this day provide inspirational role models of successful women in the bioacoustics field. To all six of my committee members, my most sincere thanks for your patience in guiding me, for sharing your evident passion for science and for helping me find the best fit of a professional path matched to my skills and interests.

At Scripps, I am also eternally indebted to Michael Buckingham for originally taking the chance to bring me as his student, as well as to his lab personnel (Fernando,

Eric), who guided my initial steps into the world of oceanography. I want to particularly acknowledge three professors whose teaching abilities I greatly admire: Peter Franks, Clint Winant and Bill Hodgkiss are geniuses at graduate level education, to the point that all these years later I still know how f-ratio is defined or when to spot a hydraulic jump on a breaking wave…

The Thode lab (Rob, Delphine) were the best possible partners in the challenges of preparing and executing demanding field work in remote locations and with complex instrumentation. Thank you, Rob, for making sure all of our electronics performed flawlessly and were always ready to go at a moment's notice. And thank you Delphine, for making the long rides down the Baja peninsula (and other exotic places in the world) always so much fun! To the many other lab interns that came and went through the years (Diana, Alyssa, Florian, Katie) and postdoc (Dawn), I owe greatly for lending a hand!

After my time at Scripps, I have been incredibly lucky to continue my professional growth and development at the Bioacoustics Research Program at Cornell University. I would like to express my great appreciation to the entire BRP team, but particularly to my supervisors Chris Clark and Aaron Rice, who have supported me when I have make mistakes and empowered me to believe in getting "back on the horse". Chris has opened extraordinary doors and opportunities for me and trusted that I can (and deserve to) seize them. His compassion, commitment and wisdom are a daily source of inspiration; I feel extremely fortunate to be trained by such a legend of the bioacoustics field.

The work presented in Chapter 2 is part of an ongoing collaboration between SIO and Greeneridge Sciences Ltd. Working alongside with distinguished scientists like Susanna Blackwell, Charles Greene and Katherine Kim tremendously improved my knowledge on the field and introduced me to the Arctic environment that I have come to love. Special thanks too, to the crewmembers of the R/V Norseman II and the R/V Alpha Helix, especially Scotty, Bobo and Ben who remain dear friends in my life many years later. Many thanks to Michael Macrander of Shell Co. for financing the Beaufort monitoring project that provided the data used here.

The work in Laguna San Ignacio (Chapter 3) was made possible thanks to the determined efforts of two legendary gray whale scientists, Steve Swartz and Jorge Urban through the Laguna San Ignacio Ecosystem Science Project (LSIESP). In their presence, it is impossible not to get infected with their enthusiastic passion for marine mammal research and their life-long commitment to their conservation. Over many Baja dessert camping nights and long work days on a panga baked under the sun, I learned why our work matters beyond the Ivory Tower and the socio-economic difference it can make directly on local people. I hold many great memories from all former UABCS' grad students and volunteers that participated in the lagoon field work, season after season, especially Sergio, Anaid, Mauricio "Milhouse", Benjamin, Jen, Svenja, Kyla and Angie. Success of the San Ignacio effort would not have been possible without the major assistance of Kuyima Ecoturismo in supplying us the basics: feeding us, housing us and navigating us on the lagoon waters, every season, until our instruments were all safely collected. Also at the lagoon, Sheyna W. became

a cherished friend and mentor, teaching me the many skills required to working creatively in remote locations and pushing me to let go of the “spoiled princess” in me. All of our work at Punta Piedra was enabled by the wonderful folks of Baja Discovery, especially Karen, Jose Luis, Cindy, Jim, Tito, Tony, Socorro and Pilar. Muchas gracias! Big thanks to Celia and Art and all personnel onboard the F/V Searcher, who helped us transport gear between San Diego and San Ignacio. With his piloting skills, quick, creative thinking and spirited humor, Eddie K (Oceans Aloft) was also instrumental in securely deploying and recovering our sensors every year and continues to be a limitless well of resourceful ideas and solutions, which I am lucky to be able to tap into.

On the administrative side at SIO, I am infinitely grateful to the Graduate Office (Krystle, Josh, Dawn, Denise, Becky) and the Development Office (John, Anne, Edwina), who through their impeccable work, seamlessly take care of critical student-life related issues, allowing us to solely focus on what’s important: our science and our surfing. The Development Office connected me to a remarkably generous individual, Mr. Irving Tragen, who for the most part of my schooling funded me through the Latin American Fellowship. Thank you, I couldn’t have done it without you! On top of handling all of our day-to-day affairs with flair, Evelyn always added a (literal) touch of sweetness to our routines and a sense of serenity to the hectic pace of the MPL/NTV halls. She is greatly missed.

Many thanks to the Outreach personnel at Birch Aquarium (Catherine, Staci, Jessica) who generously provided a venue for me to share my many amazing

experiences with the curious public, and taught me how crucial it is for scientists to effectively communicate their knowledge with general audiences of all ages and backgrounds. More than once did I run into the SIO dive locker (Rich, Christian) or the SIO machine shop (Rob, George, Ken) squealing crazy, urgent requests that required their resourceful skills and their generous help! Thank you for always seeing to it that I never walked out empty handed!

In general to UCSD and SIO, I owe much of whom I have become and many of the doors that will surely open in my professional future. I feel incredibly privileged to have attended such special institutions that genuinely care about and continuously invest on their students.

SIO surrounded me with a great support network of brilliant friends and fellow young scientists. It is an honor to now follow the development of their successful research careers and know that I have prime access to their insightful minds and compassionate words of advice, both on professional and personal matters. Loren, Sheila, Jess C, JMeir, Megan, Tali, Cass, Dalal and Fiona filled my days with sunshine, brunches and intellectually challenging debates. Together we built solid beach pyramids and friendships that will extend way beyond the SoCal sunsets. The "Friday Dinners & Hot-Tub Crew": Caglar, Flavia & Nico, Jit, Kaus & Anjali, Fernando & Karen and Gino & Susan represent the ultimate loyal friends, who may occasionally laugh at you but always, through it all, stick by you. We all come from different places in the world, but share in our curiosity and enthusiasm about exploring it. I hope to take many more exotic trips with all of you in the years to come!

Particularly to Jit, thank you for rescuing me out of countless crises (both Matlab-related and otherwise) and never wavering in helping a hand. Through this journey, you have been like a steady GPS (bad analogy?) that always points in the direction of things being OK!

LoraLora singlehandedly made this journey fun when times got tough. Her ever-present smile made sunny San Diego even brighter and our epic adventures together leave memorable stories behind and the promise of many more to come.

I always knew that I could count on Nacho, Leah, BenPNeal, Chris C., Genaro, John H., Makela, Guillaume and Becca to provide wisdom or to share delicious meals. You are friends that keep my soul happy!

Outside of SIO, but right next door, I have made even more exceptional friends through NOAA/SWFC. Anne & Paul, Fionna, Siri, Amy, Tony & Kristen, Rosa, Ryan, Rich & Jen, Katrina & Jefferson, you are colleagues that I hope to cross paths with again in our careers, because I admire your passion and dedication, and how much fun you have in the process!

The San Diego community brought many more magical people into my life. The GA gang: Debbie, Vica, Mike, Joel, Aleksey, also known as “my other life”, spiced up my days with variety and entertainment, but also kind encouragement and continuous cheering. I do not remember what life was like before meeting Diego & Patrick, Rob & Sarah, Ann & Matt, since I rely on them so frequently to feel sane and leveled. Thank you for taking care of me and making sure I always feel loved. I could never summarize how thankful I am to have met Pinsuda, a friend who challenges me

to take risks, push boundaries and reach for new heights. Without a doubt, I am a better person with you in my life!

In a short but intense time, the folks of Toastmasters (TM) of La Jolla added so much new wisdom to my life. I hope to someday be able to command an audience like a true TM should!

And at the end of the day, home life at The Villa was always a peaceful sanctuary to return to thanks to Colleen P., Aileen M., Meghan M., Megan L., Anne F., Laurie and Lana A., Victoria R. and the Guarino family. Thank you for creating a California home where I could recharge enough energy to take on the world day after day.

Like a gushing Texan oil well, love has continually flowed from my previous Texas home and my Cajun family in Houston. Sha' Tom and Becky G, all's y'all are forever a second home to me.

Although far away, in Costa Rica, I have never stopped feeling the presence of my two lifelong gals: Diana and Ingrid, are more than friends, they are my sisters. In the time I have taken to birth this dissertation, they have built families with wonderful husbands and children and I am proud to learn from their example as compassionate, empowered, modern women who can balance multiple spinning plates with style and confidence. The dear friendships of Jaime, Marco M., Sylvia, Ligia, Monse, Caricaco, Jorge C., Iva, Hans R., Luly, Alejandra and many others, remind me every day of what is truly important in life and their unwavering faith in me often uplifts me when I doubt myself.

Finalmente, mi eterno agradecimiento pertenece sobretodo a mis papás Jorge y Marcela y mi “little bro” Hernán, quienes a través de mi vida se han asegurado de que yo creciera con ilimitado acceso a las mejores oportunidades posibles. Desde mis pequeños hasta mis (relativamente más) grandes logros, el crédito es todo suyo por su amor incondicional,paciente comprensión, generoso apoyo y completa fe en mí. Aún cuando esos logros han implicado que esté geográficamente lejos, nunca han dejado de estar cerca en mi mente y sus valiosas lecciones de vida siempre me guían al tomar decisiones importantes. Mis dos abuelos, Mayor Domo Tito Periquito y Papi Ciro inspiraron en mí desde pequeña el amor por aprender, leer y por la ciencia: Tito con sus poemas escritos en servilletas me sensibilizo a lo que ocurre en el mundo y Papi Ciro con su regalo sobre el descubrimiento de Troya me hizo desear explorarlo. Para ellos y para toda mi extendida familia Guerra y Carrillo, este humilde documento es el único remplazo que puedo proveer a cambio de haberme perdido muchas celebraciones familiares, cumpleaños, Navidades, TitoBingos, etc. A pesar de la distancia, gracias por enseñarme la fuerza de la sangre y el valor de la unión familiar.

And finally, to the person to whom I made a promise a long time ago that I would be here… I hope you are proud.

MATERIAL SUBMITTED FOR PUBLICATION IN THE DISSERTATION

Chapter 2,in full is a reprint of material as it appears in the Journal of the Acoustical Society of America, 2011.Guerra, Melania; Thode, Aaron M; Blackwell, Susanna B.; Macrander, A. Michael. “Quantifying seismic survey reverberation off the

Alaskan North Slope.", Volume 130, Issue 5, pp.3046-3058, 2011. The dissertation author was the primary investigator and author of this paper.

Chapter 3, in part is currently being prepared for submission for publication of the material. Guerra, Melania; Thode, Aaron M. The dissertation author was the primary investigator and author of this material.

CURRICULUM VITAE

Education

2001 Bachelor of Science Degree
Mechanical Engineering
University de Costa Rica, San Jose, Costa Rica

2010 Master of Science Degree
Scripps Institution of Oceanography
University of California, San Diego, CA

2011-2013 Visiting Scholar
Bioacoustics Research Lab
Cornell Lab of Ornithology

2013 Doctor of Philosophy Degree
Scripps Institution of Oceanography
University of California, San Diego, CA

Publications

Blackwell, S. B., Nations, C. S., McDonald, T. L., Greene, C. R., Thode, A., and **Guerra, M**. **(2013)**. Effects of airgun sounds on bowhead whale calling rates in the Alaskan Beaufort Sea. Marine Mammal Science. 29: E342–E365.

Ponce, D., Thode, A. M., **Guerra, M.**, Urbán R, J., and Swartz, S. **(2012)**. Relationship between visual counts and call detection rates of gray whales (*Eschrichtius robustus*) in Laguna San Ignacio, Mexico. Journal of the Acoustical Society of America, 131(4), 2700–2713.

Guerra, M., Thode, A. M., Blackwell, S. B., and Macrander, A. M.**(2011).** Quantifying seismic survey reverberation off the Alaskan North Slope. Journal of the Acoustical Society of America, 130(5), 3046–3058.

Thode, A. M., Gerstoft, P., Burgess, W. C., Sabra, K. G., **Guerra, M.**, Stokes, M. D., and Cato, D. H. **(2006).** "A Portable Matched-Field Processing System Using Passive Acoustic Time Synchronization," IEEE Journal of Oceanic Engineering **31**: 696–710.

Thode, A. M., Gerstoft, P., **Guerra, M.,** Stokes, D. M., Burgess, W. C., Noad, M. J., and Cato, D. H. **(2004)**. "Range-depth tracking of humpback whales using autonomous acoustic recorders." The Journal of the Acoustical Society of America 116: 2589.

Fields of Study:

Marine mammal bioacoustics

Acoustic ecology

Underwater ambient noise

Potential impacts from increasing anthropogenic noise

Digital signal processing

ABSTRACT OF THE DISSERTATION

Studies of ambient noise in shallow water environments off Mexico and Alaska: characteristics, metrics and time-synchronization applications

by

Melania Guerra

Doctor of Philosophy in Oceanography

University of California, San Diego, 2013

Aaron M. Thode, Chair

There is a silence where hath been no sound,
There is silence where no sound may be,
In the cold grave — under the deep, deep sea…
Thomas Hood

Sound in the ocean originates from multiple mechanisms, both natural and anthropogenic. Collectively, underwater ambient noise accumulates valuable information about both its sources and the oceanic environment that propagates this noise. Characterizing the features of ambient noise source mechanisms is challenging, but essential, for properly describing an acoustic environment.

Disturbances to a local acoustic environment may affect many aquatic species that have adapted to be heavily dependent on this particular sense for survival

functions. In the case of marine mammals, which are federally protected, demand exists for understanding such potential impacts, which drives important scientific efforts that utilize passive acoustic monitoring (PAM) tools to inform regulatory decisions.

This dissertation presents two independent studies that use PAM data to investigate the characteristics of source mechanisms that dominate ambient noise in two diverse shallow water environments.

The study in Chapter 2 directly addresses the concern of how anthropogenic activities can degrade the effectiveness of PAM. In the Alaskan Beaufort Sea, an environment where ambient noise is normally dominated by natural causes, seismic surveys create impulsive sounds to map the composition of the bottom. By inspecting single-sensor PAM data, the spectral characteristics of seismic survey airgun reverberation are measured, and their contribution to the overall ambient noise is quantified. This work is relevant to multiple ongoing mitigation protocols that rely on PAM to acoustically detect marine mammal presence during industrial operations.

Meanwhile, Chapter 3 demonstrates that by analyzing data from multiple PAM sensors, features embedded in both directional and omni-directional ambient noise can be used to develop new time-synchronization processing techniques for aligning autonomous elements of an acoustic array, a tool commonly used in PAM for detecting and tracking marine mammals. Using the time-synchronization procedures shown here, arrays may be built out of stand-alone recorders that simplify the deployment logistics and can be arranged in multiple configurations.

Given increasing economic pressures worldwide, anthropogenic activities in the ocean are only expected to expand, and their ambient noise contributions will continue to rise. These studies provide baseline knowledge and practical tools to help properly assess the impact of such source mechanisms in shallow-water acoustic environments.

CHAPTER 1:

Introduction

I. INTRODUCTION

Despite the descriptive title of Jacques Cousteau's iconic 1954 work, "The Silent World" (Cousteau and Dumas, 1954), it is now well established that the ocean is filled with noise generated by a variety of sources, including a diversity of marine fauna, natural physical processes, and in contemporary times, inescapably, anthropogenic industrial activities (Hildebrand, 2009). These different source mechanisms collectively imprint the underwater acoustic environment with a variety of acoustic signatures that can vary in magnitude levels, spectral content, temporal structure and spatial extent (reviewed in Urick, 1983). Each source signature itself is distorted further by its interaction with the particular environment in which it propagates, confounding attempts to define a "generic" description of an acoustic environment.

The earliest studies to describe the nature of underwater ambient noise (Ross, 1976; Knudsen *et al.*, 1948; Wenz, 1962;Wenz, 1972) identified a variety of abiotic and biotic source mechanisms. The first category corresponds with sources that originate from geophysical phenomena, including wind-generated waves (Perrone, 1969), earthquakes, rainfall, and cracking ice; whereas biotic sources comprise sounds made by organisms like marine mammals, fish or invertebrates. These source categories are classically represented by the so-called Wenz curves (Figure 1.1), which classify the different mechanisms across spectral dimensions of frequency and averaged power spectrum received levels. For instance, the signatures of earthquakes and seismic waves can be found in the frequency range below 100 Hz, whereas wind-

driven noise extends to the several kHz range, across received levels between 20-80 dB re: 1 μPa, depending on sea state. Although the processes by which this acoustic energy is coupled into the ocean are well understood, quantification of the relative contributions of the various mechanisms to the overall noise budget remains an active and essential area of research (Hatch *et al*., 2008).

Even in these initial studies the presence of anthropogenic sources was already identified as a prominent contributor to ambient noise; for example, Figure 1-1 shows that distant and near-by shipping are a dominant source between 10 and 3000 Hz (McKenna *et al.*, 2012). Over the decades since Wenz's work, other marine industrial activities that also radiate noise underwater have become widespread, among them offshore oil and gas exploration or extraction (Greene and Richardson, 1988), construction and dredging (Greene, 1987) and military exercises. Given global economic pressures, these activities are becoming more ubiquitous (Andrew *et al*., 2002; Halpern *et al*., 2008) and consequently concerns have been raised about how this addition of noise may impact marine life and its acoustic ecology (Barlow and Gisiner, 2006; Nowacek *et al*., 2007; Richardson *et al*., 1986; Tyack, 2008)

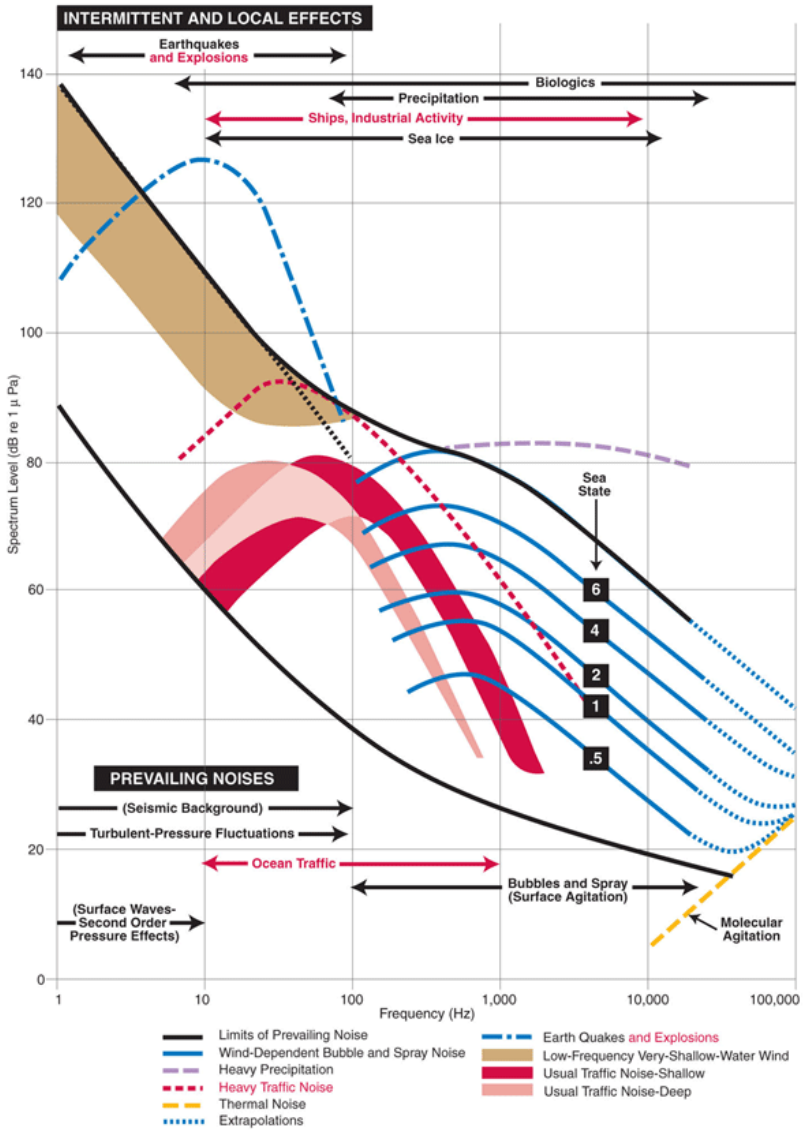

Figure 1-1: Reproduction of Wenz curves (1962) displaying power spectrum corresponding to a variety of ocean ambient noise sources at different frequencies. (Source: Discovery of Sound in the Sea www.dosits.org).

In this context marine mammals are of special concern, since so many of their basic survival functions rely on their acoustic perception: from communication with conspecifics to the ability to echolocate (which enables foraging, detection of

predators and navigation) (Norris, 1969; Ketten, 1992). Within U.S. waters. all cetaceans are federally protected by the Marine Mammal Protection Act of 1972 (16 U.S.C. § 1361 et seq.) (MMPA; Roman *et al*., 2013) and the Endangered Species Act (1973, 7 U.S.C. § 136, 16 U.S.C. § 1531 et seq.), which aim "to maintain marine mammals as a significant functioning element in the ecosystem of which they are a part." Under those statutes the U.S. National Marine Fisheries Service (NMFS) manages and regulates activities that may injure, impair or impact a population, including those that produce high noise levels in their vicinity (NRC, 2005).

In order to minimize their exposure to high-intensity anthropogenic noise, a variety of monitoring and mitigation strategies have been implemented around known critical habitats or along migration routes. Passive Acoustic Monitoring (PAM, Sousa-Lima and Norris, 2013; Zimmer, 2011) has been proven a useful complementary tool in acoustically surveying cetacean populations (Barlow and Taylor, 2005; McDonald and Fox, 1999), measuring exposure effects over long temporal and spatial scales (Blackwell *et al*., 2013) and evaluating the resulting outcome of such mitigation strategies (Van Parijs *et al*., 2009). Thus, it is of relevance to study how ambient noise interacts with PAM tools, as well as characterizing the large variation in spectral and directional features of its multiple sources.

This dissertation presents two independent studies that combine PAM data with external environmental measurements, with the ultimate goal of investigating the characteristics of ambient noise and its sources in two disparate shallow water environments. Acoustic propagation in shallow water is dominated by the interaction

of the pressure wave with the boundaries of an ocean waveguide, generating strong site-specific propagation effects (Jensen *et al.*, 1993) that can be difficult to separate from the inherent characteristics of the source mechanisms themselves (Cato, 1997; Kuperman and Lynch, 2004, Jensen and Kuperman, 1983). At the same time, shallow-water environments often present situations where large groupings of marine mammals overlap spatially and temporally with anthropogenic activities (shipping ports, offshore energy exploration, wind farm construction).

The two primary chapters (Chapters 2 and 3) of this dissertation align with two current and significant directions in the scientific study of ocean ambient noise: the effects of anthropogenic noise on marine mammals, and the extraction of information about the ocean environment from ambient noise. The next sub-sections provide relevant contextual details about these research trends and help frame the novel contributions of this dissertation within this established knowledge.

II. BACKGROUND ON CHAPTER 2: THE EFFECTS OF NOISE ON MARINE MAMMALS

Chapter 2 presents a study that evidences the impact of a seismic airgun source on the local diffuse ambient noise conditions of a shallow water environment. The results demonstrate that the backscattered energy (reverberation) can significantly contribute to raising ambient noise levels during the inter-impulse interval (between seismic airgun shots), which under certain circumstances can degrade the detection capabilities of PAM tools. By extension, it could also be hypothesized that seismic

reverberation could potentially impact local populations of marine mammals, such as the endangered bowhead whale (*Balaena mysticetus*), which uses the study region as a migration corridor.

The introduction of underwater noise into the marine environment can adversely impact marine mammals in a variety of ways. Figure 1-2 (based on concepts from Richardson *et. al.,* 1995) provides a convenient framework for cataloging all the possible types of disturbance on cetaceans, portrayed as zones of potential impact from a single point source (at the center) in order of decreasing severity, as a function of distance from the source. These effects may range from fatal at close range, to no-impact at all beyond a certain "safe" distance.

Historically, concerns for these impacts first focused on physiological injuries to individuals from acute exposure to high noise levels. It has been observed that as a result of such exposure, tissue ruptures could compromise some species' auditory systems, leading to mass strandings and mortality (bright pink zone in Fig. 1-2) (D'Amico *et al*., 2009; Filadelfo *et al*., 2009). Hearing losses in marine mammals are classified as both temporary threshold shifts (TTS), which indicate a short-lived period during which a sound must be louder than normal in order to be detected, heard or understood; or permanent threshold shifts (PTS), recognized essentially as permanent partial hearing losses. Because recovery from TTS is possible, it can be experimentally induced and studied with captive animals and a large body of knowledge has been accumulated about this phenomenon in various (mostly odontocete) species (e.g. Finneran *et al.*, 2010; Kastelein *et al.*, 2013; Schlundt *et al.*,

2008). Comprehension about permanent damage (such as PTS) or of these injuries in the wild remains still largely unclear (Southall *et al.*, 2007).

Longer-term studies and observations have also reported that underwater noise can be associated with modifications to natural behaviors (Kight and Swaddle, 2011). It is considerably more difficult to interpret these behavioral disruptions within the context of a wild animal's life history (for example, in terms of energetic cost or missed feeding opportunities) and to relate their significance to the viability of an entire population. Dedicated controlled exposure experiments (CEE; also referred to as behavioral response studies, BRS; DeRuiter *et al.*, 2012; Gordon *et al.*, 2003) are still attempting to answer these questions.

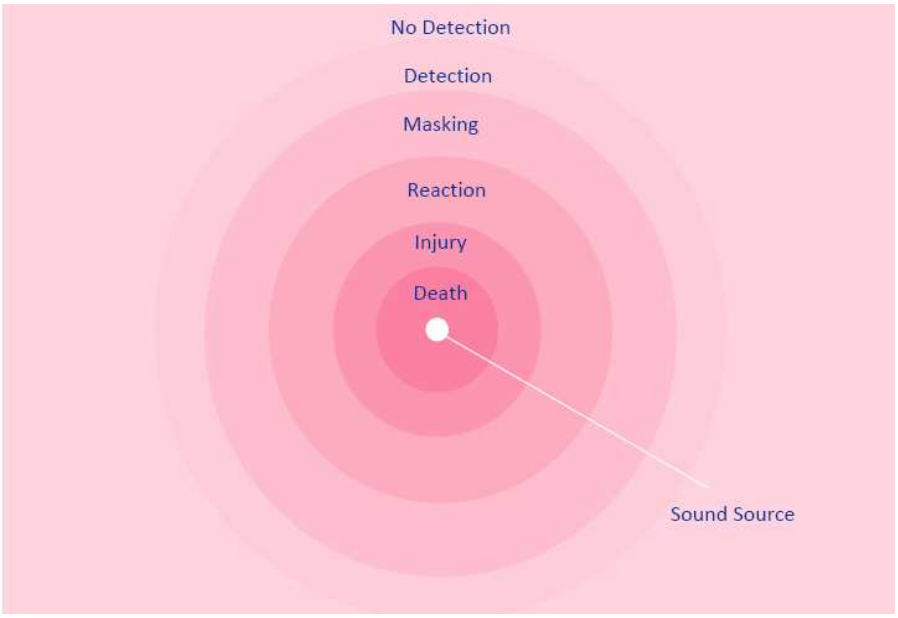

Figure 1-2: Schematic based on Richardson *et al.* (1995) showing the continuum in zones of impact, arranged in order of increasing potential seriousness to the health and well-being of a marine mammal.

Following the scientific insights about these potential effects, almost all of the regulatory and impact-assessment approaches started by identifying received level thresholds that would predict these extreme responses to noise exposure (Southall *et al.*, 2007). Mitigation strategies implement such thresholds in the practice, with the goal of preventing or minimizing the cases of exposure to those onset levels.

What has become apparent in recent times is that the early acute approach to assessing impacts can overlook the potential long-term, population-level effects of chronic noise exposure, especially considering that marine mammals are relatively long-lived species. Thus, concerns have shifted to also considering the possible adverse effects from prolonged exposure to long-term gradual increases in ambient noise. For example, elevated anthropogenic levels of ambient noise may lead to a reduction in the area over which an animal can successfully communicate, defined by Clark *et al*. (2009) as “communication masking”. By adding an obstacle to behaviors that rely on the effective communication between conspecifics or the detection of relevant acoustic cues, increased ambient noise level may thus lead to reduced reproductive rates or rates of survival, impairing the viability of the population in the long-term. Consequently, masking is now viewed as yet another potential stressor impacting species that are already facing other forms of habitat degradation (Rolland *et al.*, 2012). In that context, the characterization of ambient noise becomes a fundamental element to understanding the spatial extent of an animal’s communication range and thus its overall acoustic ecology (Hastings and Au, 2012).

With this new long-term, large-scale perspective in mind, recent studies have resulted in various additional criteria being proposed (Ellison *et al*., 2012; Moore *et al*., 2012; Southall *et al*., 2007)for assessing the likely impacts of noise exposure on marine mammals. Unfortunately, numerous other factors come into play when considering these potential long-term effects, including general behavioral states of the population; characteristics, location, and movement of the sound source; previous exposure histories of individuals, and other ecosystem changes. These science-based recommendations are starting to permeate into the regulatory realm and are being considered in the process of developing new marine mammal acoustic guidelines (Scholik-Schlomer, 2012).

Yet another recent shift in the assessment of noise impacts on marine mammals is the awareness that impulsive sources should be regarded as a distinct type of acoustic disturbance (in contrast to continuous noise sources), one that may induce certain kinds of impacts and may require particular regulations. Of the impulsive sources, seismic surveys are of special interest because of their wide-reaching use and highly energetic output (Castellote *et al*., 2012; Di Iorio and Clark, 2010; Nieukirk *et al*., 2004). Seismic surveys are conducted by towing arrays of airguns behind a vessel that is moving along survey lines as it shoots transient, broadband impulses. “Streamers” of hydrophones listen for their corresponding echoes and interpret the received seismic data to locate buried deposits of oil and gas. While seismic surveys have been taking place for decades, advances in technologies and expansion into formerly inaccessible grounds (for example, the Arctic) are increasing their use and

the resultant concern about harm to marine life. Concern has focused primarily on the impulse event itself, where most of the energy is concentrated, but as seismic surveys spread into shallow water, reverberation in between shots has become an unavoidable issue.

In view of these considerations and based on this previous knowledge, Chapter 2 addresses the specific issue of masking caused by seismic survey reverberation.

III. BACKGROUND ON CHAPTER 3: EXTRACTING ENVIRONMENTAL INFORMATION FROM AMBIENT NOISE

Considering the background established for Chapter 2 about how routine anthropogenic noise sources in the ocean have become and the consequent concerns for potential impacts on marine mammals, it is understood that PAM technologies that enable the detection and localization of vocally active marine mammals have become a critical component of the required mitigation efforts (Ireland *et al.*, 2009). In addition, acoustic monitoring recorders can collect substantial information about the local underwater propagation environment. This is especially true in shallow water environments, as a propagating sound wave can reflect multiple times between the surface and the bottom before reaching the PAM receiver. By exploiting this environmental knowledge, Chapter 3 demonstrates a method that enables individual autonomous PAM sensors to be synchronized as a unified array.

Acoustic arrays are a common PAM tool for estimating a marine mammal's position, as they have the ability to simultaneously collect acoustic data at different

spatial locations (e.g. Cato, 1998; Sonntag *et al*., 1986; Morrissey *et al*., 2006; Simard *et al.*, 2008; Thode *et al*., 2012; Tiemann *et al.*, 2002; Wladichuk *et al.*, 2008). However, such equipment is usually bulky and heavy, because all the sensors are electrically connected to a single central data acquisition system. As an alternative, arrays constructed out of autonomous recording packages may be attractive, since they offer advantages in terms of configuration and portability (Greene *et al.*, 2004; Thode *et al.*, 2006; Wiggins and Hildebrand, 2003). On the downside, given that autonomous elements have independent timing clocks, they experience a temporal offset both relative to each other and relative to an absolute time standard. Resolving these offsets generally requires the use of an active acoustic source, but given the protected status of many marine mammal species, controlled sound playbacks can be problematic.

In that context, Chapter 3 explores a passive approach to time-synchronization that takes advantage of the information about the acoustic field embedded within the diffuse ambient noise recorded by two separate recorders. The environment in which this study takes place is a shallow lagoon, whose ambient noise incorporates wind-driven noise, and biologic sources (Figure 1-1) such as croaker fish (Sciaenidae), snapping shrimp (*Alpheus heterochaelis)* and sounds of the gray whale (*Eschrichtius robustus),* a species that visits these protected waters yearly to mate and give birth to its young (Jones *et al*., 1984; Urban *et al*., 2003). During the winter months, whale-watching tourism is a major socio-economic activity that supports several regional communities. However, the noise spectrum of whale-watching boats (called “pangas”) may overlap with the acoustic niche of gray whale calls, creating a potential situation

for communication masking (Clark *et al.*, 2009). The work in Chapter 3 is based on data collected as part of a long-term, scientific effort, that seeks to measure the health of this lagoon's ecosystem and conserve the sustainability of its ecosystem services (Ruckelshaus *et al*., 2013; Worm *et al*., 2006). Acoustic arrays built out of autonomous sensors were deployed with the long-term goal of localizing and tracking gray whales; however, time-synchronization of the acoustic data is a necessary first step towards achieving those objectives.

Over the past decade it has been shown that the cross correlation of an ambient noise field recorded at two points can lead to an approximation of the time-domain Green's function (TDGF; e.g. Brooks and Gerstoft, 2009; Buckingham, 2012; Sabra *et al*., 2005a), which describes the environment's impulse response. Additional work has extended this principle to developing time-synchronization methods that utilize long-time averaged cross correlation estimates between sensors corresponding to two different arrays (Figure 1-3 taken from Sabra *et al*., 2005b; Fried *et al*., 2008) separated by 28-115m.

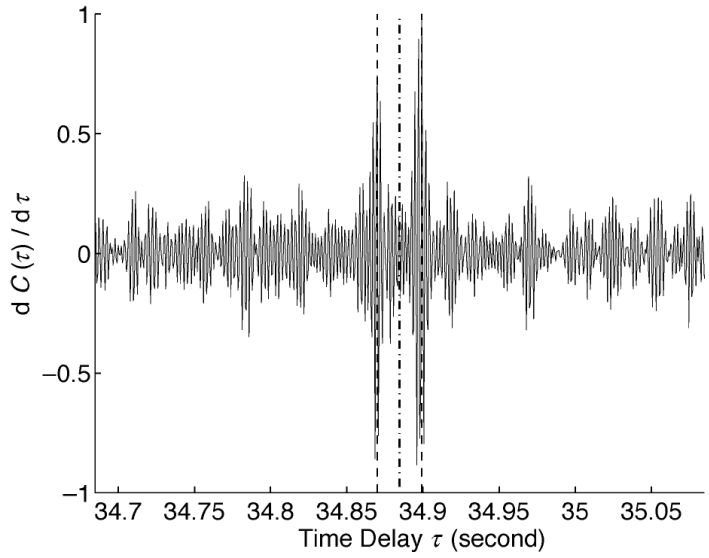

Figure 1-3: Reproduction of results showing the emergence of a time delay offset, computed from the long-term averaging of the time-derivative of the ambient noise cross correlation function as recorded by two elements from separate horizontal arrays (Figure 8 in Sabra *et al.*, 2005b).

A similar approach is tested in Chapter 3 with two closely-spaced PAM instruments and the resulting timing estimates are compared with estimates obtained from a traditional synchronizing method that relies on a transient discrete sound source, in this case a passing panga. Furthermore, the emergence of correlation peaks revealed new knowledge about the spatial and temporal distribution of various ambient noise sources at the lagoon.

IV. OUTLINE OF THE DISSERTATION

The research questions pursued by this dissertation are motivated by a basic need for a more comprehensive understanding of ambient noise and the characteristics of its source mechanisms. Although the two studies presented here describe independent investigations, at the core they both address the following research questions:

1) Is it possible to combine PAM data with independent environmental measurements to identify and characterize the source mechanisms of ambient noise in shallow water?
2) Are there practical applications to such knowledge about source mechanism features that could help improve PAM surveying tools or their effectiveness?

Chapter 2 shows how the use of PAM data combined with external, environmental measurements, can successfully identify source mechanisms for ambient noise. Specifically, independent measurements of wind speed (derived from scatterometry satellites) are combined with single-hydrophone PAM data to determine whether noise levels at a given frequency range, location and time associate with natural (wind) or anthropogenic (seismic reverberation) sources. The chapter then characterizes the spectral features of an impulsive seismic survey used in offshore oil and gas exploration, and quantifies its contribution to the overall underwater ambient noise budget in the shallow water environment of the continental shelf off the Alaskan Beaufort Sea. Contrary to most other oceans of the world, this low-frequency acoustic environment is generally dominated by natural sources during extensive times of the

year, making it a unique setting in which to isolate the impact of one predominant type of anthropogenic disturbance, present exclusively during the open water season (September and October). Results indicate that even at distances above 100 km seismic airgun impulses raise ambient levels by a few dB over the natural baseline, but as expected, much more elevated increases can be perceived at closer range to the source. As discussed previously, this work is specifically applicable to concerns about communication masking and degradation of PAM monitoring and mitigation capabilities.

In a second case study (Chapter 3) sufficient PAM data exists (i.e. multiple hydrophones) so that the source mechanisms can be identified by acoustic recordings alone; for example, data obtained from two closely-spaced hydrophones can be enough for determining the directionality of ambient noise sources.

The chapter then describes a computational time-synchronization procedure that exploits this directionality, enabling independent acoustic sensors to be used as a synchronized array. In order to demonstrate the practicality of this method, a study was performed at Laguna San Ignacio (LSI) in Baja California, Mexico, which deployed autonomous instruments separated by tens of meters in an environment where both an anthropogenic component of continuous noise exists (local whale-watching boats), as well as other diffuse biotic sources (for example, croaker fish). We then applied a traditional method of synchronizing (using the boat as a controlled source) and a novel time-synchronization method (based on the correlation of non-directional ambient noise) to time-align the sensors, followed by a discussion on the

temporal resolutions achieved by each method. The significance of time synchronization of autonomous recorders is considered in the context of a multi-scientific, collaborative project that can then apply these technologies for further marine mammal PAM research.

Finally, Chapter 4 summarizes the major conclusions resulting from this research, places their implications into the broader context of current scientific knowledge, and indicates potential future applications and supplementary studies.

V. REFERENCES

Andrew, R. K., Howe, B. M., Mercer, J. A., and Dzieciuch, M. A. (**2002**). "Ocean ambient sound: Comparing the 1960's with the 1990's for a receiver off the California coast," Acoust. Res. Lett. Online, **3**, 65–70.

Barlow, J., and Gisiner, R. (**2006**). "Mitigating , monitoring and assessing the effects of anthropogenic sound on beaked whales," J. Cetacean Res. Manag., **7**, 239–249.

Barlow, J., and Taylor, B. L. (**2005**). "Estimates of sperm whale abundance in the northeastern temperate Pacific from a combined acoustic and visual survey," Mar. Mammal Sci., **21**, 429–445.

Blackwell, S. B., Nations, C. S., McDonald, T. L., Greene, C. R., Thode, A., and Guerra, M. (**2013**). "Effects of airgun sounds on bowhead whale calling rates in the Alaskan Beaufort Sea," Mar. Mammal Sci., **29**, E342–E365.

Brooks, L. A, and Gerstoft, P. (**2009**). “Green’s function approximation from cross-correlations of 20-100 Hz noise during a tropical storm,” J. Acoust. Soc. Am., **125**, 723–734.

Buckingham, M. J. (**2012**). “Cross-correlation in band-limited ocean ambient noise fields,” J. Acoust. Soc. Am., **131**, 2643–2657.

Castellote, M., Clark, C. W., and Lammers, M. O. **(2012).** "Acoustic and behavioural changes by fin whales (*Balaenoptera physalus*) in response to shipping and airgun noise,"Biological Conservation, **147**, 115–122.

Cato, D. H. (**1998**). "Simple methods of estimating source levels and locations of marine animal sounds," J Acoust Soc Am **104**, 1667-1678.

Cato, D. H. (**1997**). “Features of Ambient Noise in Shallow Water,” Shallow Water Acoust., pp. 385–390.

Clark, C., Ellison, W., Southall, B., Hatch, L., Van Parijs, S., Frankel, A., and Ponirakis, D. (**2009**). “Acoustic masking in marine ecosystems: intuitions, analysis, and implication,” Mar. Ecol. Prog. Ser., **395**, 201–222.

Cousteau, J. Y., and Dumas, F. **(1954)**. Le monde du silence. (Éditions de Paris), pp.1-139.

D'Amico, A., Gisiner, R. C., Ketten, D. R., Hammock, J. A., Johnson, C., Tyack, P. L., and Mead, J. G. (**2009**). "Beaked Whale Strandings and Naval Exercises," Aquat. Mamm., **35**, 452-472.

Di Iorio, L., and Clark, C. W. (**2010**). "Exposure to seismic survey alters blue whale acoustic communication," Biol. Lett., **6**, 51–54.

DeRuiter, S. L., Southall, B. L., Calambokidis, J., Moretti, D., Abraham, B., and Tyack, P.L. (**2012**). "Marine Mammal Behavioral Response Studies in Southern California: Advances in Technology and Experimental Methods," Mar. Technol. Soc. J., **46**, 48-59.

Ellison, W. T., Southall, B. L., Clark, C. W., and Frankel, A. S. (**2012**). "A new context-based approach to assess marine mammal behavioral responses to anthropogenic sounds," Conserv. Biol., **26**, 21–28.

Filadelfo, R. J., Mintz, J., Michlovich, E., D'Amico, A., Tyack, P. L., and Ketten, D. R. (**2009**). "Correlating Military Sonar Use with Beaked Whale Mass Strandings: What Do the Historical Data Show?," Aquat. Mamm., **35**, 435–444.

Finneran, J. J., Carder, D. A., Schlundt, C. E., and Dear, R. L. (**2010**). "Temporary threshold shift in a bottlenose dolphin (*Tursiops truncatus*) exposed to intermittent tones," J. Acoust. Soc. Am., **127**, 3267–3272.

Fried, S. E., Kuperman, W. A., Sabra, K. G., and Roux, P. (**2008**). "Extracting the local Green's function on a horizontal array from ambient ocean noise," J. Acoust. Soc. Am., **124**, EL183–188.

Gordon, J., Tyack, P., and Thompson, D. (**2003**). "Controlled Exposure Experiments to Determine the Effects of Noise on Marine Mammals," Mar. Technol. Soc. J.,. **37**, 41-53.

Greene, C. R. J. (**1987**). "Characteristics of oil industry dredge and drilling sounds in the Beaufort Sea," J. Acoust. Soc. Am., **82**, 1315–1324.

Greene, C. R. J., and Richardson, W. J. (**1988**). "Characteristics of marine seismic survey sounds in the Beaufort Sea," J. Acoust. Soc. Am., **83**, 2246-2254.

Greene, C. R., McLennan, M. W., Norman, R. G., McDonald, T. L., Jakubczak, R. S., and Richardson, W. J. (**2004**). "Directional frequency and recording (DIFAR) sensors in seafloor recorders to locate calling bowhead whales during their fall migration," J. Acoust. Soc. Am., **116**, 799.

Halpern, B. S., Walbridge, S., Selkoe, K. A., Kappel, C. V, Micheli, F., D'Agrosa, C., Bruno, J. F., *et al*. (**2008**). "A global map of human impact on marine ecosystems," Science, **319**, 948–952.

Hastings, M. C., and Au, W. L. (**2012**). "Marine bioacoustics and technology: The new world of marine acoustic ecology," **273**, 273–282.

Hatch, L., Clark, C., Merrick, R., Van Parijs, S., Ponirakis, D., Schwehr, K., Thompson, M., *et al*. (**2008**). "Characterizing the relative contributions of large vessels to total ocean noise fields: a case study using the Gerry E Studds Stellwagen Bank National Marine Sanctuary," Environ. Manage., **44**, 735–752.

Hildebrand, J. (**2009**). "Anthropogenic and natural sources of ambient noise in the ocean," Mar. Ecol. Prog. Ser., **395**, 5–20.

Ireland, D. S., Funk, D. W., Rodrigues, R., and Koski, W. R. (**2009**). "Joint Monitoring Program in the Chukchi and Beaufort Seas, open water season, 2006-2007." in LGL Alaska Report P971-2 (LGL Ltd., Environmental Research Associates, King City, Ont., JASCO Research Ltd., Victoria, BC, and Greeneridge Sciences, Inc., Santa Barbara, CA, for Shell Offshore, Inc. Anchorage, AK, ConocoPhillips Alaska, Inc., Anchorage, AK, and the National Marine Fisheries Service, Anchorage, AK.).

Jensen, F. B., Kuperman, W. A., Porter, M. B., and Schmidt, H. **(1993)**. Computational Ocean Acoustics (Springer, New York), pp. 1-578.

Jensen, F. B., and Kuperman, W. A. **(1983)**. "Optimum frequency of propagation in shallow water environments,"J. Acoust. Soc. Am., **73**, 813.

Jones, M. L., Swartz, S. L., and Leatherwood, S. (**1984**). *The gray whale (Eschrichtius robustus)*. (Academic Press, London), i-xxiv, 1-600.

Kastelein, R. A., Gransier, R., and Hoek, L. (**2013**). "Comparative temporary threshold shifts in a harbor porpoise and harbor seal, and severe shift in a seal," J. Acoust. Soc. Am., **134**, 13.

Ketten, D. R. **(1992)**. The marine mammal ear: specializations for aquatic audition and echolocation. In:*The evolutionary biology of hearing*. (Springer New York). pp. 717-750

Kight, C. R., and Swaddle, J. P. (**2011**). “How and why environmental noise impacts animals: an integrative, mechanistic review,” Ecol. Lett., **14**, 1052–1061.

Knudsen, V. O., Alford, R. S., and Emling, J. W. (**1948**). "Underwater ambient noise," Journal of Marine Research **7**, 410-429.

Kuperman, W. A., and Lynch, J. F. (**2004**). “Shallow-water acoustics,” Phys. Today, **57**, 55–61.

McDonald, M. A., and Fox, C. G. (**1999**). “Passive acoustic methods applied to fin whale population density estimation,” J. Acoust. Soc. Am., **105**, 2643.

McKenna, M. F., Ross, D., Wiggins, S. M., and Hildebrand, J. A. (**2012**). “Underwater radiated noise from modern commercial ships,” J. Acoust. Soc. Am., **131**, 92–103.

Moore, S. E., Reeves, R. R., Southall, B. L., Ragen, T. J., Robert, S., Clark, C. W., and Suydam, R. S. (**2012**). “A New Framework for Assessing the Effects of Anthropogenic Sound on Marine Mammals in a Rapidly Changing Arctic,” Bioscience, **62**, 289–295.

Morrissey, R. P., Ward, J., DiMarzio, N., Jarvis, S., and Moretti, D. J. (**2006**). "Passive acoustic detection and localization of sperm whales (*Physeter macrocephalus*) in the tongue of the ocean," Appl. Acoust., **67**, 1091–1105.

National Research Council (NRC) **(2005).**"Marine Mammal Populations and Ocean Noise; Determining When Noise Causes Biologically Significant Effects" (National Academic Press Washington, D.C.), pp. 23–34.

Nieukirk, S. L., Stafford, K. M., Mellinger, D. K., Dziak, R. P., and Fox, C. G. (**2004**). "Low-frequency whale and seismic airgun sounds recorded in the mid-Atlantic Ocean," J. Acoust. Soc. Am., **115**, 1832-1843.

Norris, K.S. **(1969)**. The echolocation of marine mammals, in: Anderson, T.H. (Ed.) The Biology of Marine Mammals. pp. 391-423.

Nowacek, D. P., Thorne, L. H., Johnston, D. W., and Tyack, P. L. (**2007**). "Responses of cetaceans to anthropogenic noise," Mamm. Rev., **37**, 81–115.

Perrone, A. (**1969**). "Deep-Ocean Ambient-Noise Spectra in the Northwest Atlantic," J. Acoust. Soc. Am., **46**, 762–770.

Richardson, W. J., Greene C. R. Jr., Malme C. I., and Thomson D. H. (Eds). **(1995)**. Marine Mammals and Noise. (Academic Press, San Diego, CA), pp. 1-576.

Richardson, W. J., Würsig, B., and Greene, C. R. (**1986**). "Reactions of bowhead whales, Balaena mysticetus, to seismic exploration in the Canadian Beaufort Sea," J. Acoust. Soc. Am., **79**, 1117–1128.

Rolland, R. M., Parks, S. E., Hunt, K. E., Castellote, M., Corkeron, P. J., Nowacek, D. P., Wasser, S. K., *et al*. (**2012**). "Evidence that ship noise increases stress in right whales," Proc. Biol. Sci., **279**, 2363–2368.

Roman, J., Altman, I., Dunphy-Daly, M. M., Campbell, C., Jasny, M., and Read, A. J. (**2013**). "The Marine Mammal Protection Act at 40: status, recovery, and future of US marine mammals," Ann. N. Y. Acad. Sci., **1286**, 29-49.

Ross, D. **(1976)**. Mechanics of underwater noise. (Pergamon Press, New York), pp. 1-287.

Ruckelshaus, M., Doney, S. C., Galindo, H. M., Barry, J. P., Chan, F., Duffy, J. E., English, C. a., *et al*. (**2013**). "Securing ocean benefits for society in the face of climate change," Mar. Policy, **40**, 154–159.

Sabra, K. G., Roux, P., and Kuperman, W. A. (**2005a**). "Arrival-time structure of the time-averaged ambient noise cross-correlation function in an oceanic waveguide," J. Acoust. Soc. Am., **117**, 164-174.

Sabra, K. G., Roux, P., Thode, A. M., D'Spain, G. L., Hodgkiss, W. S., and Kuperman, W. A. (**2005b**). "Using Ocean Ambient Noise for Array Self-Localization and Self-Synchronization," IEEE J. Ocean. Eng., **30**, 338–347.

Schlundt, C. E., Finneran, J. J., and Carder, D. A. (**2008**). “Temporary threshold shift: Sam Ridgway’s contribution to an important and not-so-temporary line of marine mammal research,” J. Acoust. Soc. Am., **124**, 2466.

Scholik-Schlomer, A. R. **(2012)**. "Status of NOAA’s guidelines for assessing impacts of anthropogenic sound on marine life," in: The effects of noise on aquatic life. (Springer-Verlag, New York, NY), pp. 557-562.

Simard, Y., Roy, N., and Gervaise, C. (**2008**). “Passive acoustic detection and localization of whales: effects of shipping noise in Saguenay-St Lawrence Marine Park,” J. Acoust. Soc. Am., **123**, 4109–4117.

Sonntag, R., Ellison, W. T., Clark, C. W., Corbit, D. R., and Krogman, B. D. (**1986**). "A description of a tracking algorithm and its application to bowhead whaleacoustic location data collected during the spring migration near Point Barrow, Alaska 1984-85," International Whaling Commission Report of theCommission **36**, 299-310.

Sousa-Lima, R., and Norris, T. (**2013**). “A review and inventory of fixed autonomous recorders for passive acoustic monitoring of marine mammals,” Aquat. Mamm., **39**, 23–53.

Southall, B., Bowles, A., and Ellison, W. (**2007**). “Marine mammal noise exposure criteria: initial scientific recommendations,” Aquat. Mamm., **33**, 411–521.

Thode, A. M., Kim, K. H., Blackwell, S. B., Greene, C. R., Nations, C. S., McDonald, T. L., and Macrander, A. M. (**2012**). “Automated detection and localization of

bowhead whale sounds in the presence of seismic airgun surveys," J. Acoust. Soc. Am., **131**, 3726–47.

Thode, A. M., Gerstoft, P., Burgess, W. C., Sabra, K. G., Guerra, M., Stokes, M. D., and Cato, D. H. **(2006).** "A Portable Matched-Field Processing System Using Passive Acoustic Time Synchronization," IEEE Journal of Oceanic Engineering **31**: 696–710.

Tiemann, C. O., Porter, M. B., and Hildebrand, J. A. (**2002**). "A robust model-based algorithm for localizing marine mammal transients," Impact Littoral Environ. Var. Acoust. Predict. Sonar Perform., (Springer Netherlnds), pp. 523–530.

Tyack, P. L. (**2008**). "Implications for marine mammals of large-scale changes in the marine acoustic environment," J. Mammal., **89**, 549–558.

Urban R, J., Rojas-Bracho, L., Perez-Cortes, H., Gomez-Gallardo, A., Swartz, S. L., Ludwig, S., and Brownell, R. L., Jr. (**2003**). "A review of gray whales (*Eschrichtius robustus*) on their wintering grounds in Mexican waters,"Journal of Cetacean Research and Management **5**, 281-295.

Urick, R. J. (**1983**). Principles of Underwater Sound. (McGraw-Hill, New York), pp. 1-423.

Van Parijs, S., Clark, C., Sousa-Lima, R., Parks, S., Rankin, S., Risch, D., and Van Opzeeland, I. (**2009**). "Management and research applications of real-time and archival passive acoustic sensors over varying temporal and spatial scales," Mar. Ecol. Prog. Ser., **395**, 21–36.

Wenz, G. M. (**1962**). “Acoustic ambient noise in the ocean: Spectra and sources,” J. Acoust. Soc. Am., **34**, 1936–1956.

Wenz, G. M. (**1972**). “Review of Underwater Acoustics Research: Noise,” J. Acoust. Soc. Am., **51**, 1010–1024.

Wiggins, S., and Hildebrand, J. A. (**2003**). “Autonomous Acoustic Recording Packages (ARPs) for Long-Term Monitoring of Whale Sounds,” Mar. Technol. Soc. J.,. **37**, 13-22.

Wladichuk, J. L., Megill, W. M., and Blondel, P. (**2008**). “Passive acoustic localization techniques of Eastern Pacific grey whales,” J. Acoust. Soc. Am., **123**, 3207.

Worm, B., Barbier, E. B., Beaumont, N., Duffy, J. E., Folke, C., Halpern, B. S., Jackson, J. B. C., *et al*. (**2006**). “Impacts of biodiversity loss on ocean ecosystem services,” Science, **314**, 787–90.

Zimmer, W. M. **(2011)**. Passive acoustic monitoring of cetaceans. Cambridge University Press. Cambridge. 1-356.

CHAPTER 2:

Quantifying seismic survey reverberation off the Alaskan North Slope

ABSTRACT

Shallow-water airgun survey activities off the North Slope of Alaska generate impulsive sounds that are the focus of much regulatory attention. Reverberation from repetitive airgun shots, however, can also increase background noise levels, which can decrease the detection range of nearby passive acoustic monitoring (PAM) systems. Typical acoustic metrics for impulsive signals provide no quantitative information about reverberation or its relative effect on the ambient acoustic environment. Here, two conservative metrics are defined for quantifying reverberation: a minimum level metric measures reverberation levels that exist between airgun pulse arrivals, while a reverberation metric estimates the relative magnitude of reverberation vs. expected ambient levels in the hypothetical absence of airgun activity, using satellite-measured wind data. The metrics are applied to acoustic data measured by autonomous recorders in the Alaskan Beaufort Sea in 2008 and demonstrate how seismic surveys can increase the background noise over natural ambient levels by 30-45 dB within 1 km of the activity, by 10-25 dB within 15 km of the activity, and by a few dB at 128 km range. These results suggest that shallow-water reverberation would reduce the performance of nearby PAM systems when monitoring for marine mammals within a few kilometers of shallow-water seismic surveys.

I. INTRODUCTION

The Beaufort Sea borders the Alaskan North Slope along a 340 km swath of northern Alaska. The continental shelf along this coast is relatively narrow, between 60 and 120 km. Its depth can reach a few hundred meters, but in this paper a 'shallow-water environment' will refer to continental shelf water depths of 50 m or less. The Beaufort Sea, along with the adjacent Chukchi Sea, is home to a variety of whales, seals and other marine mammals that may be sensitive to the sounds of increasing industrial activities in the area.

During the ice-free months of 2006-2009 multiple overlapping anthropogenic activities by several independent companies and government agencies were conducted in this region. Of particular concern to regulators are sounds originating from seismic airgun surveys (Barger and Hamblen, 1980; Greene and Richardson, 1988). Quantifying the potential long-term impacts of these surveys on the viability of marine mammal populations faces numerous challenges, beginning with the problem of defining the relevant measurement metrics. Some consensus is emerging about metrics of impulsive signals that are appropriate in terms of estimating auditory injury to animals (Madsen, 2005; Southall *et al.*, 2007; Kastak *et al.*, 2005). These measurements include peak-to-peak amplitude, root-mean-square (rms) amplitude, and sound exposure (SE) (Urick, 1983; Madsen, 2005). Limited laboratory data on marine mammal hearing, reviewed in Southall *et al.* (2007), suggest that sound exposure level (SEL) in particular, may be a biologically relevant metric for predicting the degree of

temporary and permanent threshold shift in individuals exposed to high-intensity sounds; however, there has been little research on the long-term impacts of chronic acoustic exposure on marine mammal populations, nor are there formal regulations for quantifying communication masking effects in marine mammals.

In shallow-water environments additional factors arise when characterizing the sounds from a seismic airgun survey. In shallow water no direct path exists between the airgun source and a receiver; instead, the pulse energy arrives as a series of multipath (normal mode) arrivals, each with a different arrival time at the receiver. Due to frequency-dependent geometric dispersion effects, the time-dependent frequency structure and duration of each modal multipath arrival changes, complicating attempts to estimate the biologically relevant sound exposure. A portion of the pulse energy also travels through the ocean floor and re-emerges into the water column as a head wave, which can provide a significant fraction of the total signal energy below 50 Hz.

Yet another consequence of shallow-water propagation is the substantial reverberation that follows all modal arrivals. As the pulse propagates through shallow water, it interacts multiple times with the ocean surface, bottom, and substrate, scattering energy incoherently throughout the water column in the form of reverberation. Although the received levels of reverberation are generally lower than peak or rms measurements of the coherent arrivals, they can be greater than natural ambient noise levels. Reverberation can persist over timescales much longer than the duration of the dispersed coherent arrivals, even persisting until the start of the next

seismic airgun shot. Thus, seismic airgun reverberation can continuously elevate the background noise field during a survey, even during times between airgun shots. In general, modeling or predicting reverberation is difficult; reverberation characteristics are highly dependent on the local bathymetry and propagation environment.

The presence of reverberation in shallow water has two important consequences when trying to understand the potential impact of seismic airgun activities on marine mammals. First, the elevated background noise levels arising from reverberation would be expected to reduce the range at which passive acoustic monitoring (PAM) systems could detect and localize marine mammal sounds near shallow-water seismic airgun activities. Second, seismic airgun reverberation may reduce the 'communication space' between animals like the bowhead whale, and thereby impact quantitative estimates of information masking (Richardson *et al.*, 1986; Clark *et al.*, 2009; Di Iorio and Clark, 2009). Thus simple metrics are desired to quantify how reverberation increases background noise above ambient levels in shallow water. This paper defines two metrics: a *minimum level metric (MLM)* and a *reverberation metric (RM).* The former simply reports the minimum sound levels detected over a given time window, while the latter estimates how much seismic airgun reverberation increases background noise over what would have existed in the absence of such activity. For the continental shelf off the Alaskan North Slope, the RM is derived from wind speed estimates obtained from satellite observations, which are then used to empirically model what wind-driven ambient noise levels would have been at a specific location. These modeled ambient levels are then compared with the

MLM to generate the RM. The RM is a conservative measure of the contribution of reverberation to the background noise environment because it only applies to times when reverberation is continuously present. The RM does not apply to situations where reverberation is present, but fades away to ambient levels between airgun shots.

Section II gives details about the data used for this analysis: acoustic recordings obtained in 2008 at a variety of ranges from seismic airgun activities off the North Slope of Alaska. Section III defines the two metrics in detail and discusses the global database used to estimate sea surface wind speeds derived from satellite data. Section IV applies these metrics to the data described in Section II, producing information about the temporal and spatial distribution of reverberation generated by a seismic airgun survey operating between 2-128 km from acoustic receivers.

II. DATA DESCRIPTION

A. Seismic airgun survey

The reverberation data presented here arose from a seismic airgun survey generated from the M/V Gilavar in the Beaufort Sea in 2008. The Gilavar towed two WesternGeco arrays of Bolt airguns (Ireland *et al.*, 2009) approximately 275 m behind the vessel. Each array consisted of 24 airguns, distributed into three sub-arrays of 1049 in^3 volume each, for a total volume of 3147 in^3 operated at an air pressure of 2000 psi. Full airgun operations were preceded by ramp-up procedures, during which marine mammal observers (MMO) visually searched the surrounding area for evidence of

marine mammal presence. During standard operation airguns were shot at intervals of 25 m (~9 s) while the vessel traveled at speeds between 4 and 5 knots. The seismic survey vessel usually rastered across a region, moving in a straight line over an area of interest, then making a 180 degree turn and shooting another line parallel to the previous course. During the process of turning the vessel around, activity is reduced to a mitigation-gun condition, when only one of the airguns remains active at a volume of 30 in^3.

B. Passive acoustic data

Between August 11th and October 9th 2008 a network of 40 Directional Autonomous Seafloor Acoustic Recorders (DASARs-C08) (Greene *et al.*, 2004) were deployed offshore in the Alaskan Beaufort Sea, covering a coastal distance of approximately 280 km (174 mi) between the village of Kaktovik in the east and Harrison Bay in the west (Figure 2-1). DASARs were deployed on the seafloor at depths between 15 and 54 m, and were arranged into five groups, or 'sites' labeled 1 through 5 from west to east. Each site is configured into an extended array of seven DASARs, labeled A-G from south to north, with the instruments placed at the vertices of equilateral triangles of sides 7 km in length. Site 1 had the shallowest mean water depth of all the sites (20.5 m) while Site 5 had the deepest (48.9 m). The DASARs recorded continuously at a sampling rate of 1 kHz, and the sensitivity of the omni-directional (pressure) hydrophone was -149 dB re 1 µPa/V, with a high-pass frequency response of around 20 dB per decade, in order to pre-whiten the expected ambient

noise spectrum. To recover the calibrated time series, the data were passed through a single-pole IIR low-pass filter cascaded with a Butterworth high-pass filter with a 10 Hz cutoff frequency. The low-frequency cutoff was chosen to remove the effects of flow noise, as well as seismic interface and head waves. While IIR filters can be unstable, producing 'ringing' in response to a large-amplitude impulsive signal, a review of the calibrated vs. un-calibrated data confirmed that the reverberation data reported here are not filtering artifacts.

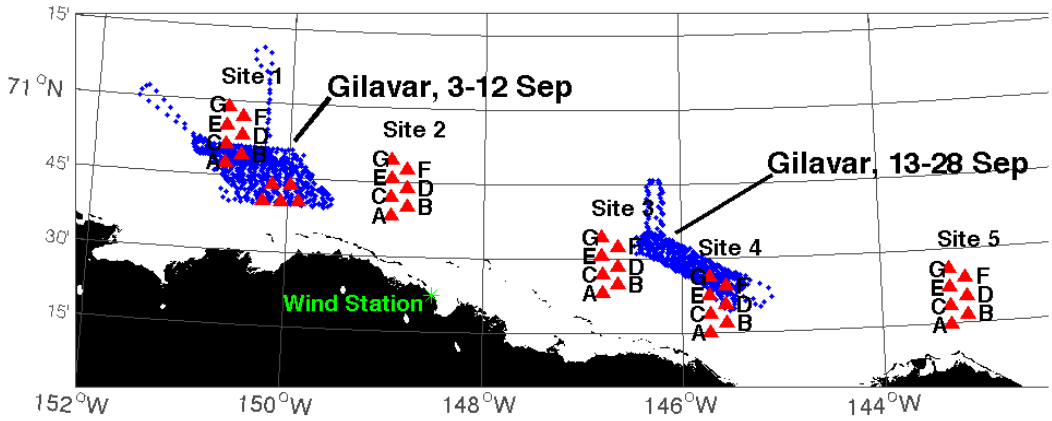

Figure 2-1: Location of DASAR deployments, arranged by site, plotted alongside with tracks and dates of extended seismic airgun surveys. Within each site DASARs are labeled A to G from south to north. The location of the Prudhoe Bay land-based wind station is also marked.

Figure 2-1 illustrates the track lines of the M/V Gilavar plotted alongside the DASAR locations, revealing two bouts of concentrated survey activity. One bout occurred around Site 1 from September 3rd through the 12th, 2008, and the second bout occurred between Sites 3 and 4, from September 13th through the 28th, 2008. The analyses that follow incorporate data from the shallowest (A) and deepest (G) DASARs at all sites within those date ranges. Reverberation from other DASARs at

intermediate depths at a site generally lay between the levels obtained from the A and G DASARs. The land-based weather station at Prudhoe Bay, marked on Figure 2-1, was used to confirm wind speeds downloaded from satellite scatterometry databases (Zhang *et al.*, 2006). The closest DASAR to the weather station was 2A.

III. ANALYSIS PROCEDURE

A. Review of fundamental level metrics

The metrics defined in this paper are intended to complement the concepts of sound exposure level (SEL) and root-mean-square sound pressure level (rms SPL) of a transient sound, in that they provide additional information not captured by these metrics. However, the metric definitions originate from SEL and SPL, and so their definitions are reviewed here.

The term sound exposure (SE), with units of Pa^2-s, is frequently used as a proxy for energy flux density. Studies of mammalian ears (Young and Wenner, 1970; Yost, 1994; Madsen, 2005) suggest that, for signals of relatively short duration (under 1 s) their perception of loudness is based on both the intensity and the duration of a received signal. However, SE is not a direct measure of the physical energy flux density, because measuring the true energy flux would require an independent measurement of acoustic particle velocity (D'Spain *et al.*, 1991). Following the definitions from Southall *et al.* (2007) and Madsen (2005), the SE of an equalized transient pulse at a given absolute time index *i* is computed as follows:

$$SE_i(t) = \int_{T_{i-1}}^{T_i} \left[p^{\,2}(t) \right] dt_i = \int_{f_1}^{f_2} \left| P(f) \right|^2 df \approx \sum_{k=k_1}^{k_2} \frac{\left| \hat{P}(k) \right|^2}{NF_s} \tag{1}$$

where *p(t)* refers to a band-limited pressure time series, *i* indicates the time index defined over a period $\Delta T_i = T_i - T_{i-1}$, and *P(f)* is the analytic Fourier Transform of *p(t)*, with *p(t)* set to zero outside the time interval defined here. The second equality is a consequence of Parseval's Theorem. The third approximate equality shows how the SE is computed from the Fast Fourier Transform (FFT) $\hat{P}(k)$, derived from *N* samples of a pressure time series discretely sampled F_s times per second, such that $N=\Delta T_i F_s$. Eq. (1) is frequency-dependent as it implicitly assumes the pressure time series *p(t)* has been bandpass-filtered over a specific frequency range of interest between f_1 and f_2.

A variant of Eq. (1) subtracts an estimate of the root-mean-square background noise from $p^2(t)$ in an attempt to estimate the pressure contribution from the transient signal alone, and not the combined transient and background pressure, but when defining the new metrics here, the definition as presented in Eq. (1) will be used.

The rms sound pressure (SP) is simply the square root of SE divided by ΔT_i and has units of pressure:

$$SP_i(t) = \sqrt{\frac{1}{T_i - T_{i-1}} \int_{T_{i-1}}^{T_i} \left(p^2(t) dt \right)} \equiv \sqrt{\frac{SE_i(t)}{T_i - T_{i-1}}} \tag{2}$$

The decibel measure of SE, the sound exposure level (SEL), is

$SEL_i = 10\log_{10}(SE_i/SE_{ref})$ with a reference quantity of 1 μPa^2-s. The rms sound pressure level (SPL) is $SPL_i = 20\log_{10}(SP_i/SP_{ref})$, with a reference quantity of 1 μPa.

B. Minimum level metric (MLM)

This section describes how to obtain a minimum level metric (MLM) from recordings of seismic airgun surveys. The importance of the metric is that it provides a convenient approach for measuring background noise levels that exist between airgun pulses, and thus reverberation effects. In order to generate a MLM from a raw time series, three steps have to be taken, and each step requires a decision concerning the choice of a particular time scale for processing the data.

The first step is to convert the raw time series into a series of overlapping FFTs, from which SE or SP estimates can be derived using Eqs. (1) and (2); however, both equations were originally defined for deterministic impulsive signals that are clearly distinguishable from diffuse background noise within a given time interval ΔT_i. The first decision that arises when attempting to apply these definitions to stochastic signals like seismic airgun reverberation is how long a time period ΔT_i is needed to compute the SE or SP. Stated another way, what FFT length N should be selected to compute these levels? In the absence of a sharply-defined transient pulse, it is difficult to determine how long a time sample is needed to provide a SE or SP estimate of the background noise.

In this paper ΔT_i (and thus the FFT length N) is related to the estimated integration time of the mammalian hearing mechanism of concern; given the lack of

such information for various species of interest, including the bowhead whale, this integration time ΔT_i is postulated to be the typical call duration from the species. For example, for a bowhead whale the integration interval would be on the order of 1 to 2 s (Ljungblad *et al.*, 1980; Clark and Johnson, 1984). Thus a value of ΔT_i of 1.024 s will be used in Section IV, which translates into a FFT length of 1024 points at a 1 kHz sampling rate. Having chosen the time window, a set of overlapping FFTs are calculated over the entire time series, regardless of whether or not a seismic airgun pulse is present within a particular FFT time window. The FFT snapshots are then converted into a series of SE values using the last equality in Eq. (1).

The second step in computing the MLM is averaging sequential SE or SP estimates over a short time window, in order to reduce the variance of the result. The need for this step arises from the fact that SE or SP estimates derived from a stochastic signal fluctuate over time, even if the underlying statistical distribution of the noise properties (e.g. power spectral density) remains constant.

To achieve this step, one must decide how many FFT snapshots can be averaged to generate a 'well-behaved' estimate of the stochastic signal's SE or SP. Thus a second (averaging) timescale must be determined. This new timescale estimates a time window over which certain statistical properties of the noise are assumed to be invariant, or *stationary*, an assumption that permits the SE or SP estimates generated from data from within that time window to be averaged together. In the signal processing literature, a certain kind of stationary signal is designated *wide-sense stationary* (WSS) if both the mean and autocorrelation (i.e. the first two

moments) of a stochastic signal do not change over the time period in question. Roughly stated, a WSS signal maintains the same underlying power spectrum over time, and thus sequential estimates of SE or SP can be averaged.

Reverberation in an ocean waveguide is time-dependent, in that both its magnitude and spectral content clearly evolve over time as the reverberation fades away. A time window ΔT_{WSS} can be identified, however, wherein the WSS assumption holds. If $\Delta T_{WSS} > \Delta T_{i,}$ then an integer number $N_{samples}$ of adjacent or overlapping SP or SE estimates can be averaged together, reducing the variance in accordance with Welch's method (Oppenheim, 1999). Thus, for SE measurements of background noise,

$$\overline{SE_i} = \frac{1}{N_{samples}} \sum_{j=i}^{i+N_{samples}} SE_j \tag{3}$$

The duration of ΔT_{WSS} is always less than the interval between airgun pulses, thus ensuring that some values of SE_i will have been averaged over a time window that excludes an airgun signal. In Section IV a ΔT_{WSS} value of 2 s is used.

The final step in computing the MLM is determining the minimum value produced by Eq. (3) over a third time window $\Delta T_{min.}$ Completing this step requires a final decision over what timescale the minimum should be sought. Whereas the first two timescales defined relatively short time windows of 1 to 2 s, the ΔT_{min} window generally must be much longer, encompassing several airgun pulse arrivals. Yet, the third time window cannot be chosen to be so long that it fails to capture gradual

changes in the background reverberation caused by changes in source/receiver distance and other aspects of the operation.

Therefore $\Delta T_{min}$is defined as the time scale over which there are no significant changes in the source/receiver range, orientation, and/or propagation environment. Once $\Delta T_{min}$is determined, a MLM can be defined using either SE or SP, or equivalently SEL or SPL:

$$SPL_i^{\min} = \min\left\{SPL_i,\ SPL_{i+1},\ SPL_{i+2},\ \ldots SPL_{i+N_{\min}}\right\} \tag{4}$$

$$SEL_i^{\min} = \min\left\{SEL_i,\ SEL_{i+1},\ SEL_{i+2},\ \ldots SEL_{i+N_{\min}}\right\} \tag{5}$$

where $N_{min}$is the number of averaged samples generated by Eq. (3) that lie within the ΔT_{min}time window. In Section IV a time window of 30 min was estimated to be the interval over which reverberation levels do not change. The units of this MLM are identical to that of a standard SPL or SEL level: dB re 1 µPa for SPL, dB re 1 µPa^2-s for SEL.

In summary, deriving a MLM from raw acoustic data requires three steps: generating a series of time-overlapped FFT snapshots of the data, averaging adjacent snapshots together to reduce the estimate's variance, and then selecting the minimum averaged value that occurs over a long-term time window. The three time scales that need to be defined to obtain the metric have been labeled ΔT_i,$\Delta T_{WSS,}$ and ΔT_{min}. These values represent: (1) the assumed biologically-relevant energy-integration time scale of a species' hearing mechanism, which determines the FFT length used on the data; (2) the time scale over which the noise can be considered wide-sense stationary, which

determines how many SE or SP estimates can be appropriately averaged over time; and (3) the time scale over which no significant changes take place in the source-receiver separation and propagation environment, which determines the time window over which to extract the minimum level value. The final result is a time-dependent estimate of minimum background noise level that removes any contribution from transient components of the airgun signal, including all modal and substrate arrivals.

C. Reverberation metric (RM)

To convert the MLM into a dimensionless reverberation metric (RM), an independent estimate of baseline ambient sound levels must be made in the absence of seismic airgun survey activity. The dB values of these estimates are then subtracted from the dB values of the MLM to generate the RM, with an interpretation analogous to that of signal-to-noise ratio (SNR). For example, a value of 0 dB or less for the RM would indicate that the reverberation from an airgun shot decays to natural ambient levels before the next shot occurs.

Unfortunately, no universal procedure for estimating or modeling ambient noise can be recommended, because the sources of ambient noise are highly dependent on a particular location and season. Three possible methods can be suggested, all of which require assumptions behind the ambient noise mechanisms. The first method is to simply assume that the MLM values measured before the onset of a particular anthropogenic activity would have remained at that level during the activity (temporal consistency). The second method is to measure the MLM simultaneously at two

locations: one close to the anthropogenic activity, and one so distant that contributions from that activity are assumed negligible (spatial consistency). The final method assumes that the MLM can be accurately modeled using independent measurements of other environmental parameters, such as wind, rainfall, tides, levels of shipping activity, etc (environmental consistency). The results in Section IV.C use this third method, because empirical measurements of ambient noise in this open-water Arctic environment correlate well with local surface wind speed measurements. Winds agitate the ocean surface, creating waves, bubbles, and other physical processes that dominate the acoustic noise environment. Noise from shipping is negligible in this region. These assumptions are consistent with previous ambient noise observations in the region (Ireland *et al.*, 2009; Wenz, 1962; Figure 2.7 of Blackwell *et al.*, 2006). The wind speeds for this work were obtained from the online NOAA Blended Sea Winds database (Zhang *et al.*, 2006), which combines scatterometer observations from multiple satellites to produce a set of global gridded wind speeds, averaged in 6-hour increments and gridded with 0.25º spatial resolution in latitude and longitude. For every time increment, the wind speed values of the four grid-points closest to a given DASAR location were spatially averaged to produce a best-estimate of the wind speed at the DASAR location at that time. The dB values of the MLM were then averaged over 6 hour increments (i.e., the ambient noise values are geometrically averaged) to produce a time series with the same sampling interval as the spatially-averaged blended wind data. Finally, the correlation coefficient was computed between the MLM and the spatially-averaged wind data, using relative time offsets of 0, 6 and 12

hours, where the MLM was delayed from the wind. Periods when seismic airgun survey activities were occurring in close proximity were rejected from the regressions. The time offset that produced the best correlation was then used to compute a set of linear regressions between the blended database wind speeds and MLM, a process discussed in more detail in Section IV.C. The dB levels of the resulting modeled ambient noise levels are then subtracted from the MLM derived for all times, including times of seismic airgun survey activity, generating the RM.

IV. RESULTS

A. Reverberation examples

Figure 2-2 presents representative calibrated spectrograms of seismic airgun survey impulses generated by the Gilavar in 2008, as recorded by DASARs at Sites 1 and 4. All spectrograms are computed using a 256-point FFT with 75% overlap. Figures 2-2(a) and 2(b) show spectrograms of seismic impulses recorded at DASAR 1A, the shallowest DASAR at Site 1, on September 9th at ranges of 18.5 km and 6.5 km, respectively. Figure 2-2(a) illustrates a 60 s portion of the mitigation-gun procedure that occurs as the vessel reverses course between transects, during which only one gun fires at a volume of 30 in^3. Subplot 2(b) illustrates the received signal from the full airgun array firing 24 guns (for a total volume of 3147 in^3) at a range of 6.5 km, with pulses generated at approximately 9 s intervals. Finally, Figure 2-2(c) displays a 60 s-long spectrogram of airgun pulses from the full airgun array, but

recorded at the deepest DASAR of Site 4 (DASAR 4G) at a range of 17.5 km on September 25th. These spectrograms demonstrate how different source ranges affect the modal airgun arrivals. The exact nature of reverberation is highly site dependent; one can see that the power spectral density from reverberation varies from site to site, even when the same airgun source is used.

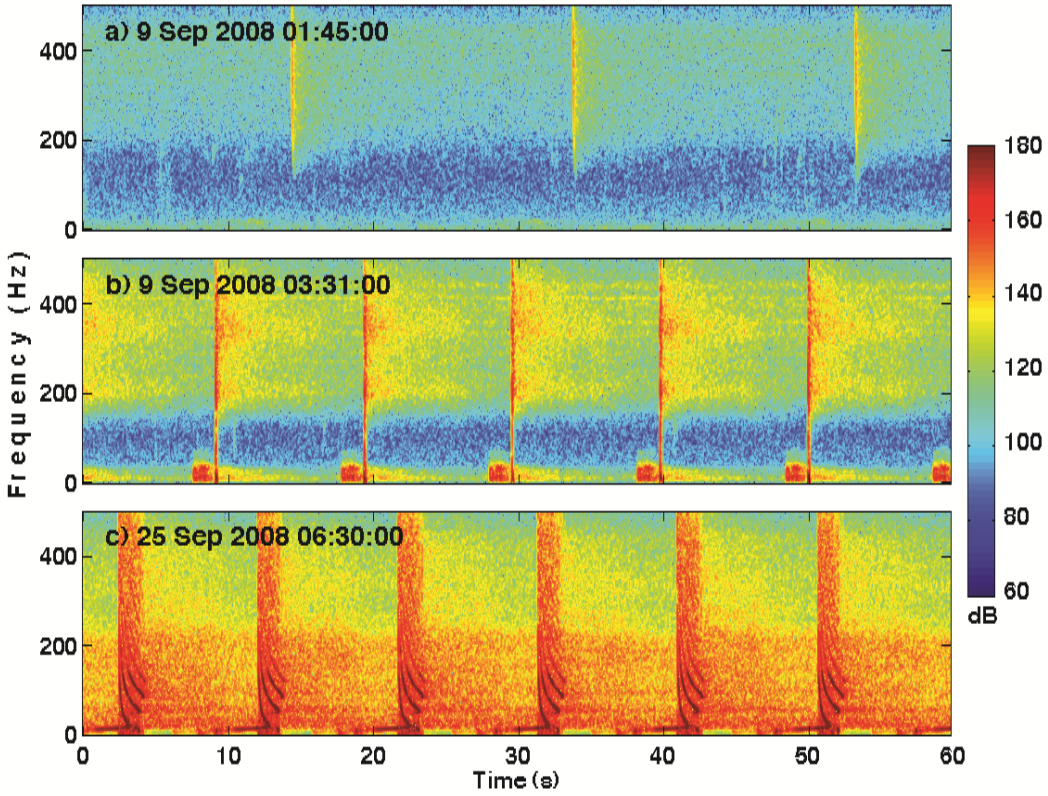

Figure 2-2: Representative spectrograms of seismic activity from the M/V Gilavar: (a) mitigation gun at 18.5 km range recorded at DASAR 1A (the shallowest DASAR at Site 1) on September 9th, 2008 at 01:45; (b) full airgun array at 6.5 km range, at DASAR 1A on September 9th, 2008 at 03:31; (c) full airgun array at 17.5 km range at DASAR 4G (the deepest DASAR at Site 4) on September 25th, 2008 at 06:30. The sub-50 Hz arrival visible before the main pulse arrival in (b) arises from a head-wave leaking from the substrate, and the frequency-modulated down-sweep visible in (c) arise from the geometric dispersion of various normal mode arrivals.

Figures 2-2(b) and 2-2(c) also show head wave arrivals from the substrate (Frisk, 1994), visible below 50 Hz.

B. Minimum level metric (MLM) estimates

Figures 2-3 through 2-8 display the MLM [Eq. (5)] derived for all 30-min samples of the dataset, including periods with seismic activity. To compute this metric, a series of Fast Fourier Transforms (FFTs) were computed, using 1024-point snapshot sizes, with 50% overlap between subsequent snapshots. A 1024-point FFT corresponds to an energy integration time ΔT_i of 1.024 s, the rough mean duration of an average bowhead whale call. The time scale ΔT_{WSS} was selected to be 2 s, and ΔT_{min} was chosen to be 1800 s, or 30 min. ΔT_{WSS} is less than the interval between seismic airgun shots (about 9 s), thus guaranteeing that some outputs of this operation will not be contaminated by energy from the direct shots visible in Figure 2-2.

Figure 2-3(a)-(d) shows the broadband (10-450 Hz) MLM in units of SPL, for the shallowest (A) and deepest (G) DASARs at Sites 1 and 4. It is worth re-emphasizing that Figure 2-3 and subsequent figures do not display any properties of the dispersed airgun pulse arrivals; instead, they quantify the reverberation that persists *between* airgun pulse arrivals. Note that the time scales in Figure 2-3 cover the entire deployment period, not just times when local seismic airgun surveys are present.

The long-term broadband MLM results, shown in Figure 2-3, are influenced by changes in ambient noise levels, as well as the presence of reverberation from

anthropogenic sources. Substantial changes in the broadband natural ambient levels can be observed, varying by over 30 dB, but tend to occur over relatively long time scales (e.g. over the course of a day), as seen between September 14th and 19th in Figure 2-3(a) and 2-3(b). By contrast, seismic airgun surveys produce relatively rapid fluctuations ('comb patterns') in background levels over timescales of only a few hours, as the ship constantly varies its distance to a given DASAR while rastering across the site. This rapid variation is emphasized by the fact that the vessel reduces the number of airguns firing while it is turning around, allowing background levels to briefly return to ambient baselines, before the survey activates the full airgun array again. MLM levels at Site 4 can vary by up to 30 dB, as can be seen between September 20th and 28th [Figure 2-3(c) and 2-3(d)], as the vessel transits between the furthest and closet ranges relative to the DASAR.

Figure 2-4 displays the same metric as in Figure 2-3, but computed for DASAR 1A only, over four 100-Hz frequency bands: 10-110 Hz, 110-210 Hz, 260-360 Hz and 360-460 Hz. The same periods of seismic airgun activity seen in Figure 2-3 can be recognized here due to the distinctive 'comb pattern'. During these times, MLM values are greatest at frequencies above 260 Hz [Figure 2-4(b)], regardless of vessel range and orientation to the receiver, indicating that the spectral composition of this reverberation is strongly dependent on local propagation conditions, such as local water depth. Figures 2-5 and 2-6 plot the MLM as a function of frequency, time, and location. Figure 2-5 plots the results obtained at the shallowest DASAR at each of the five sites (DASARs A), while Figure 2-6 plots results on the same intensity scale for

the deepest DASARs at each of the five sites (DASARs G). The frequency dependence has been computed over eight overlapping (50%) frequency bands between 10 and 460 Hz, each band covering a 100 Hz bandwidth.

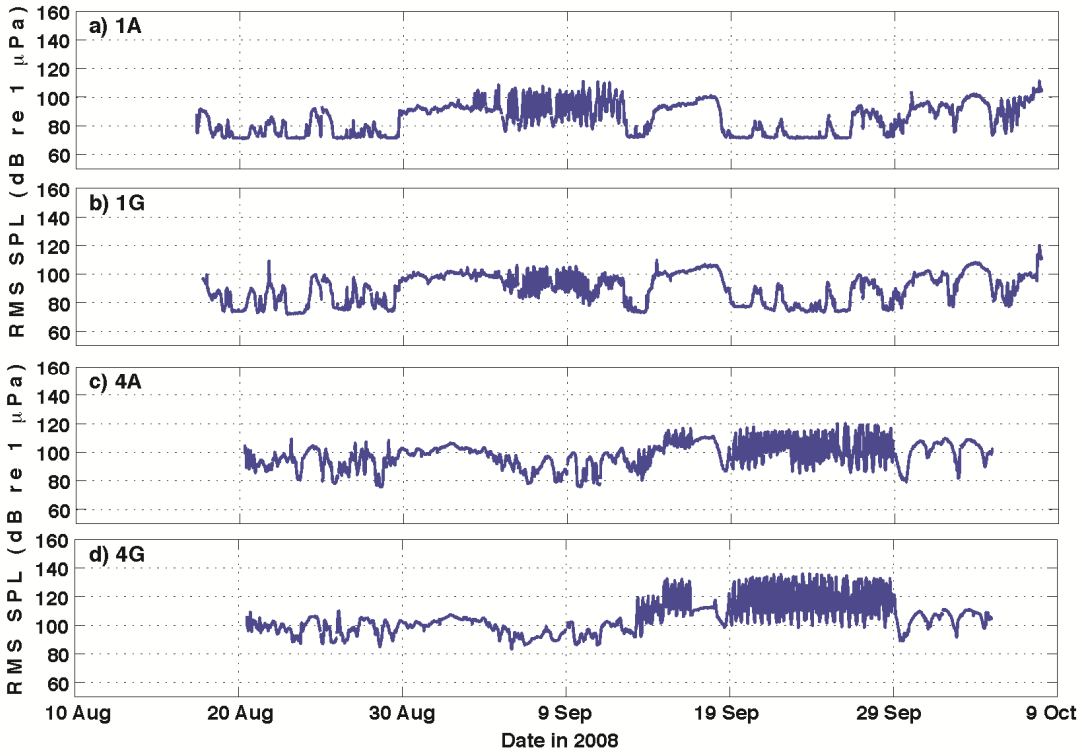

Figure 2-3: Broadband (10-450 Hz) MLM (in SPL units) at the shallowest and deepest locations of Sites 1 and 4, computed for the entire duration of deployment, using a 30 minute long-term window: (a) DASAR 1A; (b) DASAR 1G; (c) DASAR 4A; (d) DASAR 4G. DASAR A locations are the shallowest, DASAR G locations, the deepest.

.

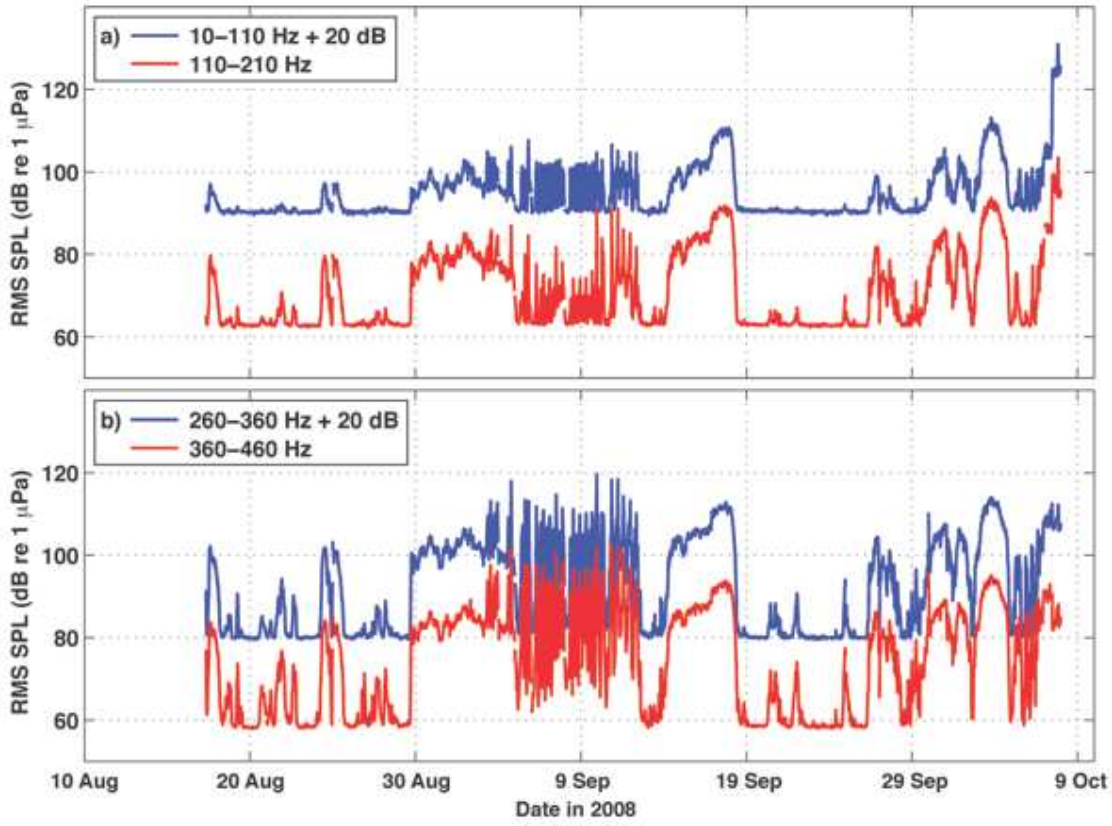

Figure 2-4: 100-Hz narrowband MLM (SPL units) for DASAR 1A, over the same timescale and using the same analysis parameters: (a) 10-110 Hz and 110-210 Hz; (b) 260-360 and 360-460 Hz. Note that a +20 dB offset has been applied to the upper time series.

.

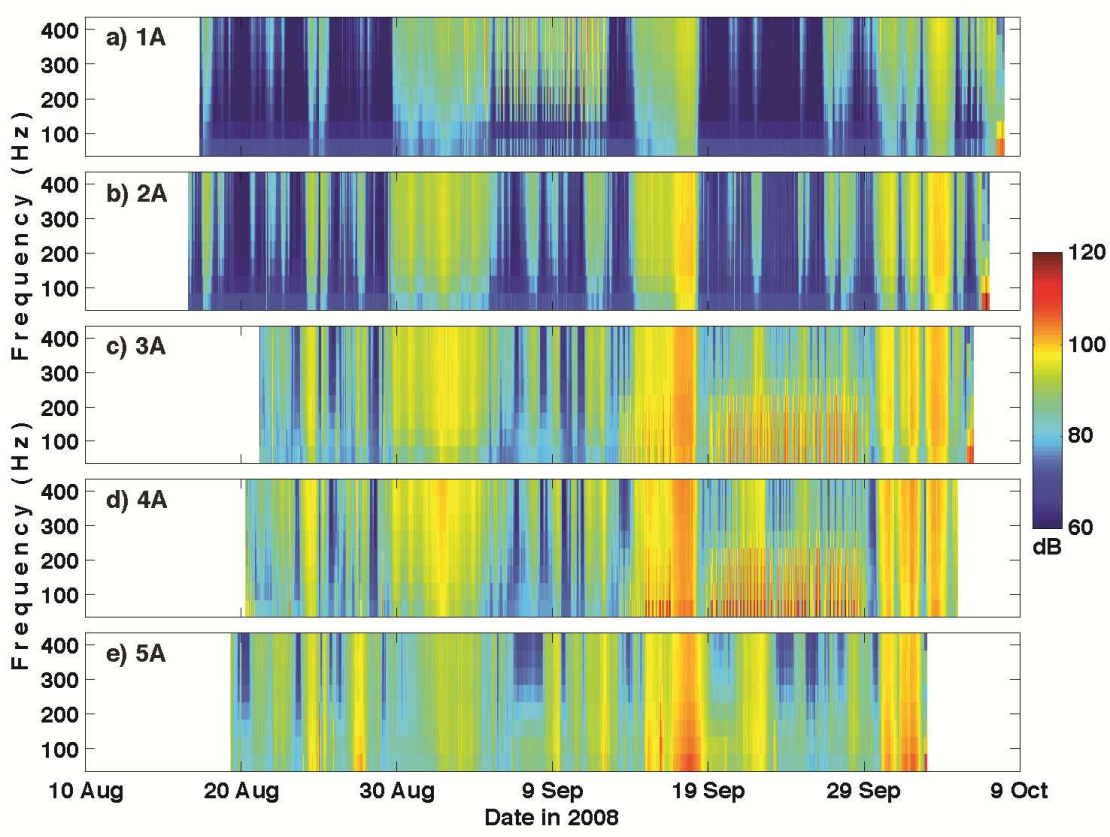

Figure 2-5: MLM (SPL units) as a function of frequency and time at shallowest locations (A DASARs) at all five sites. The metric was computed in eight frequency ranges of 100-Hz bandwidth, overlapping 50% (10-110 Hz, 60-160 Hz, 110-210 Hz, 160-260 Hz, etc.) between 10 and 460 Hz. Other analysis parameters remain the same as Figures 2-3 and 2-4.

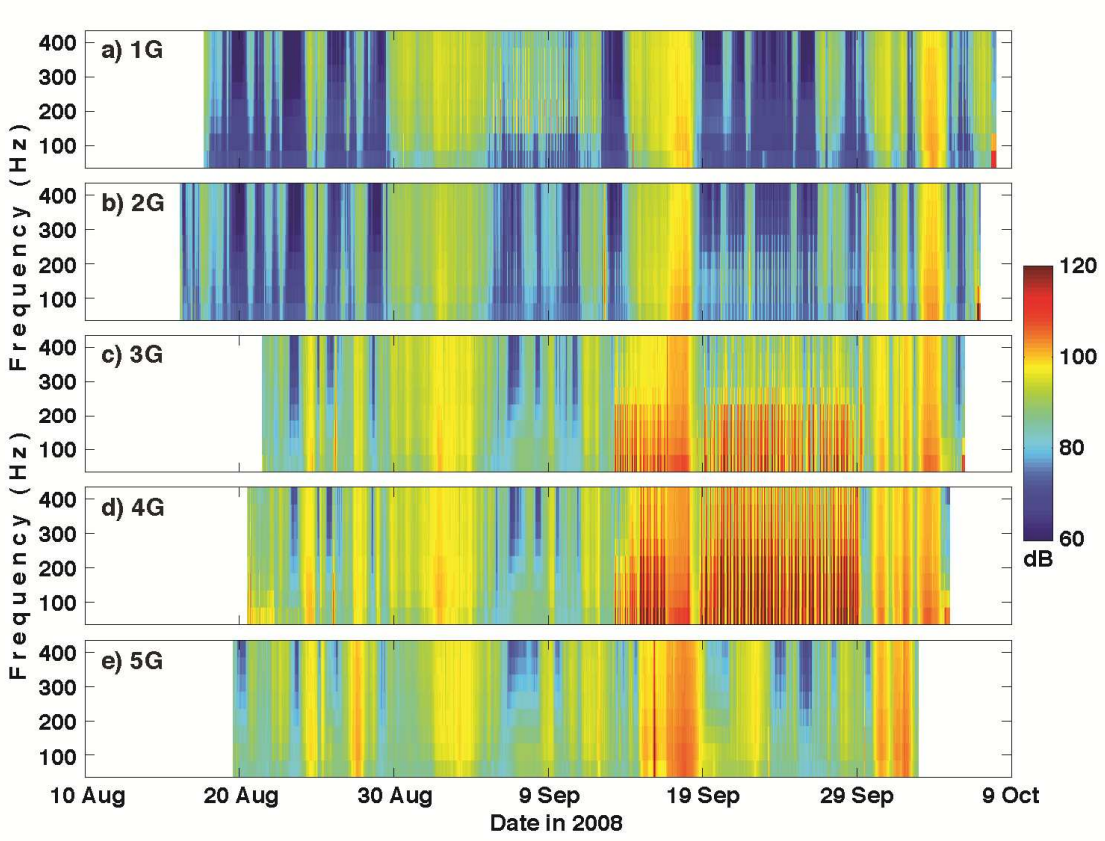

Figure 2-6: MLM (SPL units) as a function of frequency and time at deepest locations (G DASARs) at all five sites. Analysis parameters are identical to those in Figure 2-5.

Two one-week periods of particularly intense seismic airgun survey activity are emphasized in Figures 2-7 and 2-8, which simply expand the time scales of Figures 2-5 and 2-6. Figure 2-7 shows the MLM during the week of September6th-14th, when the survey operated at Site 1, while Figure 2-8 shows the corresponding levels between September 20th and 28th, when the survey operated between Sites 3 and 4. Generally, when the seismic airgun survey occurred between September 3rd and 12th in close proximity to Site 1, MLM levels were more intense at the shallower DASARs, when compared to the deeper DASARs (Figure 2-7). The opposite is true

when the seismic airgun survey operated between Sites 3 and 4: received levels of the MLM were higher at the deeper DASARs compared to the shallower DASARs (Figure 2-8).

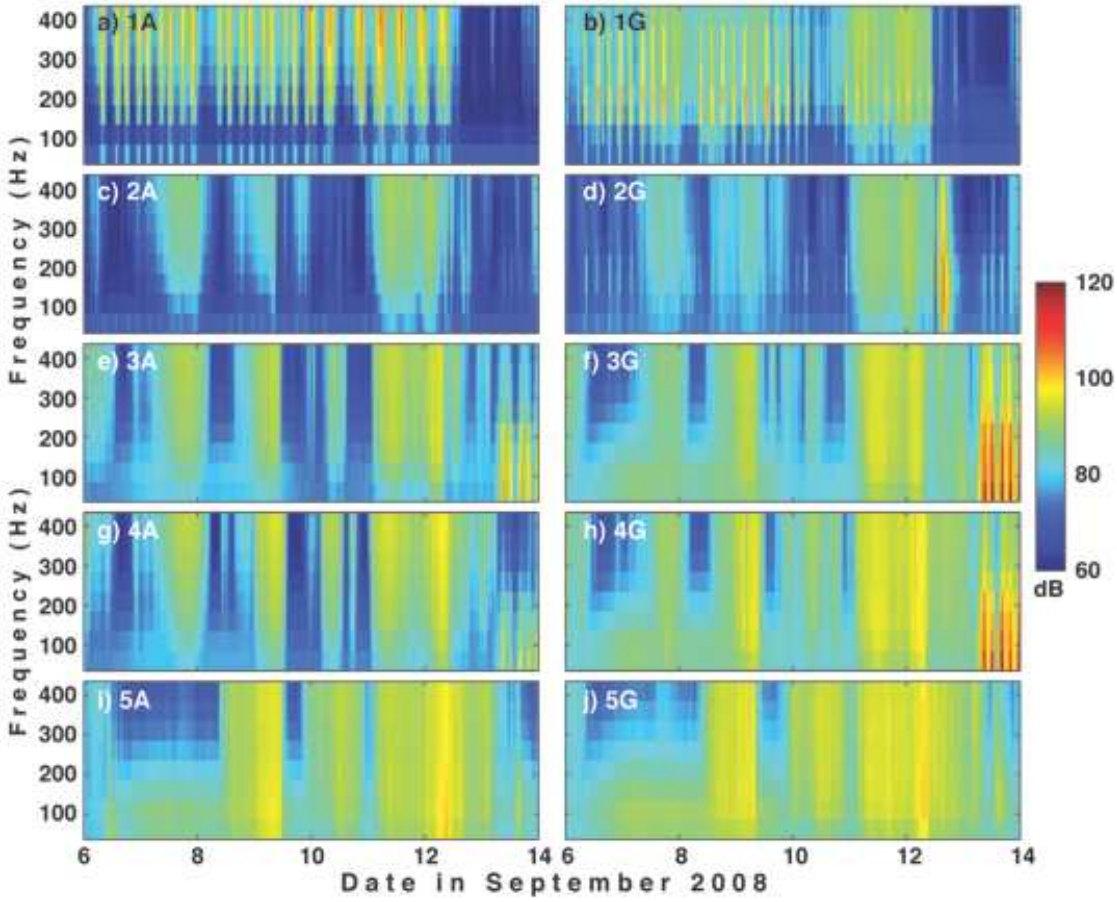

Figure 2-7: Expanded views of Figures 2-5 and 2-6, covering seismic airgun activities between September 6th-14th. The left column plots the MLM (SPL units) of the shallowest DASAR at each site (A); the right column plots the metric for the deepest DASAR at each site (G). The rows correspond to the different sites and follow the format of Figure 2-5.

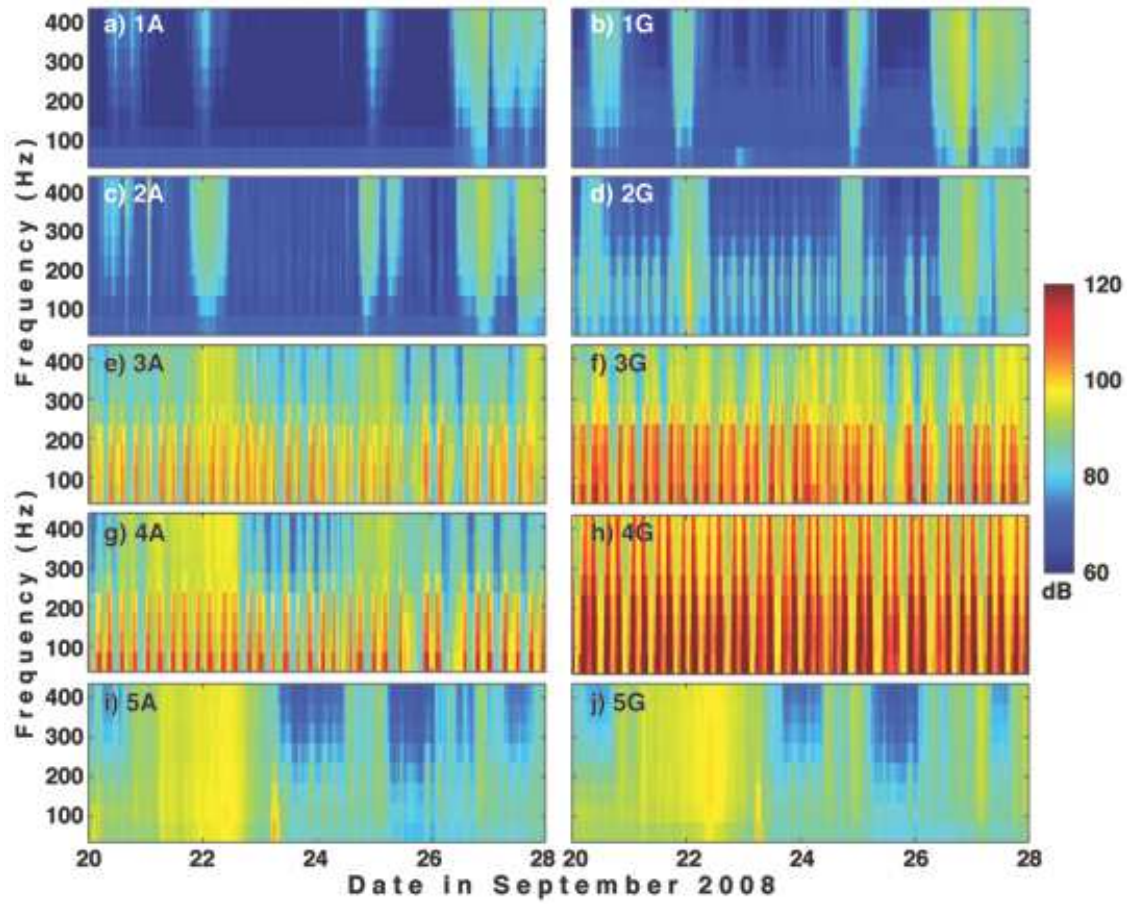

Figure 2-8: Expanded views of Figures 2-5 and 2-6, covering seismic airgun activities between September 20th-28th during peak seismic airgun activity in close proximity to Sites 3 and 4. The left column plots the MLM (SPL units) of the shallowest DASAR at each site (A); the right column plots the metric for the deepest DASAR at each site (G). The rows correspond to the different sites and follow the same order as the rows of Figure 2-5.

.

C. Reverberation metric (RM) estimates

As mentioned in the Data Description (Section II), the RM for this location is estimated by first empirically modeling the ambient noise using remotely-sensed wind speeds [e.g. Figure 2.7 in (Blackwell *et al.*, 2006)].

Figure 2-9 illustrates the process for one particular frequency band using DASAR 2A, the shallowest DASAR (21 m depth) at Site 2. Figure 2-9(a) plots the 6-hour average of the MLM time series, calculated over the frequency band 60-160 Hz. Figure 2-9(b) plots the 6-hour average of wind speed (in m/s) obtained from the Sea Winds database, using a 0.5º x 0.5º area (four closest grid-point values averaged together) around the coordinates of 2A. The times between September 3rd and 12th in the time series correspond to periods when seismic airgun activity is occurring, so these periods are excluded from the correlation. The correlation coefficient between the MLM and wind speed are illustrated by the graphical matrix in Figure 2-9(c) as a function of frequency band and time offset between the wind and noise data. This matrix was used to determine the optimal time offset to apply to the regression model, which was +6 hrs, since at that time delay, the correlation coefficient is greatest for all frequency bands. Between 60 and 160 Hz the wind speed and MLM are highly correlated ($R^2_{correlation}$ =0.8621) with a 6-hr time lag. Figure 2-9(c) shows that this correlation diminishes slightly at higher frequency ranges (i.e. $R^2_{correlation}$ =0.7880 at 360-460 Hz). Figure 2-9(d) plots the MLM between 60 and 160 Hz vs. wind speed at the best time offset of +6 hrs, or where the MLM is advanced 6 hours with respect to the wind times. This regression is re-computed for a total of eight 100-Hz frequency bands between 10 and 460 Hz.

Visual inspections of all the correlation plots across the DASARs suggested natural break points for three separate linear regressions that could be applied over three distinct regimes of wind speed: winds under 5 m/s [B_1], winds between 5-10 m/s

[B_2] and winds exceeding 10 m/s [B_3]. Figure 2-9(d) shows the optimal linear regressions, although the third regression may not be valid as the number of data points available is small. A standardized Student's T test (Zar, 1984) was performed to establish the probability that such a fit would occur from a cloud of uncorrelated points. The resulting P values obtained from Figure 2-9(d) are on the order of 8.8e-05, reflecting the low likelihood that the two variables are uncorrelated.

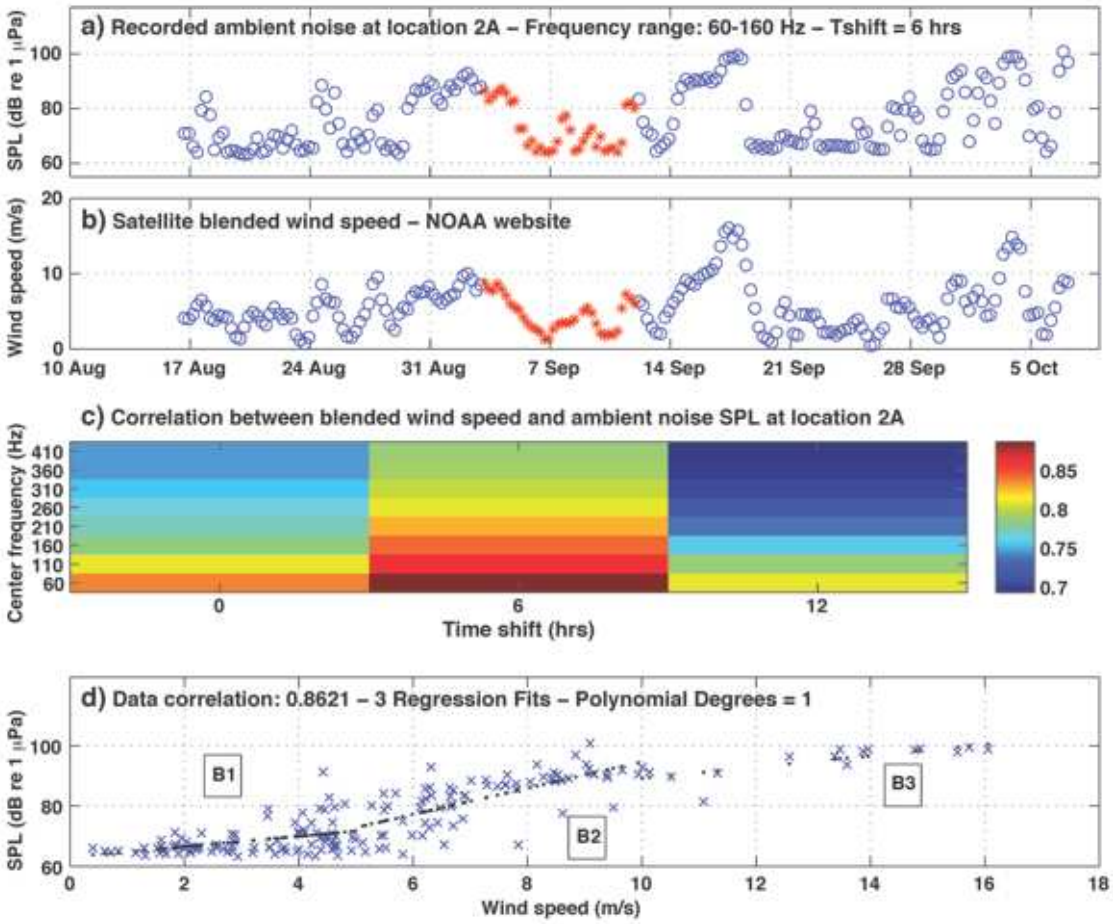

Figure 2-9: Relationship between MLM and wind speed dataset: (a) MLM for DASAR 2A at 60-160 Hz, averaged over 6-hr intervals; (b) Blended wind speed time series in m/s, which consist of 6-hr averages of wind speed around a 0.5 x 0.5 deg grid surrounding the DASAR; (c) Correlation coefficient between MLM (at DASAR 2A) and wind speed at different time delays and frequency ranges; (d) Three linear regression fits between reverberation and wind. Corresponding slopes in dB/(m/s): $B_1 = 63.046 \pm 1.708$; $B_2 = 51.006 \pm 4.363$; $B_3 = 70.405 \pm 1.878$. Corresponding regression Student's test P-values: $P_1 = 1.9707e\text{-}05$; $P_2 = 1.2187e\text{-}10$; $P_3 = 2.4536e\text{-}04$.

Figure 2-10(a) plots the two-dimensional MLM at DASAR 2A [Figure 2-5(b)]. Figure 2-10(b) presents the modeled noise levels derived from applying the regression equations performed at each one of the eight frequency bands, like the one illustrated in Figure 2-9(d), to the wind record in Figure 2-9(b). In effect, remotely-sensed satellite data have been used to predict the temporal and spectral levels of the MLM [Figure 2-10(b)]. The results of subtracting in dB-space (effectively, dividing) these modeled ambient noise levels from the MLM [Figure 2-10(a)] creates Figure 2-10(c), the RM, with units of dB SNR. Over this time period there was no detectable seismic airgun activity, so ideally, if wind alone explained ambient noise levels, the value of the metric should be 0 dB across all times and frequency ranges. The scatter of the points around the linear fit in Figure 2-9(d), however, ensures that the RM will be nonzero even at times of no activity. The distribution of these non-zero fluctuations does not display a regular temporal pattern.

Finally, Figure 2-11 shows the RM estimates for the same locations and time intervals shown in Figure 2-8, computed for the shallowest and deepest DASAR at each of the five sites. The time scale covers September 20th-28th, 2008, a time of heavy seismic airgun survey activity occurring close to Sites 3 and 4. The seismic airgun survey leaves distinctive, temporally regular signatures at DASARs in close proximity to the seismic airgun activity [e.g., Figure 2-11(f) and 2-11(h)]. Figure 2-11 demonstrates the efficacy of the RM in quantifying the effects of seismic airgun reverberation on background noise in a shallow-water environment.

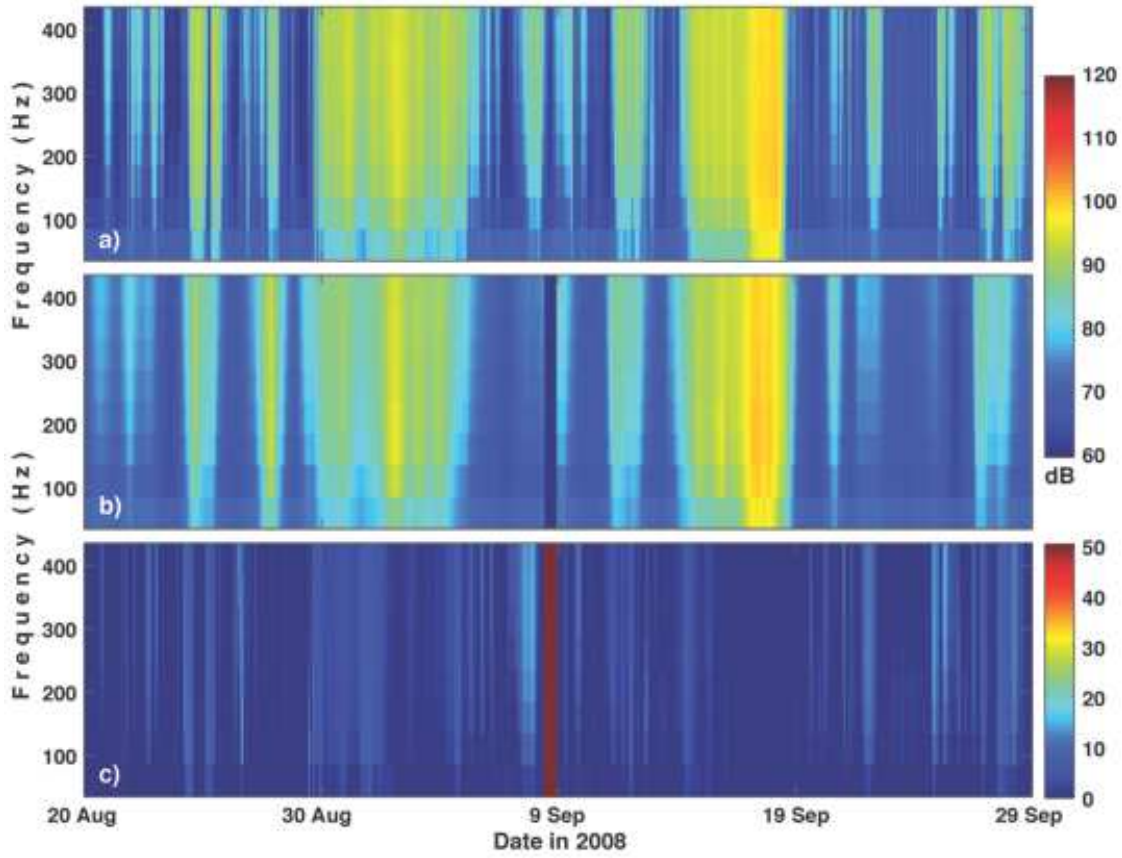

Figure 2-10: Example of reverberation metric (RM): (a) Time-frequency MLM for DASAR 2A; (b) Time-frequency model of underwater wind noise from satellite observation data; (c) RM (ratio of measured to modeled MLM, or difference in dB). All units are shown in terms of dB intensity ratios. The red band represents times when satellite wind data are unavailable.

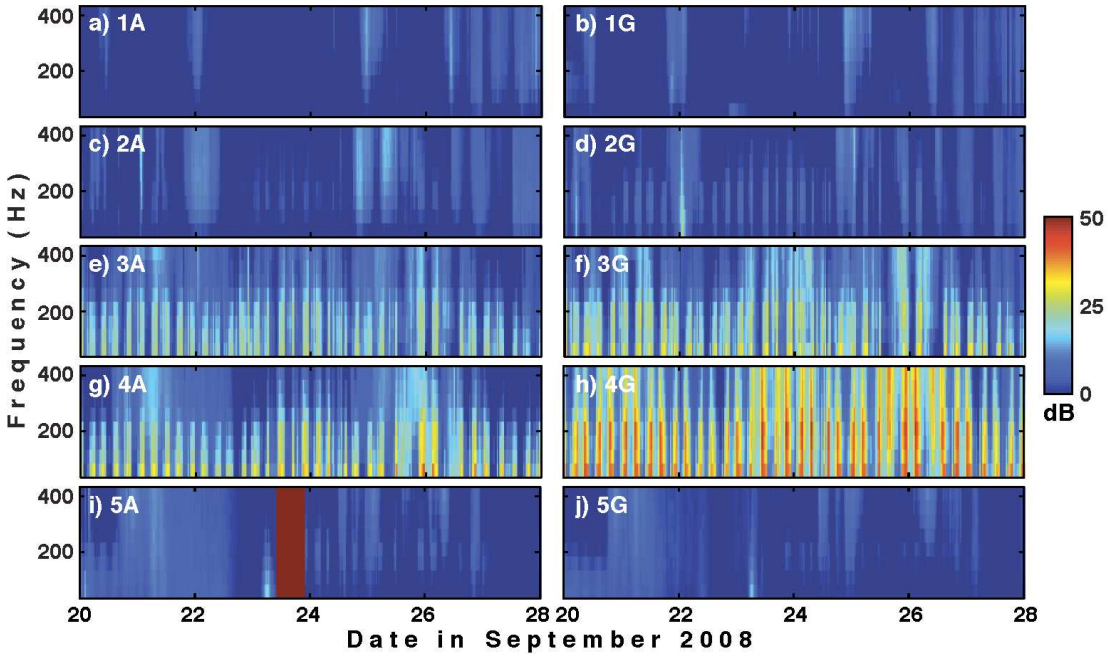

Figure 2-11: Expanded views of the RM covering seismic airgun activities between September 20th-28th. The left column plots the RM of the shallowest DASAR at each site and the right column plots the same metric for the deepest DASAR at each site. The rows correspond to different sites, and follow the same order as the rows of Figures 2-7 and 2-8. Compare with Figure 2-8, which shows the associated MLM.

V. DISCUSSION

A. Minimum level metric (MLM) observations

The broadband MLM values in Figure 2-3 indicate that the seismic airgun surveys generated sustained broadband changes in background noise levels while the survey took place. Two periods of substantial seismic airgun activity can be identified at Sites 1 and 4 from the temporal pattern alone. In general, for DASARs within 10

km of the seismic airgun activities, the highest MLM values generated by the reverberation matched or exceeded the MLM values attained during periods when seismic activity was absent. As expected, reverberation effects are greatest at DASARs closest to the activities; the shallowest DASAR at Site 1 [Figure 2-3(a)] and the deepest DASAR at Site 4 [Figure 2-3(d)].

Figures 2-5 through 2-8, which present the frequency and time dependence of the MLM at all five sites, reinforce these observations. Reverberation effects from airgun shots are again clearly recognizable, due to the 'comb-like' pattern apparent in the MLM, which occurs because the seismic vessel rasters away and towards the recorder. For example, Figures 2-8(f) and 2-8(h), centered on September 24th, demonstrate that MLM levels are high at Site 4 when they are low at Site 3, coinciding with the vessel traveling from Site 3 towards Site 4, and vice versa. Wind-driven changes in the MLM arising from changes in the ambient noise are seen to occur over longer time scales and over wider geographic areas, being recorded at multiple DASARs (e.g. the surge in ambient noise on September 9th in Figure 2-7).

Airgun shots fired between Sites 3 and 4, occurring between September 20th and 28th, produced the overall highest reverberation detected throughout the two-month period [Figures 2-6(c), 2-6(d) and 2-8(f) and 2-8(h)]. Reverberation from this airgun activity can be observed on Site 4, Site 3 (up to 85 km away), and even at Site 5 (93 km away) and Site 2 (128 km away). The earlier seismic airgun survey between September 3rd and 12th had much weaker impacts on background noise levels beyond Site 1, only influencing the deeper waters of Site 2 (62 km away).Just as changes in

water depth and/or bottom composition generate different reverberation effects (Figure 2-2), these factors might also explain why reverberation decreases more rapidly with range at Site 1, the shallowest of all the sites. As seen in Figure 2-2(b), reverberation effects generated by the survey at Site 1 had higher frequency content, relative to the later survey between Sites 3 and 4 [Figure 2-2(c)]. Since higher frequencies experience relatively greater propagation loss with range at shallow water depths between 25 and 50 m, it is not surprising that the reverberation effects from the Site 1 survey decay much more quickly with range than the later surveys. It remains puzzling why Site 5 is little affected by reverberation from the Site 3/Site 4 survey [Figs. 2-8(j) and 2-11(j)], compared with Site 2 [Figs. 2-8(d) and 2-11(d)].

B. Wind driven ambient noise and the reverberation metric RM

Figure 2-9 illustrates the strong relationship between wind speed [Figure 2-9(b)] and the MLM at DASAR 2A [Figure 2-9(a)], which was distant to most seismic airgun activities. While Figures 2-9(a) and 2-9(d) only show this relationship over a particular frequency band (60-160 Hz), Figure 2-9(c) demonstrates that a correlation exists at all frequencies between 10 and 460 Hz, although the quality of the reverberation-wind correlation coefficient degrades with increasing frequency. The reverberation measurement times must be delayed 6 hours with respect to the wind times to achieve the best correlation. These conclusions were verified by repeating the analysis using hourly wind data measurements from the Prudhoe Bay land-based weather station shown in Figure 2-1. That analysis also found a high correlation

between the MLM and wind speed and required a relative time delay of seven hours to maximize the correlation. The implication of these time shifts is that it takes ocean ambient noise levels about 6-7 hours to respond to a change in wind speed.

A 6-hr time shift was selected for regression analysis between the MLM and database wind speeds, and Figure 2-9(d) shows an example of the set of linear regressions at one of the eight frequency ranges (60-160 Hz). Once all regression equations were computed for the corresponding eight frequency bands at every DASAR, all of them at a delay of 6 hrs, the MLM across all DASARs was modeled using the appropriate local wind time series. Figure 2-10(b) shows how the piecewise linear regressions capture much of the variability in the natural fluctuations of the MLM at Site 2A [Figure 2-10(a)], and thus the difference between the recorded and modeled MLM (i.e. the RM) suppresses large-scale natural ambient noise fluctuations [Figure 2-10(c)]. Occasionally, short periods exist when local wind data were not available. These data 'dropouts' result in blank regions, as occurs on September 9th in Figures 2-10(b-c). The fact that wind is the most significant contributor to ambient noise levels below 500 Hz is unusual; in most oceans, distant shipping noise dominates this band (Wenz, 1962). The absence of shipping noise in the low-frequency band of the Arctic acoustic environment may currently represent the closest oceanic scenario to pre-industrial ambient noise conditions.

When the RM is computed at all sites (Figure 2-11), using specific regressions computed at each DASAR with satellite-derived wind speeds, the relative changes in the ambient noise levels due to patterns of airgun reverberation become clearly visible,

e.g. at Sites 2, 3 and 4, particularly in the deepest (northern) DASARs, at depths between 30 and 50 m [Figure 2-11(d), (f), and (h)]. Thus, seismic airgun reverberation can produce measureable effects at distances of up to 128 km. Specifically, Figure 2-11 indicates that at water depths of 50 m or less, seismic airgun activity within 1 km of a DASAR can increase noise levels by 30-45 dB over ambient levels (deep DASARs at Sites 3 and 4), by 10-25 dB within 15 km range of the survey (shallow DASARs at Sites 3 and 4), and by a few dB at ranges out to 128 km (Site 2).

VI. CONCLUSION

Two metrics have been defined for characterizing reverberation from seismic airgun surveys in shallow water, which can complement standard metrics that focus on the coherent airgun pulse arrivals, such as the SPL and SEL. The minimum level metric (MLM) captures the minimum background sound level detected over a fixed time window, thus allowing it to capture long-term changes in background noise that arise *between* airgun pulses, while rejecting effects from dispersed modal and substrate transient arrivals. To compute the MLM three time-scale parameters were selected: a time over which to generate a single estimate of SE or SP, a time over which it is permissible to average sequential SE or SP estimates to reduce their variance, and a time over which the minimum value is selected. The MLM was applied to airgun signals recorded between 15 and 54 m depth in the Arctic Beaufort

Sea in 2008. The resulting MLM shows that the spectral composition of reverberation is heavily dependent on receiving location, particularly water depth.

A second dimensionless metric, the reverberation metric (RM), can be derived from the MLM in various ways; in the results presented here, wind measurements were found to be highly correlated with the MLM over most frequency bands in the absence of seismic airgun activity. Thus the ambient noise field was empirically modeled from satellite-derived wind speed estimates, and the dB levels of the models were subtracted from the MLM, yielding the RM. A RM of 0 dB would indicate that anthropogenic contributions to background levels are less than or equal to ambient contributions from other mechanisms. The RM indicates that the Gilavar shallow-water seismic airgun survey that took place between September 13th and 28th increased background noise levels by 30-45 dB over ambient levels within 1 km range of the survey, by 10-25 dB within 15 km range of the survey, and produced detectable modifications to background noise levels out to 128 km.

These results suggest that the range at which towed arrays or other PAM techniques would be effective for detecting the presence of marine mammal vocalizations within a few km of shallow-water seismic airgun surveys would be significantly reduced. This is because there is no time period between airgun shots when reverberation does not mask one's ability to detect and recognize calls. The results here also suggest a potential for intra-specific communication masking, as defined in Clark *et al.* (2009), as a result of seismic airgun array activities.

These metrics provide a conservative, lower bound on reverberation levels, because reverberations that do not persist over the entire period between airgun shots are not included in the two metrics presented here. Eqs. (4) and (5) could be expanded to select not just minimum levels detected, but 25% and 50% percentile levels extracted from histograms of SEL and SPL derived from Eq. (3). This approach would permit detection and characterization of reverberation that exists for only a portion of time between impulses.

While percentile levels would add additional information about reverberation effects, the MLM defined here is convenient to compute, easy to understand and makes minimal biological assumptions about a particular species. Furthermore it could easily be incorporated into standard source level verification measurements of seismic airgun and other impulsive anthropogenic activities in shallow water. By these considerations, the potential communication masking effects of seismic airgun surveys on particular species of interest could be quantified. The inclusion of these metrics in monitoring and mitigation reports would also provide regulators with valuable insight into the expected efficacy of PAM and guide management strategies as relative to seismic surveys according to site-specific features of the environment.

VII. ACKNOWLEDGEMENTS

Chapter 2, in full is a reprint of material as it appears in the Journal of the Acoustical Society of America, 2011. Guerra, Melania; Thode, Aaron M; Blackwell, Susanna B.; Macrander, A. Michael. “Quantifying seismic survey reverberation off the

Alaskan North Slope.”, Volume 130, Issue 5, pp.3046-3058, 2011. The dissertation author was the primary investigator and author of this paper.

This work was supported by Shell Exploration and Production Company (SEPCO) and Greeneridge Sciences Inc (GSI). The second author received support from the North Pacific Research Board (NPRB). We are grateful to Charles R. Greene of GSI, for making this acoustic dataset available for analysis and for valuable suggestions on the manuscript. We thank Delphine Mathias and the entire crew of the R/V Norseman II for their help in the field collecting data. We also thank Chris Nations of WEST for informing us of the existence of the Blended Wind Data Set. We thank Bruce Martin of JASCO and Ann E. Bowles of HSWRI for helpful and thoughtful comments on the manuscript.

VIII. REFERENCES

Barger, J. E., and Hamblen, W. R. (**1980**). "The air gun impulsive underwater transducer," Journal of the Acoustical Society of America **68**, 1038-1045.

Blackwell, S. B., Norman, R. G., Greene, C. R., McLennan, M. W., and Richardson, W. J. (**2006**). "Acoustic monitoring of bowhead whale migration, autumn 2005," in *Monitoring of industrial sounds, seals, and bowhead whales near BP's Northstar oil development, Alaskan Beaufort Sea, 2005: Annual summary report*, edited by W. J. Richardson (LGL Ltd., King City, Ont.).

Clark, C. W., Ellison, W. T., Southall, B. L., Hatch, L., Van Parijs, S. M., Frankel, A., and Ponirakis, D. (**2009**). "Acoustic masking in marine ecosystems: intuitions, analysis, and implication," Marine Ecology-Progress Series **395**, 201-222.

Clark, C. W., and Johnson, J. H. (**1984**). "The sounds of the bowhead whale, balaena-mysticetus, during the Spring migrations of 1979 and 1980," Canadian Journal of Zoology-Revue Canadienne De Zoologie **62**, 1436-1441.

D'Spain, G. L., Hodgkiss, W. S., and Edmonds, G. L. (**1991**). "The simultaneous measurement of infrasonic acoustic particle-velocity and acoustic pressure in the ocean by freely drifting swallow floats, " IEEE Journal of Oceanic Engineering **16**, 195-207.

Di Iorio, L., and Clark, C. W. (**2009**). "Exposure to seismic survey alters blue whale acoustic communication," Biology Letters **6**, 51-54.

Frisk, G. (**1994**). *Ocean and Seabed Acoustics: A theory of wave propagation*, (PTR Prentice Hall, Englewood Cliffs, New Jersey), pp. 89-172.

Greene, C. R., McLennan, M. W., Norman, R. G., McDonald, T. L., Jakubczak, R. S., and Richardson, W. J. (**2004**). "Directional frequency and recording (DIFAR) sensors in seafloor recorders to locate calling bowhead whales during their fall migration," Journal of the Acoustical Society of America **116**, 799-813.

Greene, C. R., and Richardson, W. J. (**1988**). "Characteristics of marine seismic survey sounds in the Beaufort sea," Journal of the Acoustical Society of America **83**, 2246-2254.

Ireland, D. S., Funk, D. W., Rodrigues, R., and Koski, W. R. (**2009**). "Joint Monitoring Program in the Chukchi and Beaufort seas, open water season, 2006-2007" in *LGL Alaska Report P971-2* (LGL Ltd, Environmental Research Associates, King City, Ont., JASCO Research Ltd., Victoria, BC, and Greeneridge Sciences, Inc., Santa Barbara, CA, for Shell Offshore, Inc. Anchorage, AK, ConocoPhillips Alaska, Inc., Anchorage, AK, and the National Marine Fisheries Service, Silver Springs, MD, and the U.S. Fish and Wildlife Service, Anchorage, AK., Anchorage. AK), p. 485 p. plus Appendices.

Kastak, D., Southall, B. L., Schusterman, R. J., and Kastak, C. R. (**2005**). "Underwater temporary threshold shift in pinnipeds: Effects of noise level and duration," Journal of the Acoustical Society of America **118**, 3154-3163.

Ljungblad, D. K., Leatherwood, S., and Dahlheim, M. E. (**1980**). "Sounds recorded in the presence of an adult and calf bowhead whale," Marine Fisheries Review **42**, 86-87.

Madsen, P. T. (**2005**). "Marine mammals and noise: Problems with root mean square sound pressure levels for transients," Journal of the Acoustical Society of America **117**, 3952-3957.

Oppenheim, A. V., Schafer, Ronald W., Buck, John R. (**1975**). *Digital signal processing.* (Prentice Hall, Englewood Cliffs, New Jersey), pp. 548–554.

Richardson, W. J., Würsig, B., and Greene, C. R. (**1986**). "Reactions of bowhead whales, *Balaena mysticetus*, to seismic exploration in the Canadian Beaufort sea," Journal of the Acoustical Society of America **79**, 1117-1128.

Southall, B. L., Bowles, A. E., Ellison, W. T., Finneran, J. J., Gentry, R. L., Greene, C. R., Jr., Kastak, D., Ketten, D. R., Miller, J. H., Nachtigall, P. E., Richardson, W. J., Thomas, J. A., and Tyack, P. L. (**2007**). "Marine mammal noise exposure criteria: Initial scientific recommendations," Aquatic Mammals **33**, 1-521.

Urick, R. J. (**1983**). *Principles of Underwater Sound.* (McGraw-Hill, New York), pp. 1-423.

Wenz, G. M. (**1962**). "Acoustic ambient noise in the ocean: spectra and sources," Journal of the Acoustical Society of America **334**, 1936-1956.

Yost, W.A. (**1994**). *Fundamentals of hearing: An introduction.* (Academic Press, San Diego), pp. 1-326.

Young, I. M., and Wenner, C. (**1970**). "Two distinct loudness functions of the ear," in *79th meeting of the Acoustical Society of America* (Acoustical Society of America, Atlantic City, NJ,), pp. 7.

Zar, J. H. (**1984**). *Biostatistical analysis*. (2nd Ed. Prentice-Hall, Engelwood Cliffs, New Jersey), pp. 97-121.

Zhang, H. M., Bates, J. J., and Reynolds, R. W. (**2006**). "Assessment of composite global sampling: Sea surface wind speed," Geophysical Research Letters **33**, L17714

CHAPTER 3:

Using ocean ambient noise to time-synchronize independent elements of a horizontal acoustic array

ABSTRACT

Due to concerns for potential impacts of anthropogenic noise on marine mammals, regulatory policies limit the application of active low-frequency sources ("pingers") in close proximity to these animals. Such devices are commonly used to time-synchronize independent sensors with the purpose of employing them collectively as a network or an array. This chapter explores the use of underwater ambient sound to time synchronize underwater recorders separated by 10 and 20 m, in an environment with strong tidal fluctuations, highly directional biological noise components and a highly variable bathymetry in azimuth and range. Two three-element passive acoustic horizontal arrays were deployed in Laguna San Ignacio, Mexico, during February and March 2010, in order to record gray whale (*Eschrichtius robustus*) sounds and ambient noise. Each array consisted of autonomous recorders separated by 10 or 20m. In the 0.05-5 kHz frequency band this underwater acoustic environment contains multiple directional anthropogenic sources (passing boats) and numerous biological sources (snapping shrimp and croaker fish). The relative clock offset and horizontal separation between the recorders was estimated by averaging pre-whitened cross correlations of ambient noise over 30 minute intervals and then selecting times of day where directional noise was relatively absent. At 10 m separation frequency components up to 1.4 kHz contained enough spatial coherence to contribute to the timing estimate. The relative clock drift between the instruments was obtained by repeating the process exactly 24 hours later; the resolution of the resulting

drift estimates was within 1 ms/day. The results are compared against offset and drift estimates derived from boat transits equipped with GPS devices.

I. INTRODUCTION

Considering the background established in Chapters 1 and 2 about how routine anthropogenic noise sources in the ocean have become and the consequent concerns for potential impacts on marine mammals, it is understood that passive acoustic monitoring (PAM) technologies that enable the detection and localization of those animals are a critical component of the required mitigation efforts (Funk et. al., 2009; Ireland et. al., 2009). In addition, PAM recorders can collect critical information about the local underwater sound field. This is especially true in shallow water environments, as the propagating sound wave can reflect multiple times between the surface and the bottom before reaching the PAM receiver. By exploiting that environmental knowledge (specifically the directionality of ambient noise source mechanisms), this chapter demonstrates a method that enables autonomous PAM sensors to be used as a synchronized array.

Currently, a wide variety of techniques exist for estimating a marine mammal's position via PAM (e.g. Sonntag *et al*., 1986; Cato, 1998). These methods vary from one-dimensional tracking methods (e.g. towed array beamforming), to two- and three-dimensional methods that include hyperbolic localization using measurements of relative time of arrival differences (TOAD), triangulation of bearings from widely-

spaced sensors (Greene *et al*., 2004) and matched field processing (MFP; Greene, 1987; Thode *et al*., 2000; Tiemann and Porter, 2003;Nosal and Frazer, 2007). All these techniques, however, share a common assumption that acoustic data collected from different spatial locations are properly time-aligned, which has often required that the sensors be connected via electric cable to a single central data acquisition system.

Arrays assembled from autonomous recording packages offer distinct advantages over cabled systems, including freedom of configuration and manageable in-situ portability (Wiggins, 2003; Greene *et al*., 2004; Thode *et al*., 2006). The corresponding disadvantage is that the recorders have independent crystal oscillators that generate slightly different timing frequencies and these frequencies are sensitive to ambient temperature. Any two autonomous recorders will thus experience a clock drift relative to each other and relative to an "absolute" time standard broadcast by GPS satellites. Hence, a challenge when using arrays constructed with autonomous sensors is their time-synchronization and this challenge is compounded when the relative positions of the underwater instruments cannot be determined precisely.

The standard approach for time-synchronization when utilizing autonomous recorders for underwater acoustic applications has relied on controlled transmissions (harmonic tones and frequency-modulated sweeps) (Greene *et al.*, 2004) or distinctive sources of opportunity located at known positions around the instruments (Hodgkiss *et al.*, 2003). If these measurements are repeated at large enough time intervals and the relative clock drift between the instruments is assumed linear with time, then the clock

offset τ_0 and drift $d\tau_d/dt$ can be estimated. This assumption of linear drift presumes that both instruments encounter the same water temperature during the entire period of data acquisition.

This chapter examines the practicality of using ambient noise to estimate the relative clock offset and relative clock drift between two autonomous sensors spaced tens of meters apart on the ocean floor, by computing the time-averaged noise correlation function (NCF) between the sensors (Sabra *et al.*, 2005a; Sabra *et al.*,2005c). Examples of potential noise sources in the environment include wind generated noise, croaker fish (Sciaenidae), gray whales (*Eschrichtius robustus)* and snapping shrimp (*Alpheus heterochaelis*) sounds. The peaks in the NCF yield information about the relative clock offset, clock drift and the physical separation between the sensors. These timing estimates are compared with estimates obtained from a transient discrete sound source, in this case transiting motorboats. In principle if a discrete, directional sound source can be used to determine the orientation of a two-element array on the ocean floor, the final synchronized array can be used to localize and track an arbitrary acoustic source.

Section II reviews time-synchronization concepts for acoustic datasets and defines symbols for clock offset (τ_0) and clock drift ($d\tau_d/dt$). Section III describes the acoustic data used in this study, collected in a sheltered lagoon in Mexico. Section IV details the analysis procedures for estimating clock offset and clock drift from both directional and diffuse noise sources. Results are presented in Section V.

II. BACKGROUND AND THEORY

A large body of previous research has demonstrated, theoretically and experimentally, that an estimate of the time-domain Green´s function (TDGF) between two sensors can be extracted by performing a cross correlation of ambient noise detected by the sensors. Roughly speaking, the TDGF represents the acoustic field received at one sensor when excited by an impulse at a second sensor. This principle has been demonstrated with multiple wave phenomena, with applications in geophysics (Shapiro and Campillo, 2004), ultrasound (Weaver and Lobkis, 2004)and underwater acoustics (Roux *et al*., 2004; Sabra *et al*., 2005c). A consistent motivation behind these studies is the desire to conduct geoacoustic inversion or acoustic tomography from the noise data.

Theoretical studies (Lobkis and Weaver, 2001) show that the time-derivative of the ensemble-averaged NCF, $C_{a,b}$, can be expressed as the summation of a forward TDGF G and a time-reversed TDGF -G between two synchronized receivers *a* and *b*, at horizontal locations r_a and r_b respectively:

$$\frac{d\langle C_{a,b}(\tau)\rangle}{d\tau} = -G(r_a, r_b, \tau) + G(r_b, r_a, -\tau) \qquad (1)$$

where τ denotes the relative time lag of the cross-correlation function and $G(r_a,r_b,\tau)$ represents the environment´s TDGF between *a* and *b.* The derivation of this expression assumes an azimuthally-symmetric ambient noise field. The TDGF estimate emerges from random noise events whose signal propagates through both *a*

and *b*, which arises when noise events are collinear with locations *a* and *b*, or "endfire" to the effective two-element array. For receiver positions separated by a few tens of meters in water depths of 10 m depth or deeper, the TDGF is dominated by the direct path arrival between the receivers. If the sensors are separated by a distance *L* and the medium sound speed is *c*, then Eq. (1) reduces to the approximate

$$\frac{d\left\langle C_{a,b}(\tau)\right\rangle}{d\tau} = \delta\left(\tau - \frac{L}{c}\right) + \delta\left(\tau + \frac{L}{c}\right) \tag{2}$$

where δ(0) is some finite value, and δ(x)=0 for x not equal to zero.

If the two independent receivers are not time-synchronized, then at an absolute reference time T_0 a relative clock offset $\tau_o(T_0)$exists between the sensors. As time progresses, the clock drift between the sensors will alter the offset. If the drift rate per unit time $d\tau_d/dt$ is linear, then at a time T_i the new clock offset $\tau_{o,i}$ becomes:

$$\tau_{o,i}(T_i) = \tau_o(T_0) + \frac{d\tau_d}{dt}(T_i - T_0) \tag{3}$$

And Eq. (2) becomes:

$$\frac{d\left\langle C_{a,b}(T_i,\tau)\right\rangle}{d\tau} = \delta\left(\tau - \frac{L}{c} + \tau_{o,i}(T_i)\right) + \delta\left(\tau + \frac{L}{c} + \tau_{o,i}(T_i)\right) \tag{4}$$

Thus, if the NCF yields two prominent peaks, then the element separation *L* and$\tau_0$can be deduced (Sabra *et al*., 2005c). The rate at which these peaks drift over longer timescales then yields the drift rate $d\tau_d/dt$. In principle, even if the ambient noise environment is not azimuthally symmetric, such that the double peak structure implied by Eq. (2) is not visible, the clock drift $d\tau_d/dt$ could still be inferred, provided

that the angular statistical distribution of the noise field remains stationary over the measurement interval of interest.

Figure 3-1 illustrates how to estimate clock offset τ_0 and clock drift $d\tau_d /dt$ from a NCF estimate in the form of Eq. (4), when the recorders are horizontally separated by distance L. The figures schematically show a stacked set of NCF estimates generated over a significant amount of time. The y-axis shows the absolute time of the start of a particular NCF estimate, and the x-axis shows the high-resolution lag time of each estimate. The red lines indicate the location of the two peaks calculated using Eq. (4).This plot format (Figure 3-1) will be used extensively when presenting the results of this chapter.

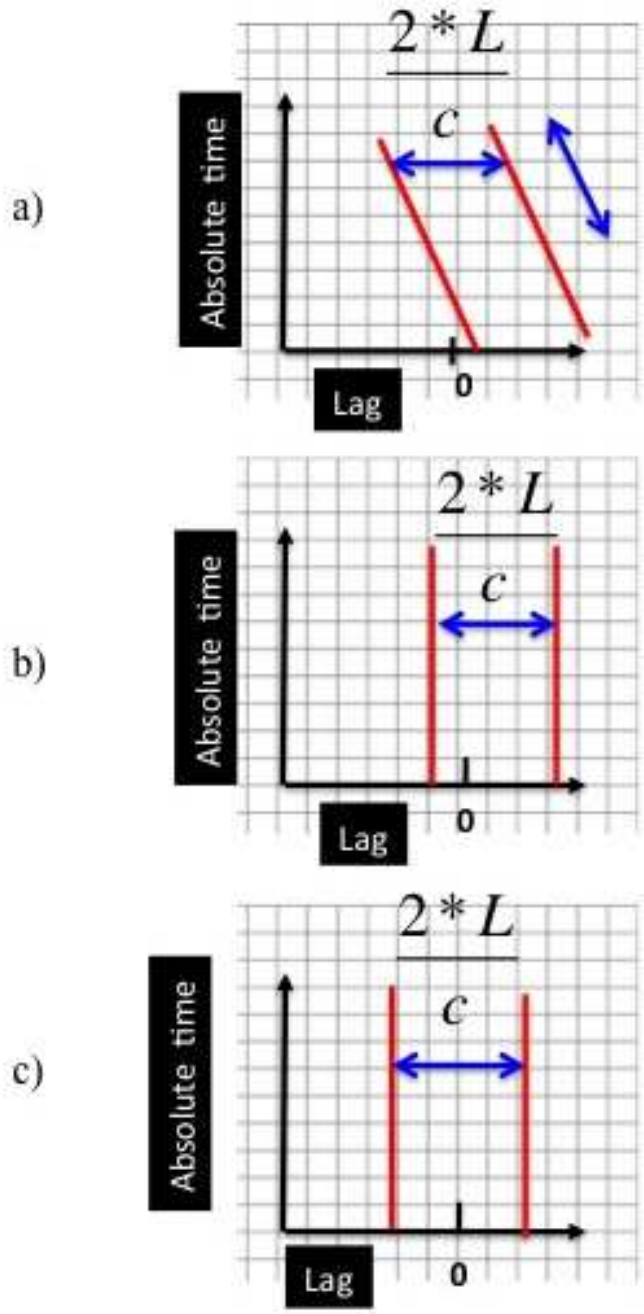

Figure 3-1: Illustration of how to extract clock offset and clock drift from ambient noise: (a) NCF structure from two unsynchronized sensors; (b) NCF structure after incorporating a clock drift estimated from the slope of the drifting peaks in (a); (c) NCF structure after applying a clock offset.

An initial approximation of clock drift $d\tau_d/dt$ can be obtained from the slope of the peak trajectories over time [red lines in Figure 3-1(a)]. An arbitrary "origin" time is chosen on the y-axis where the drift value is assumed zero. Once that clock drift estimate has been incorporated into a new set of cross-correlations, the double-peak structure stops drifting with time, appearing as vertical lines in Figure 3-1(b). If the peaks' lag times are not symmetric with respect to zero lag, then the offset τ_0 correction is simply the time shift with respect to the x-axis that makes the distributions symmetric [Figure 1(c)]. This offset is associated with the "origin" time previously discussed. Finally, the horizontal time-lag difference between the two peaks corresponds to $\tau=2L/c$, and thus the hydrophone separation L can be deduced if the local sound speed c is known.

A fundamental issue that arises when attempting to implement Eqs. (1)-(4) is determining how many averaged data snapshots are needed for the double-peak structure in Eq. (2) to emerge. Theoretical treatments (Sabra *et al.*, 2005b) suggest that the variance of the estimate is inversely proportional to the bandwidth of the signal used in Eq. (1) and the averaging time used to generate $C_{a,b}$. Experimental measurements show that averaging times on the order of 11 to 230 minutes are required in cases of element separations between 28 and 115 m, when biological noise was used to generate the estimates (Fried *et al.*, 2008).

III. DATA COLLECTION

A. Equipment

All acoustic data were collected on custom-built autonomous acoustic recorders that contain a Persistor CF-2 microprocessor powered by a bank of D-cell batteries, confined inside an acrylic cylindrical housing [Figure 3-2(a)]. The instruments continuously record for approximately 40 hours onto a 4 Gb flash-card at a 12.5 kHz sampling rate, after which the data is transferred onto an 80 Gb hard drive. No additional acoustic data are recorded during this two-hour transfer.

The relative clock drifts on these instruments were observed to be around 0.5s per day during previous experiments. HTI-96 MIN hydrophones were used with a typical sensitivity of −165 dB re 1 V/μPa and a frequency response between 2 Hz and 30 kHz.

B. Deployments

Between February 6th and March 4th 2010 two horizontal acoustic arrays of three elements each were deployed to record gray whale sounds and ambient noise in the southern section of Laguna San Ignacio (LSI) in Baja California Sur, Mexico (Figure 3-3). This lagoon is visited yearly during the winter months by a large aggregation of Eastern Pacific gray whales (*Eschrichtius robustus*) and boat-based whale-watching activities take place daily between 9:00 and 17:00 (Urban R *et al*., 2003).

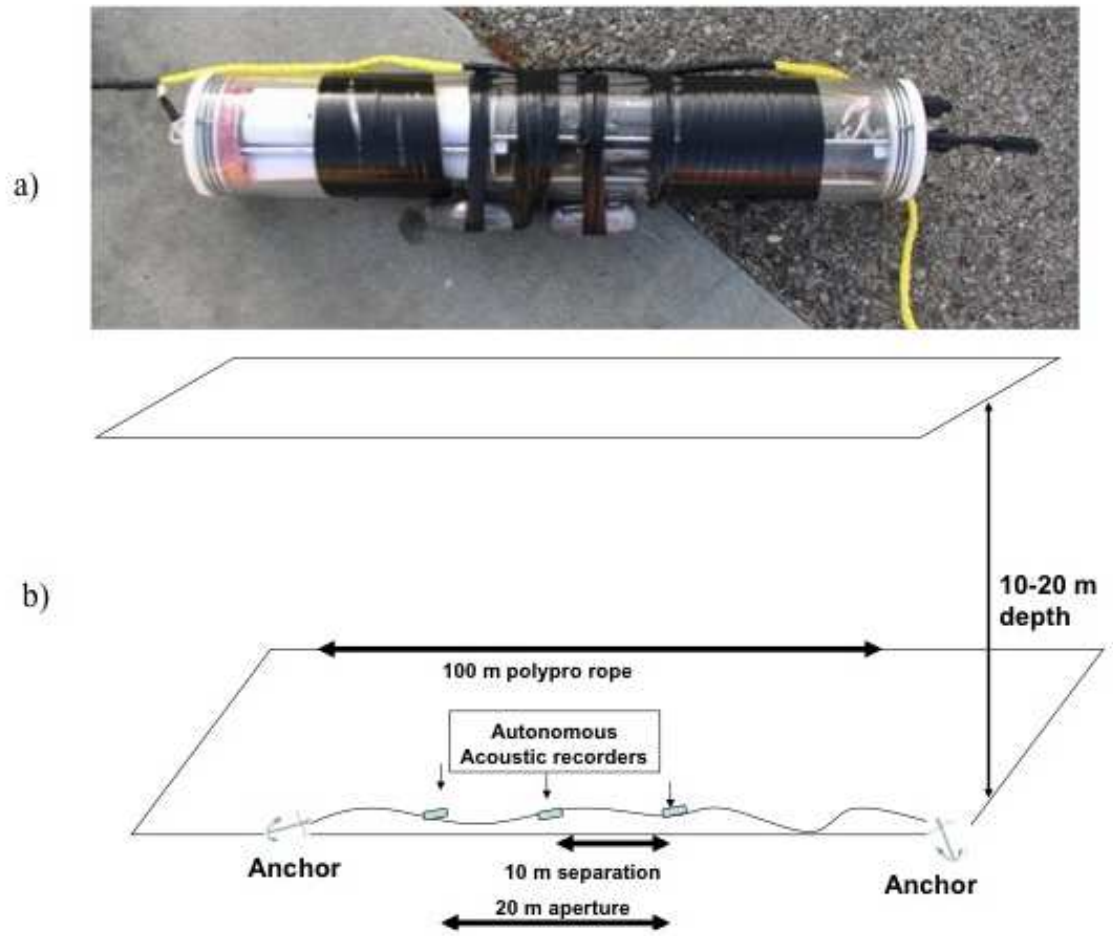

Figure 3-2: Instrumentation used for acoustic data collection in Laguna San Ignacio: (a) autonomous recorder attached to array line; (b) schematic of a horizontal three-element array.

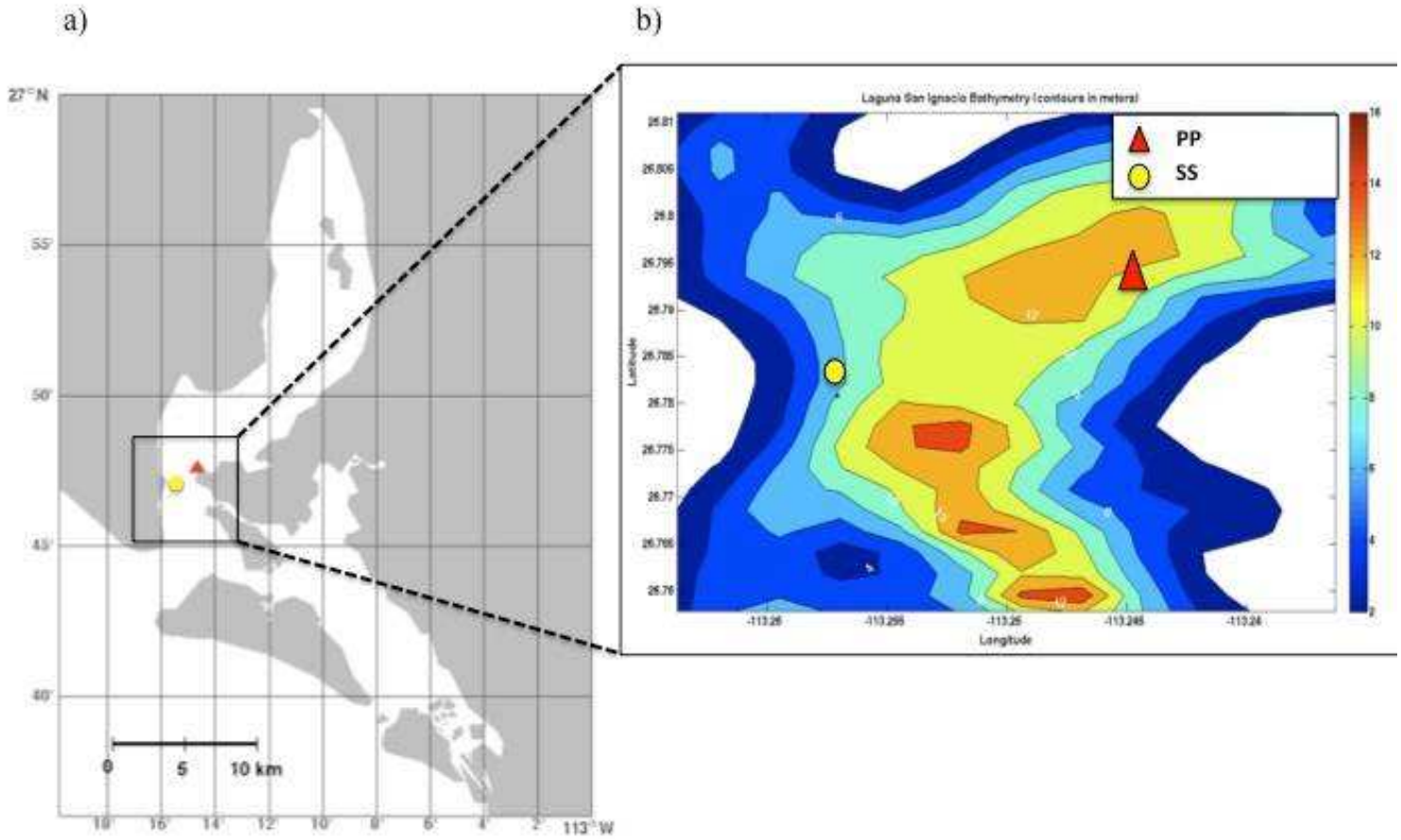

Figure 3-3: (a) Map and (b) bathymetry of Laguna San Ignacio, Baja California, Mexico. Array locations are marked for PP (triangle) and SS (circle).

A few hours before each deployment, the instrument clocks were synchronized to local GPS time. Each horizontal array was constructed by attaching three autonomous instruments to a 100 m section of nylon line [Figure 3-2(b)], with each pressure case weighted down by 5 lbs of distributed scuba diving lead weights [Figure 3-2(a)]. Two Grapnel-type anchors were used to secure the line to the bottom. The array was deployed from a small boat by lowering and securing the first anchor, followed by paying out the rest of the gear while keeping tension on the line and finally dropping the second anchor. GPS waypoint positions were taken at both anchor drop points. Because of the nature of the deployment, it is not guaranteed that the array line will lie straight on the ocean floor, so the precise separation between the recorders may differ from the measured distances along the rope. The submerged configuration [Figure 3-2(b)] leaves no surface signature, which is advantageous given the number of whales and boats transiting the area. To prepare for a contingency that strong tides would displace the set-up from its original location, a recovery transponder or "pinger" (model ORE CART) was also attached to the line, which could be queried from the surface to provide a ranging estimate.

The array was recovered by grappling perpendicularly between the anchor GPS waypoints. The northernmost array [triangle symbol in Figures 3-3(a) and 3-3(b)] is labeled "Punta Piedra" (PP) due to its proximity to a well-known local landmark of the same name. The deployment location (26°47.604' N; 113°14.674' W) was chosen to be compatible with historical baseline acoustic studies in the area, conducted in 1982-1984 (Dahlheim *et al*., 1984). The three instruments in the PP array are labeled

Units 1, 2 and 3, with adjacent units separated by 10 m. Units 1 and 3 were separated by 10 m, and Units 1 and 2 were separated by 20 m. The second underwater array [circle symbol in Figures 3-3(a) and 3-3(b)] is labeled the "Southern Station" (SS), and was deployed 1.5 km southwest of the first array (at 26°47.076' N, 113°15.436' W).

The three instruments in the SS array (Units 5, 7 and 8) were also spaced 10 m apart, with Units 5 and 8 separated by 10 m and Units 5 and 7 separated by 20 m. Unit 8 failed on February 24th. In this chapter only data from the PP station will be time-synchronized, although a sample spectrogram recorded at SS is shown for illustration purposes in Figure 3-5.

Tourist boats traveled past both locations each day. One dedicated research boat and five of 17 tourist boats were outfitted with onboard GPS devices. Each day during the 5-week monitoring period, the research boat drove two circles around each deployment (Figure 3-4) at a radius of approximately 100 m (bathymetry permitting), while attempting to maintain a constant engine cycling rate. The result was a broadband acoustic signal arriving from all azimuths around each deployment, which permitted independent estimates of clock offset and element separation for that day. The onboard GPS sampled position once a second when a circle was being performed, otherwise at one sample every 10 s while in regular transit.

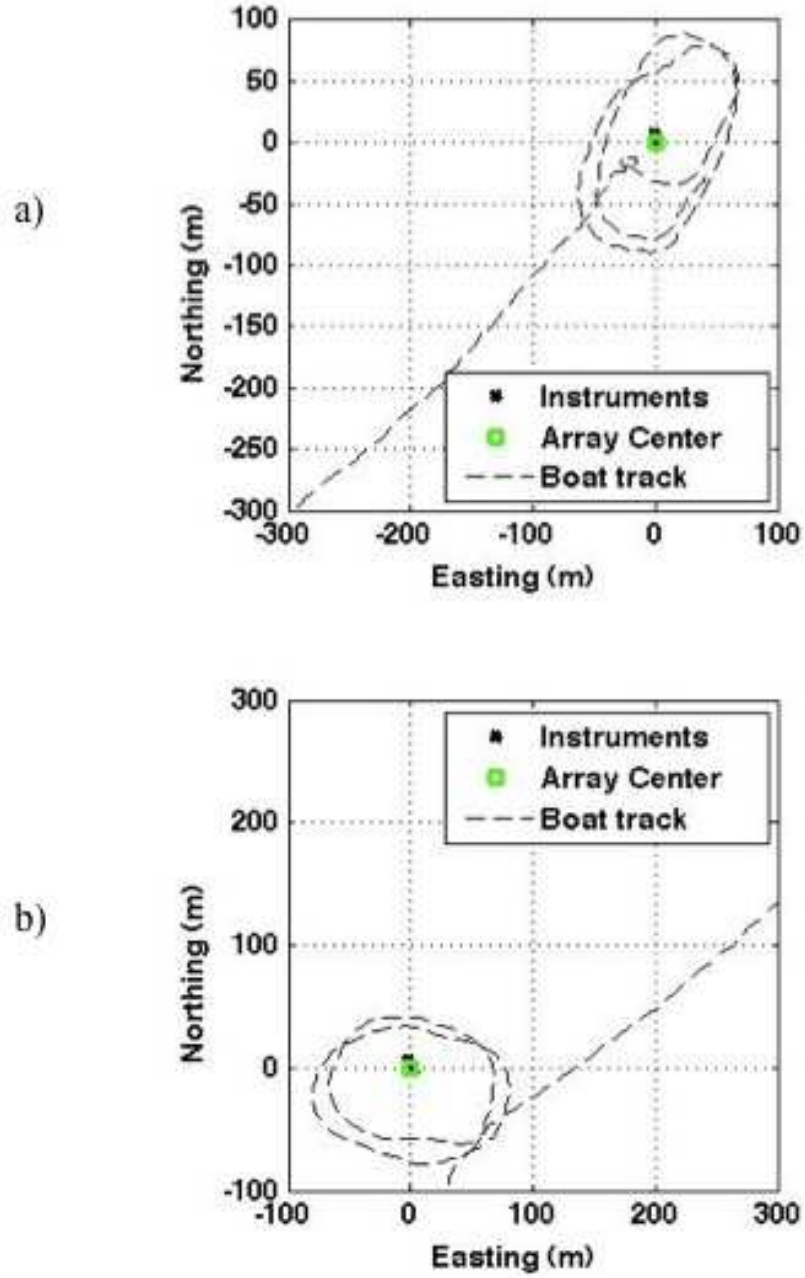

Figure 3-4: GPS tracks of research boat performing circles on March 1st, 2010: (a) around PP starting at approximately 15:44:00; (b) around SS starting at approximately 15:35:00. Also shown are the localized array instrument positions and array center. Axes are displayed in meters from the array center.

C. Acoustic environment

Historical acoustic research conducted 20 years ago at the PP site during the same winter months as this study (Dahlheim *et al*., 1984) deemed the lagoon habitat to be noisy in the 0-20 kHz range, when compared with open-ocean reference spectra from Knudsen *et al*. (1948). In particular Dahlheim found a concentration of elevated noise levels between 2-5 kHz. Although mainly dominated by biologics (fish, invertebrates and marine mammals), the local acoustic landscape also incorporates anthropogenic and physical sources, the latter associated with oceanographic processes like tidal currents and wind.

Of particular interest to this work is the ambient noise environment at 2 kHzand below. Above 1 kHz the most significant acoustic signature are biological sounds from invertebrates [Figure 3-5(a)]. Of the possible species in temperate and tropical habitats such as LSI, snapping shrimp (*Alpheus heterochaelis*) are commonly responsible for high-level noise in this frequency range (Au and Banks, 1998). The lagoon is also inhabited by a variety of croaker fish (*Sciaenidae* family) known for their sunset and sunrise choruses (D'Spain and Batchelor, 2006) in the frequency range below 100 Hz [Figure 3-5(a)].

The gray whale's dominant vocalization in LSI, the so-called type S1 pulsive call (Dahlheim *et al*., 1984) [Figure 3-5(c)], occupies the frequency range between 300-800 Hz, an acoustic niche that coincides with the "quiet" frequency band in the lagoon's ambient noise structure below snapping shrimp and above fish sounds.

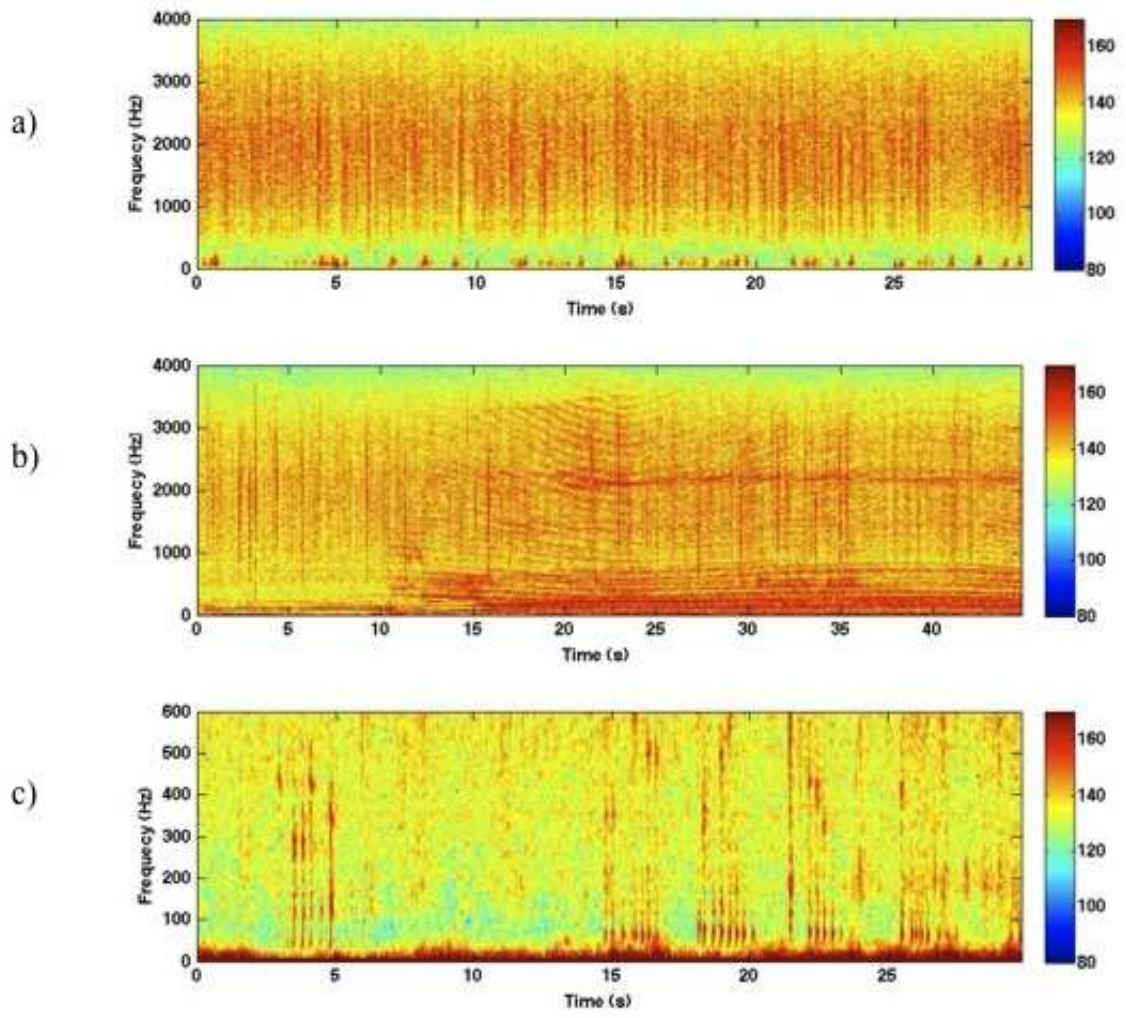

Figure 3-5: Sample spectrograms of raw acoustic data recorded at SS: (a) Underwater ambient noise recorded on March 1st, 2010 at 23:03:00; (b) Harmonics of boat noise at close approach recorded on March 1st, 2010 at 15:36:30; (c) Gray whale call type S1 recorded on March 1st, 2010 at 06:27:05. All samples correspond to the same raw data file on Unit 5. All spectrograms were computed using an FFT size of 2048 points and 75% overlap.

However due to the introduction of man-made sources this range now overlaps with a portion of the spectrum of the transiting boats [Figure 3-5(b)], creating the

potential for masking (Clark *et al*., 2009). Other gray whale vocalizations utilize slightly wider frequency ranges, as high as 2 kHz and as low as 100 Hz.

Due to the lagoon's complex bathymetry (Jones *et al*., 1984) and high evaporation rates (Winant and de Velasco, 2003), LSI experiences strong tidal currents. The average depth of the lagoon is only 3 m, because of the extensive salt flats situated to the north. The deep-water channel running along the central lagoon, adjacent to where the PP station was deployed, varies between 1.8 and 3 km in width and has an average depth of 15.2 m with a maximum depth of 25 m by the mouth of the lagoon. The water depths around a 100 m radius from where the acoustic arrays were positioned were sampled at the time of deployment and recovery, using a handheld depth finder (model: Vexilar LPS-1). On average, depths around the PP array measured between 7.6 m and 12.0 m and between 12.6 m and 20.2 m depth around SS. The bathymetry surrounding the deployments varied strongly with azimuth, especially around the PP site. Indeed, at low tide the lagoon shore would be within 100 m of the PP deployment, along the broadside array direction. By measuring how the broadband received level of transiting boat engine noise decreased with distance, a rough transmission loss formula of *27log(R)* was obtained for the PP site, indicating relatively poor propagation conditions in the lagoon.

IV. ANALYSIS PROCEDURE

A. The equalized noise covariance (EC), signed noise covariance (SC) and their time derivatives ECTD and SCTD

The noise covariance function (NCF) C_{ab} between two random timeseries $x_a$and x_b can be defined in the frequency domain as:

$$C_{ab}(\omega) = X_a(\omega)X_b^*(\omega) \tag{5}$$

where X_a and X_b are the respective Fourier transforms of x_a- $<x_a>$ and x_b - $<x_b>$. The inverse Fourier transform of Eq. (5), weighted by some choice of frequency window, is the NCF. Technically speaking, subtracting the mean value of the time series makes C_{ab} a measure of covariance, not correlation, but we will continue to use the term "noise correlation function" to be consistent with previous literature (Sabra *et al*., 2005c). The time derivative of the noise correlation function $dC_{ab}/d\tau$, expressed in the frequency domain, is

$$\frac{dC_{ab}(\omega)}{d\tau} = i\omega\ C_{ab}(\omega) \tag{6}$$

That is, the application of a frequency weighting of $i\omega$ is equivalent to a time derivative of the function in the time domain. The quantity $dC_{ab}/d\tau$ is closely related to the time-domain Green's function (TDGF) via Eq. (1) (Roux *et al*., 2005).

Eqs. (5) and (6) incorporate the spectrum of the ambient noise sources, which can lead to oddly-shaped peaks in the NCF. To generate cleaner peaks in the NCF, we define two additional functions. The equalized noise covariance $EC_{ab}(\omega)$ is defined in the frequency domain as:

$$EC_{ab}(\omega) = \frac{C_{ab}(\omega)}{T\sqrt{PSD_a(\omega)}\sqrt{PSD_b(\omega)}} \tag{7}$$

where the power spectral density $PSD_j(\omega)$ is defined as:

$$PSD_j(\omega) = E\left[\frac{|X_j(\omega)|^2}{T}\right] \tag{8}$$

where T is the time interval encompassed by the Fourier transform, and E indicates an ensemble average, or an average of a set of data snapshots.

Equation 7 is basically the Pearson's correlation coefficient of the two time series, which represents an attempt to "whiten" the noise spectrum and thus produce cleaner peaks in the frequency domain. Before applying Eq. (7) one must be confident that frequencies displaying a low power spectral density represent physical acoustic noise and not electronic noise or other artifacts. The time derivative of the equalized noise covariance (ECTD) then becomes

$$ECTD(t) = \int_{-\infty}^{\infty} W(\omega)\frac{i\omega\, C_{ab}(\omega)}{T\sqrt{PSD_a(\omega)}\sqrt{PSD_b(\omega)}}\, e^{i\omega t} d\omega \tag{9}$$

where $W(\omega)$ is a frequency weighting that acts as both a bandpass filter and a windowing function.

A second method for removing the source spectrum is to simply strip away all amplitude information by taking the sign of the time series. This 'one-bit' approach has been used frequently in the past (Sabra *et al*., 2005a; Brooks and Gerstoft, 2009). Thus if $x_a'(t)=sgn(x_a(t)-<x_a(t)>)$, and $X'_a(\omega)=F(x_a'(t))$, then both the signed noise

covariance $SC_{ab}(\omega)$ and signed noise covariance time derivative (SCTD) can be defined as simply Eqs. (7) and (9) with $X'_a(\omega)$ and $X'_b(\omega)$ substituting for $X_a(\omega)$ and $X_b(\omega)$.

The discrete time version of EC, $EC(T_l,N_{avg},N_{fft})$, is defined in the frequency domain as follows:

$$EC_{ab}(T_l, N_{avg}, N_{fft}, \omega) = \frac{\sum_{i=0}^{N_{avg}} C_{ab,l+i*N_{ovlap}}(\omega)}{\sqrt{\sum_{i=0}^{N_{avg}} \left| X_{a,l+i*N_{ovlap}}(\omega) \right|^2} \sqrt{\sum_{i=0}^{N_{avg}} \left| X_{b,l+i*N_{ovlap}}(\omega) \right|^2}} \quad (10)$$

where $X_{a,i}$ and $X_{b,i}$ are the Fast Fourier Transforms (FFT) of the respective discrete time series x_a and x_b sampled at f_s Hz, beginning at time sample j. $C_{ab,j}$ is simply the discrete-time version of Eq. (5), evaluated starting at time sample j. Each FFT uses N_{fft} samples to compute the transform. The time index l indicates an absolute time T_l, at which the ensemble time-averaging begins. N_{avg} indicates the number of data snapshots averaged together to force the emergence of the TDGF estimate, and N_{ovlap} indicates the number of samples overlapping between subsequent data snapshots, as per standard spectral density estimation methods. It was found that the numerator and denominator of Eq. (10) had to be averaged separately to produce a stable result. The time period covered by the N_{avg} data samples is assumed to be much smaller than the shift in clock offset caused by clock drift. Thus a sequence of EC estimates can be

obtained over long periods of time, indexed by *l*. The discrete-time version of the signed noise covariance $SC(T_l N_{avg} N_{fft})$ has a similar form as Eq. (10).

Both the EC and SC are time-averages of the NCF, evaluated at T_l. For sufficiently long averaging times, aspects of the TDGF should emerge in the EC and SC, in accordance to Eq. (2). While the time derivatives of the EC and SC (ECTD and SCTD) should technically be used, we have found little practical difference between using the ECTD vs. the inverse Fourier transform of the EC, and the rest of this manuscript will focus on estimating EC and SC (Roux *et al*., 2004). While both metrics EC and SC were computed, EC performed either better or similarly than SC (see EC-SC comparison in Figure 3-14), therefore results shown in Section V will mainly be based on EC calculations, as they are representative of SC results as well.

When considering the practicalities of computing EC and SC, two additional pre-processing steps were examined. First, the impact of pre-filtering the data (using both a finite impulse response (FIR) and Butterworth filters) at different frequency ranges was tested before computing the FFT, as well as using the complete bandwidth of the raw unfiltered data. The latter method generated the best overall results. Second, an event detector was investigated which rejected data samples that contained high intensity transient sounds. The use of an event detector yielded no improvement in performance either, which was surprising considering the number of boat transits and whale calls present in the lagoon. Thus all computations from this point forward represent time averages of the raw data without the removal of event detections.

B. Estimation of the relative clock offset τ_0 and clock drift $d\tau_d/dt$ from transient sources

The clock offset $\tau_0$between each pair of recorders was estimated twice, using two methods; first, using the highly directional sound field generated by the research boat circling the instruments, and then by using long-term averages of the ambient noise field.

For the first approach the initial clock offset estimate was divided into two parts:

$$\tau_0 = \tau_{TE} + \tau_{BC} \tag{11}$$

Here τ_{TE} represents a crude time alignment using the cross-correlation of a distinctive transient event, and τ_{BC} is a finer-resolution correction derived from noise from a research boat circling the instrument pair.

Before applying Eq. (11), the time series corresponding to a pair of recorders were visually inspected and aligned to within 1 s. To determine τ_{TE}, a distinctive sound (i.e. a whale call or the impulsive sound of a boat engine suddenly engaging or disengaging) was identified in spectrograms of a pair of hydrophones, and the timeseries were cross-correlated via Eq. (5). τ_{TE} is defined as the lag time of the peak of this cross-correlation. By applying the time offset τ_{TE} such that the peak cross correlation occurs at zero lag (Figure 7), we can guarantee that the data are now time-aligned to within $\pm L/c$, where L is the horizontal separation between the instruments and c the waterborne sound speed. Stated another way, since a physical signal will

display a cross-correlation peak between lags of -L/c to +L/c, by setting the peak of the cross-correlation at zero lag we ensure that the time-synchronization is off by at most L/c.

The fine-scale offset correction τ_{BC} in Eq. (11) relies on computing multiple EC estimates over the duration of the boat event, when the acoustic field is dominated by the highly directional engine and cavitation noise from the boat. The sequence of EC(T_l,N_{avg},N_{fft}), estimates are computed using the initial rough time-alignment τ_{TE}, and a small number (~4) of N_{avg} snapshots, and a large value of N_{fft}, selected such that $N_{fft} >> 2\ f_s L/c$, which ensures that the peak in the cross-correlations would be captured.

Figure 3-8 illustrates the procedure on two instruments separated by 10 m at the PP location, a result discussed in more detail in Section V.B. The figure displays a stack of EC estimates obtained from two hydrophones separated by 10 m, during times when the boat is circling the instruments, producing a 2-D image similar to the schematic shown in Figure 3-1. Thus the absolute time appears on the y-axis, and the lag time τ of the EC estimates appears on the x-axis. As seen in Figure 3-8, as the boat circles the array, the peak of the EC follows an S-shaped trajectory. Times at which the trajectory reaches an extremum with respect to τ indicate when the boat is passing endfire to the effective two-element array. When this information is combined with onboard GPS records, the orientation of the array on the ocean floor can be determined. The value of τ that lies midway between these extremes identifies τ_{BC}, and the span of τ between the endfire maxima yields the element separation via the

relationship $\tau=2L/c$. Figure 3-8 also shows that multiple peaks are visible in the EC estimates; these represent various multipath arrivals between the sensors, so when estimating L one must be cautious to choose the peaks associated with the direct path, which correspond to the S-shaped trajectories associated with the smallest absolute value of τ.

To estimate the relative clock drift $d\tau_d/d_t$ from boat data alone, the procedure described above is repeated on additional boat transits recorded at least 12 hours later (or earlier) from the initial estimate. Thus at least two clock offsets $_{\tau o}(T_0)$ and $\tau_o(T_1)$ are computed during absolute times T_o and T_1 respectively. The difference in clock offsets $\tau o(T_1)$- $\tau o(T_0)$ divided by the elapsed time (T_1-T_0) yields $d\tau_d/dt$.

C. Estimation of relative clock offset τ_0 and clock drift $d\tau_d/dt$ from ambient noise

To estimate clock drift from ambient noise, an initial clock offset estimate $\tau_0$derived from boat noise is selected. Then the EC functions are generated by averaging 500 snapshots of data with 75% overlap, with each snapshot using 82 ms of data. Thus 40.96 s of data are used to generate each EC estimate. This same analysis could also be performed with estimates of SC, ECTD or SCTD instead.

The clock drift is estimated from the ambient noise in two stages. First, a value of $d\tau_d/dt$ is measured from the slope of drifting peaks generated by a set of EC estimates over a long-term window of data. Following the clock drift correction, the

peaks should show little change in their lag time with time and the double-peak structure becomes roughly vertically aligned [Figure 3-1(b)].

Next, sets of EC functions are computed over a 30 min window, beginning every hour until all hours of a data file have been processed. Monitoring the evolution of the peak structure of the NCF, a 30 min time segment beginning at absolute time $T_{win,1}$ is selected that shows the best fit to Eq. (4); that is, over the particular 30 min interval starting at $T_{win,1}$the EC shows two strong peaks, separated by the expected value of $2L/c$. (As will be shown in the results, this structure may emerge only during certain times of the day in this environment.) A matching time window is then selected beginning at $T_{win,2}$, 24 hours before or after $T_{win,1}$. All EC estimates from both 30 min time windows are then averaged and summed to form a single NCF estimate, referred to as NCF_{total}, and the peak amplitude $A(d\tau_d/d_t)$ of NCF_{total} is measured.

Now, small corrections to the original $d\tau_d/dt$ approximation can be investigated. Over an extended period of time (i.e. a day), a horizontal shift to the EC window at $T_{win,2}$ would be equivalent to applying a slightly larger or smaller clock drift to the instrument. This horizontal drift shift corresponds to a small adjustment to the original approximation of clock drift. Thus the 30 min window starting at$T_{win,2}$ is shifted along the x-axis, before summing it with the estimate from $T_{win,1}$again, yielding a new value of A. This process is repeated until a local maximum in A has been determined and from it, a more precise estimate of $d\tau_d/dt$. The resolution of the clock drift estimate can be inferred from how quickly A decreases as a function of $T_{win,2}$ shift. Once the clock drift has been optimized, the clock offset can be fine-tuned until

the peaks are symmetrical around zero lag, and the element separation L can be derived as discussed in Section II.

D. Using boat transits to estimate bottom array orientation

Boat noise can also be used to orient the horizontal array's deployment on the ocean bottom, by transforming the time lag associated with the primary peak in the EC (equivalent to the time of arrival difference TOAD) into source bearings, and comparing these localizations with known positions derived from on-board GPS records. An approximate formula for $\Delta\tau$ can be related to the sound speed in the medium c and horizontal separation L:

$$\Delta\tau = \cos(\phi)\frac{L}{c} \tag{12}$$

where L represents the spacing between receivers and the angle ϕ determines the bearing to the source relative to the array's endfire direction. The point at which the boat crosses the array's endfire bearing will yield the largest lag and the peak of the cross-correlation function will be shifted from $\tau = 0$ by a value $\Delta\tau = |\tau_a - \tau_b|$ where τ_a is the arrival time to receiver a and τ_b to receiver b. Conversely the peak will present no lag and be centered at $\tau = 0$ if τ_a and τ_b are identical, which occurs when the source is directly broadside from the array.

However, two factors complicate the calculation. First, because the source (boat) is on the surface, while the recorders lie on the ocean floor, if the boat approaches too close to the sensors, the TOAD becomes a function of water depth,

along with azimuth and element separation. Thus all boat transits used in the analysis were required to be at least 100 m distant from both sensors in 20 m water. Second, surface-reflected multipath must be recognized and rejected if present.

V. RESULTS

A. Dates and times of data analyzed

The autonomous instruments recorded acoustic data at a sampling frequency of 12.5 kHz, so each raw data file of 3.35 Gb stored 40 hrs of data. The relative offset $\tau_0$and drift $d\tau_d/dt$ within a single acoustic file were explored by analyzing the file created between February 28thand March 2ndon all elements of the PP array.

First, in order to illustrate the acoustic environments at LSI, three sample spectrograms of raw acoustic data are shown in Figure 3-5. These were recorded at the Southern Station (SS) between February 28th and March 2nd, specifically between 06:27:05 and 23:03:30 on March 1st. The 30 s-long, nighttime spectrogram recorded at 23:03:00 [Figure 3-5(a)] demonstrates the evening predominance of biological acoustic sources in this environment, like croaker fish, which dominate below 100 Hz, and snapping shrimp sounds, seen between 1 kHz and up to 4 kHz. These biological sources are not as prevalent between 100 Hz and roughly 600 Hz. Figure 3-5(b) presents an example of boat engine noise during a circling event performed at 15:36:30 on March 1st, following the procedure described in Section III.B. Finally, Figure 3-5(c) shows an example of gray whale type S1 calls recorded between

06:27:05 and 06:27:50 on March 1st. Due to the strong propagation loss experienced in this lagoon, boat circles at one array were not recorded on the other array, 1.5 km away. However, whale calls and distinctive impulsive engine sounds were found in the recordings at both PP and SS and used to initially estimate τ_{TE} (Eq.11).

Daily boat transits were aurally and visually detected in the datasets of both array locations through the duration of this data file. Figure 3-4 shows the GPS tracks of two circles performed by the research boat on March 1st around PP [Figure 3-4(a)] and SS [Figure 3-4(b)]. The research boat circled around SS for four minutes, starting at approximately 15:36:00 [Figures 3-4(b) and 3-5(b)]. Between 15:40:00 and 15:44:00 the boat transited north in the direction toward the PP location. At 15:46:00 it began the circling around PP, finishing at approximately 15:49:00 [Figure 3-4(b)]. These GPS boat tracks were used to estimate clock offset using the procedure described in Section IV.B.

The following day (March 2nd) yielded two boat-related events that were used to estimate clock drift. At 10:39:00 the research boat made a close approach by PP, slowing down and stopping down for 3 min between 10:43:00 and 10:46:00, before accelerating and departing the area. These data were used to estimate the relative clock drift for units separated by 20 m (Figure 3-20) via the procedure detailed in Section IV.B. Later in the day, at 13:20:00, a second boat-transit signature was found in the data and used to calculate the relative clock drift between instruments separated by 10 m (Units 2 and 3) at PP (Figure 3-9). In general, the 10:39:00 boat pass had more

distinct engine start/stop characteristics, and so was used for the more difficult 20 m time synchronization.

B. Estimation of clock offset τ_0 and clock drift $d\tau_d/dt$ at PP (10 m separation)

Following the procedure detailed in Section IV.B, the clock offset τ_0 and clock drift $d\tau_d/dt$ at PP between Units 2 and 3 (10 m separation) were estimated both by means of transient events (Figures 3-6 to 3-9) and continuous ambient noise (Figures 3-10 to 3-18).

To estimate τ_0, the time series were first visually aligned within 3 s with respect to each other using spectrograms, in order to guarantee an overlap in the cross-correlation (Figure 3-6). A cross-correlation of 30 averages (FFT size of 2048 pts at 50% overlap) was performed on a 5 s-long data sample of boat-engine revving sound occurring at 15:46:33 on March 1st. The data were first bandpass-filtered using an FIR with a bandpass between 30-200 Hz. This cross-correlation produced peak output at a lag of - 0.9315 s, for a total relative offset τ_{TE} = 2.0685 s (Figure 3-7).

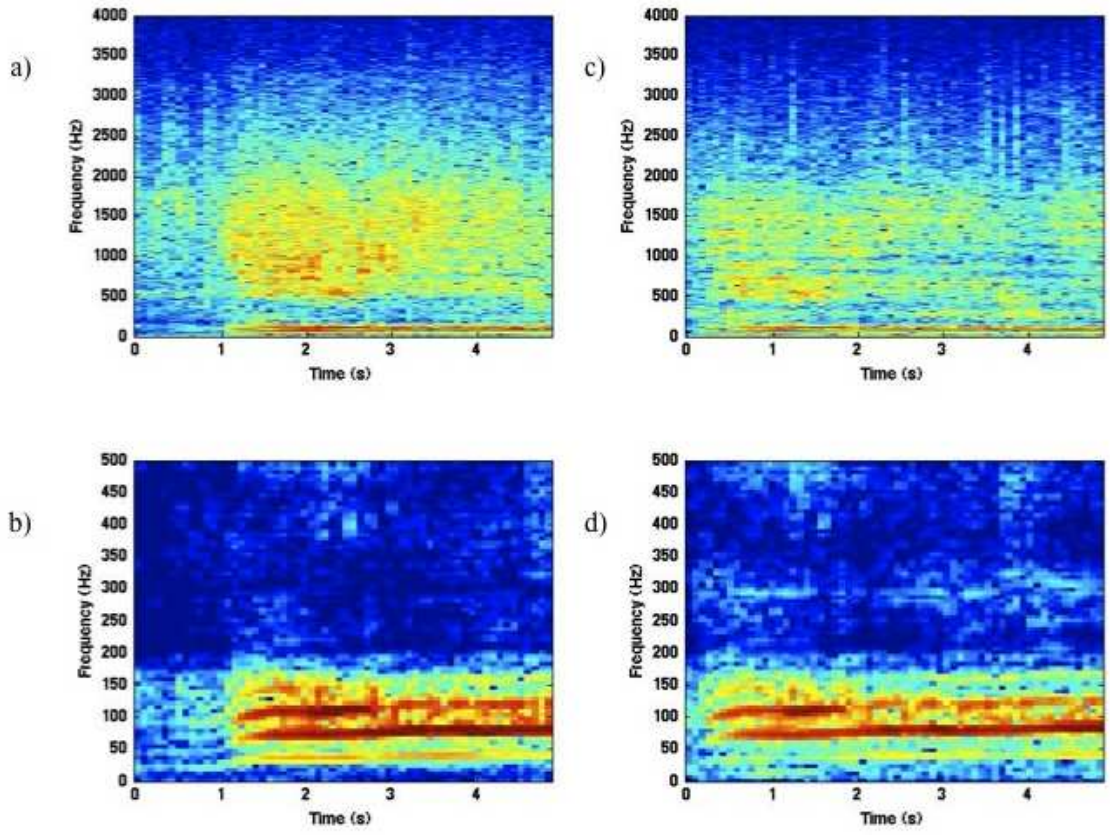

Figure 3-6: Sample data from an engine start sound, used to initially time-align two time series: (a) Raw data at Unit 2 at 15:46:33 on March 1st; (b) FIR filtered data (30-150 Hz) at Unit 2; (c) Raw data at Unit 3 at 15:46:36 on March 1st; (d) FIR filtered data (30-150 Hz) at Unit 3. All spectrograms were computed using an FFT size of 2048 points and 50% overlap.

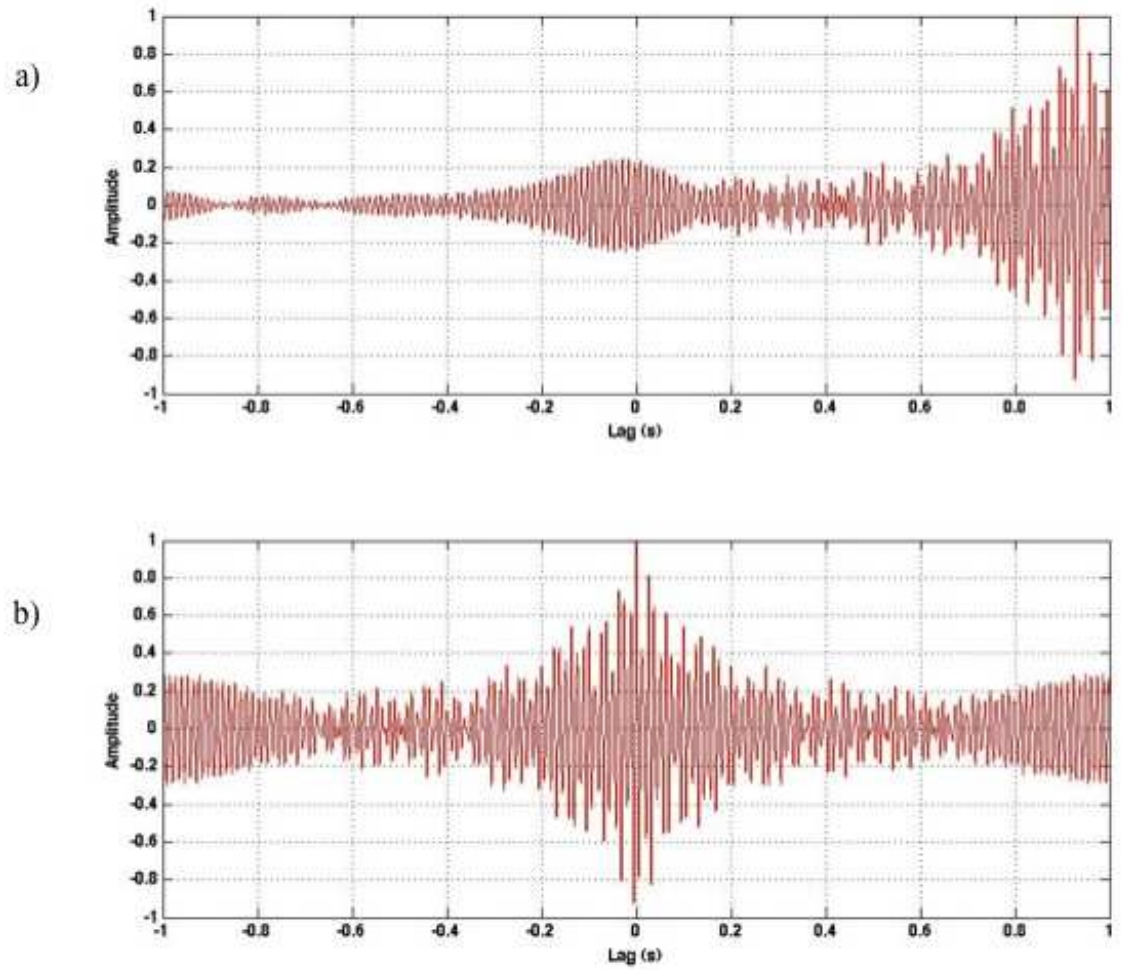

Figure 3-7: Cross-correlation between two time series in order to measure the component tTE of clock offset t0: (a) Cross-correlation of 5 s of data between Units 2 and 3; (b) Cross-correlation of the same data points, after the introduction of a tTE of - 0.9315 s.

To further refine this estimate, a set of EC functions were derived using 10 min of engine noise (Figure 3-8) originating from the boat circle around PP at 15:44:00 on March 1st [Figure 3-4(a)]. Each EC estimate was generated using 0.3277 s of data (or 4 data snapshots with FFT size 1024 pts at 75% overlap) producing the S-shaped trajectory seen in Figure 3-8. Connecting this time-lag image with GPS track data

from the boat, it is established that a negative lag corresponds to the source being located south of the array. Also, from this trajectory a value of -0.0054 s was obtained for τ_{BC}, for a total clock offset ($\tau 0 = \tau_{TE} + \tau_{BC}$) of 2.0631 s between Units 2 and 3 at 15:46:33. Note the surface-reflected multipath visible at the endfire points of the trajectory at 15:47:30 and 15:49:00 (Figure 3-8).

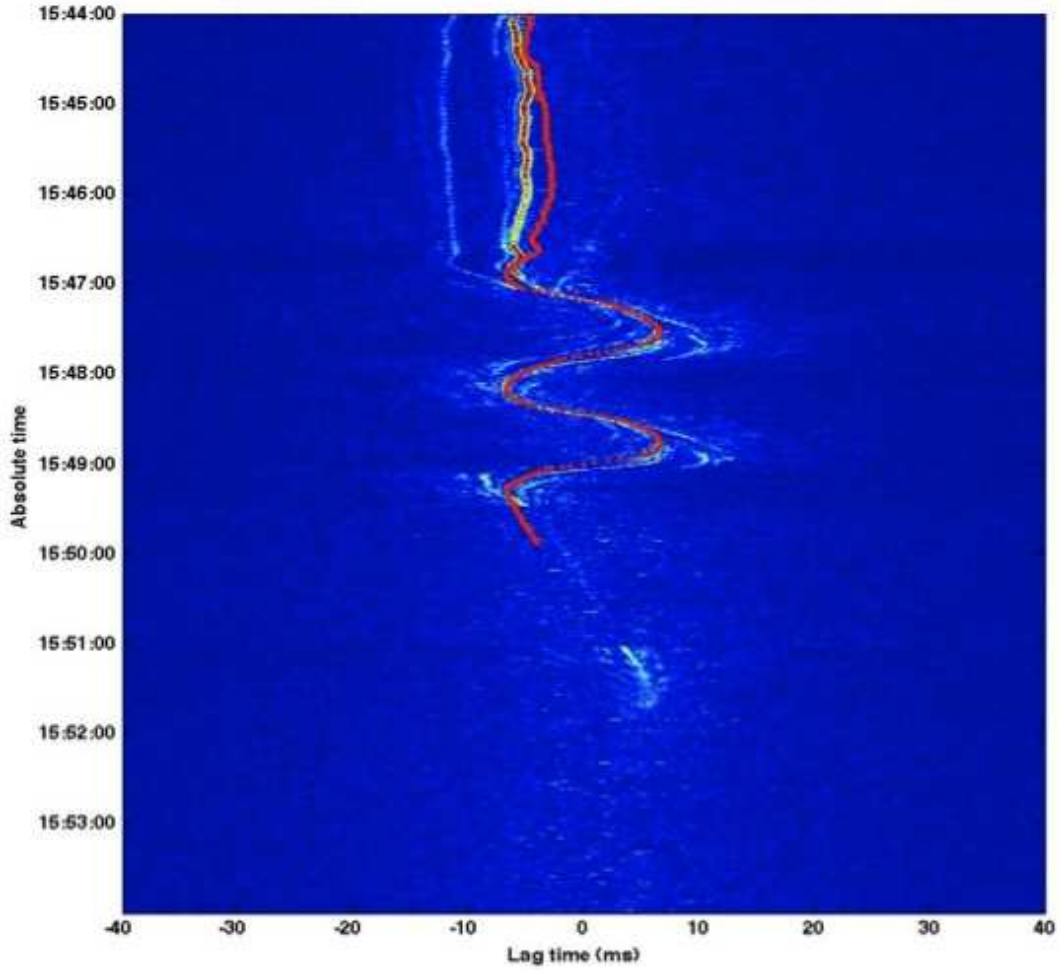

Figure 3-8: The time domain EC between two instruments 10 m apart at PP (Units 2 and 3), overlain with the time lags estimated from GPS track localizations (red dots) of a boat circle on March 1st, 2010 between 15:44:00 and 15:53:00, using a clock drift of 0.27 s per day and an initial offset of 2.0631 s.

A second close-approach boat pass occurred 22 hours later, and the EC computation was performed again using 12 min of data starting at 13:20:00 on March 2nd(Figure 3-9). On this occasion, the boat did not circle the autonomous instruments, but simply navigated transited by the array, leaving an acoustic signature between 13:23:30 and 13:26:30. The difference in clock offsets between those two boat events produced a clock drift estimate $d\tau_d/dt$ of 0.27 s per day.

Figures 3-10 to 3-18 show the derivation of clock drift $d\tau_d/dt$ and the verification of clock offset τ_0 from the lagoon's ambient noise. To estimate clock drift, long-term estimates of EC were computed per Eq. 10, where each estimate used 40.96 s of data (or 500 averages of 1024 point FFTs, overlapped 75%).

Figure 3-10 shows the values of the EC in the time and frequency domain [per Eq. (10)] computed without any clock drift correction, but with an initial offset of 2.0631 s at 15:46:33 (derived using the boat circle) over 5 hours between 15:46:00 and 20:46:00 on March 1st. The drift rate of the peaks in the corresponding time domain EC [Figure 3-10(b)] is measured and used as a first approximation of clock drift. Figure 3-11 is a re-analysis of the same time period as Figure 3-10, but using a measured approximation of clock drift of 0.2834 s per day, taken from the slope of Figure 3-10(b).

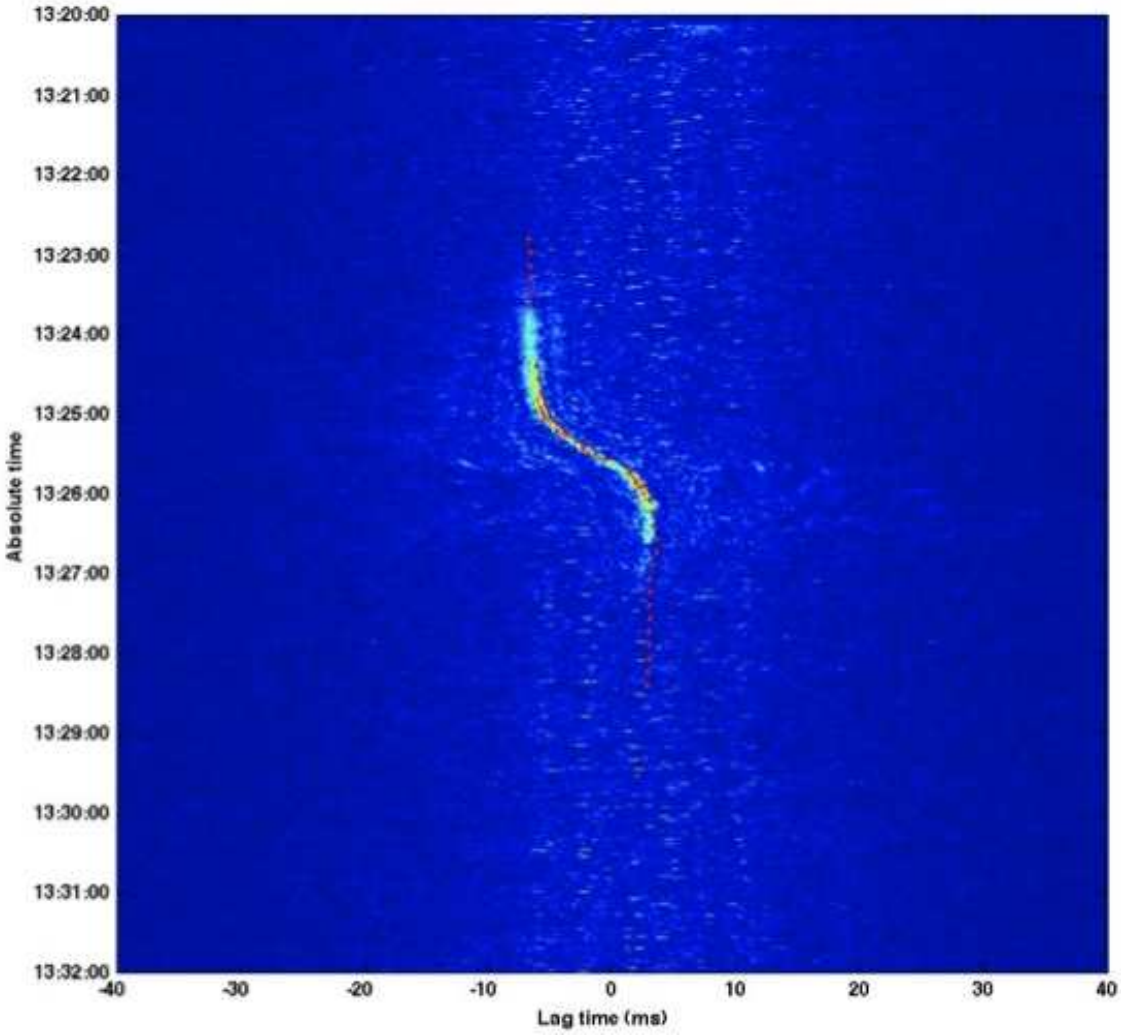

Figure 3-9: The time domain EC between two instruments 10 m apart at PP (Units 2 and 3), overlain with the time lags estimated from a GPS track of a boat transit (red dots) on March 2nd, 2010 between 13:20:00 and 13:32:00, using the same clock offset and drift as in Figure 3-8.

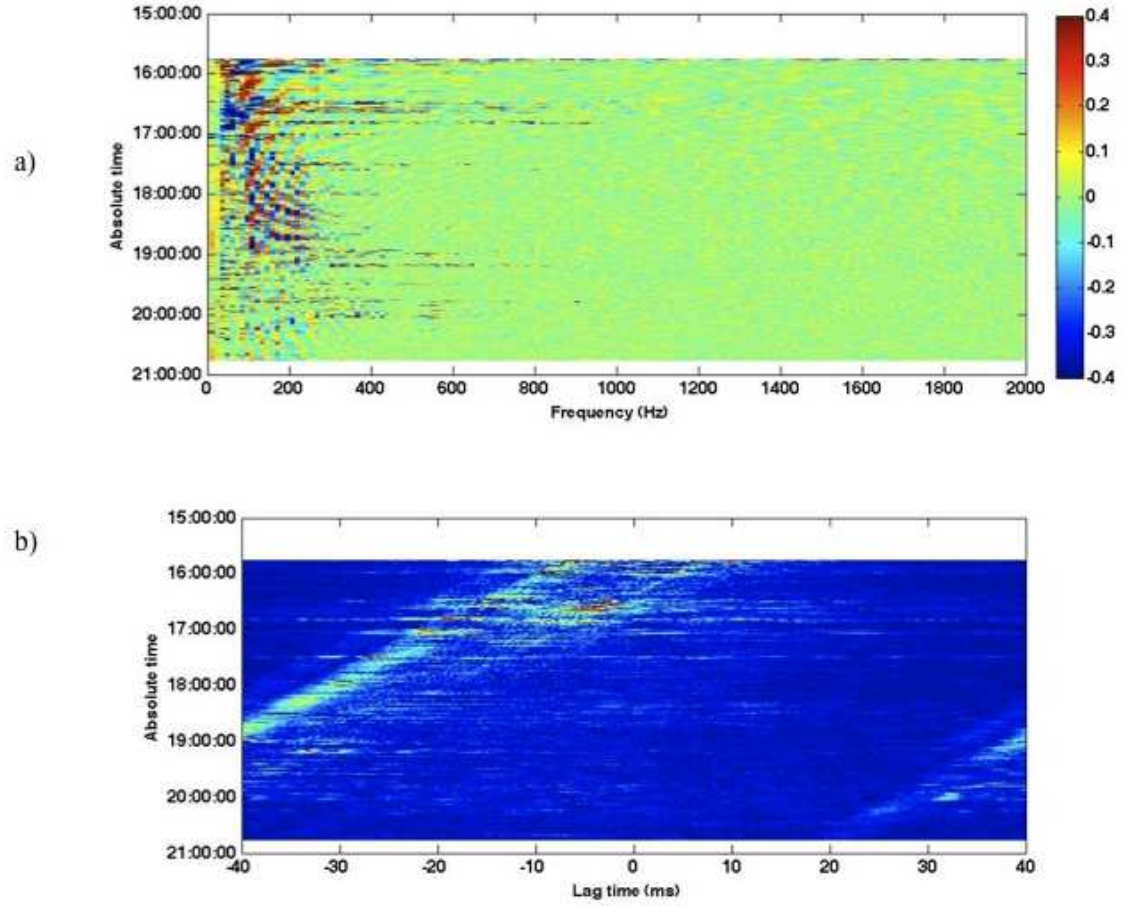

Figure 3-10: Long-term estimation of NCF between Units 2 and 3 at PP, between 15:46:00 and 20:46:00 on March 1st, 2010 using a clock offset of 2.0631 s and no clock drift: (a) Frequency-domain EC; (b) Time-domain EC as a function of lag time.

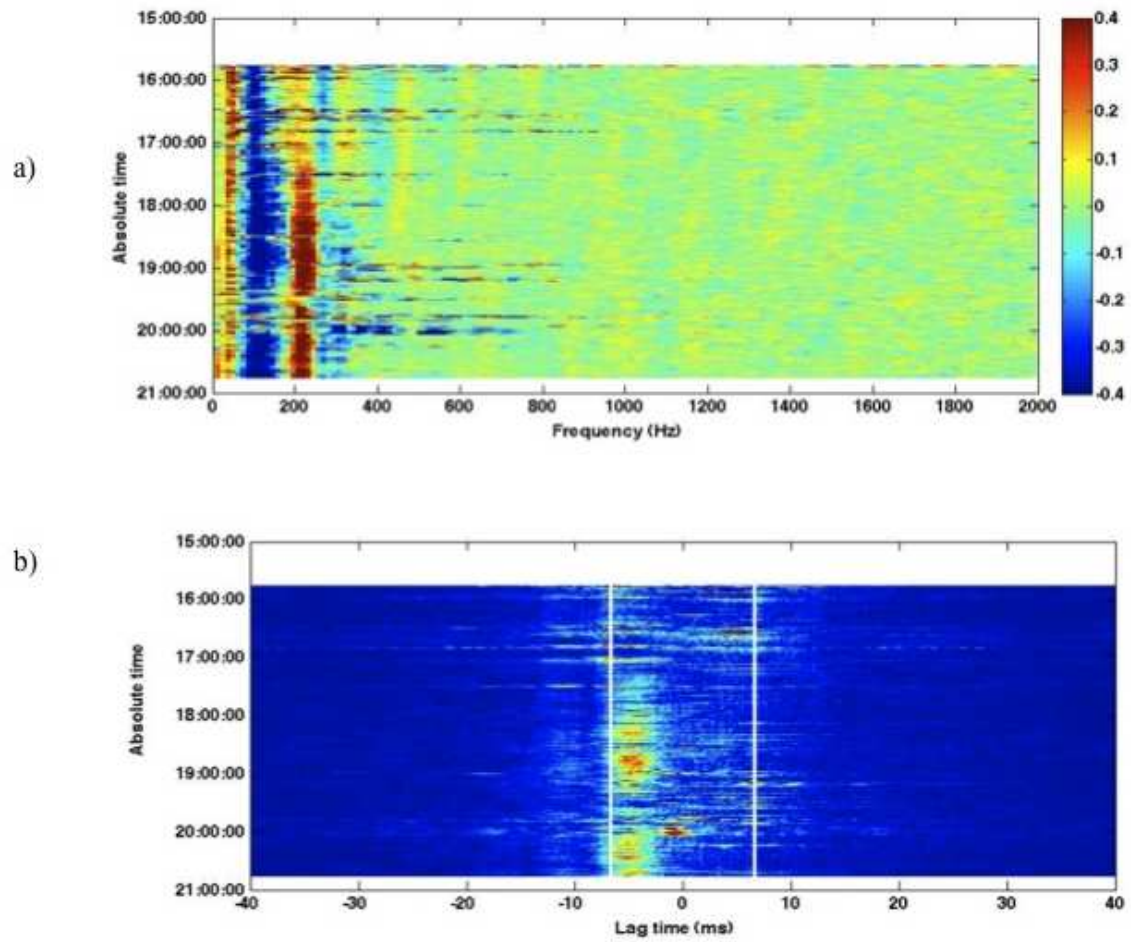

Figure 3-11: Same as Fig. 3-10, but with the introduction of a clock drift of 0.2834 s per day, measured from the drifting peaks of Fig. 3-10. The theoretical time lags corresponding to a 10 m separation (±6.7 ms) are marked with vertical lines in (b).

Both Figures 3-10(a) and 3-11(a) display the EC estimates [Eq. (10)] in the frequency domain, which provides insight into the frequency components that are spatially coherent between the sensors, and thereby contribute to the coherent peaks in the corresponding time-domain EC. A value of EC substantially different from 0 at a given frequency indicates a significant degree of spatial correlation between the sensors.

Spatial correlation generally decreases with frequency, as expected from analytical models of noise covariance (Cron and Sherman, 1962; Cox, 1973). A "ripple" interference pattern is visible in the frequency structure of the NCF [Figure 3-10(a)], and these ripples become vertical and evenly-spaced in frequency once the correct clock drift between time series has been applied [Figure 3-11(a)]. Figure 3-11(a) indicates that at 10 m separation, frequencies up to 1400 Hz have a non-zero spatial coherence, but the strongest components of the timing signal exist at 300 Hz and below.

To investigate longer-term patterns in the evolution of the spatial correlation, EC estimates are derived from 30 min-time windows of acoustic data every hour over continuous hours within a single raw data file, between 16:00 on March 1st and 04:30 on March 2nd following procedures detailed in Section IV.C. Figure 3-12 stacks these 30 min-long estimates into a continuous time record; the top subplot shows the frequency-domain structure of the EC estimate, while the bottom subplot shows the time-domain. From the relationship $2L/c$ and assuming a sound speed of 1500 m/s, a separation L of 10 m should yield theoretical twin peaks at ± 6.7 ms in Figure 3-12(b), lag times that are indicated as white, vertical bars.

Three interesting features arise from the long-term coherence plots in Figure 3-12. First, the frequency coherence plot in Figure 3-12(a) shows a strong change in the ambient noise structure in the lagoon between 18:00 (local sunset) and midnight. During this time the noise field between 50 and 250 Hz becomes strongly correlated, which corresponds with a highly directional noise source associated with peaks at lag

time of -5 ms in Figure 3-12(b). The direction of the noise is 48.6° relative to the endfire direction (Eq. 12), and given that the time lag is negative, the source is known to come from the lower (southern) portion of the lagoon.

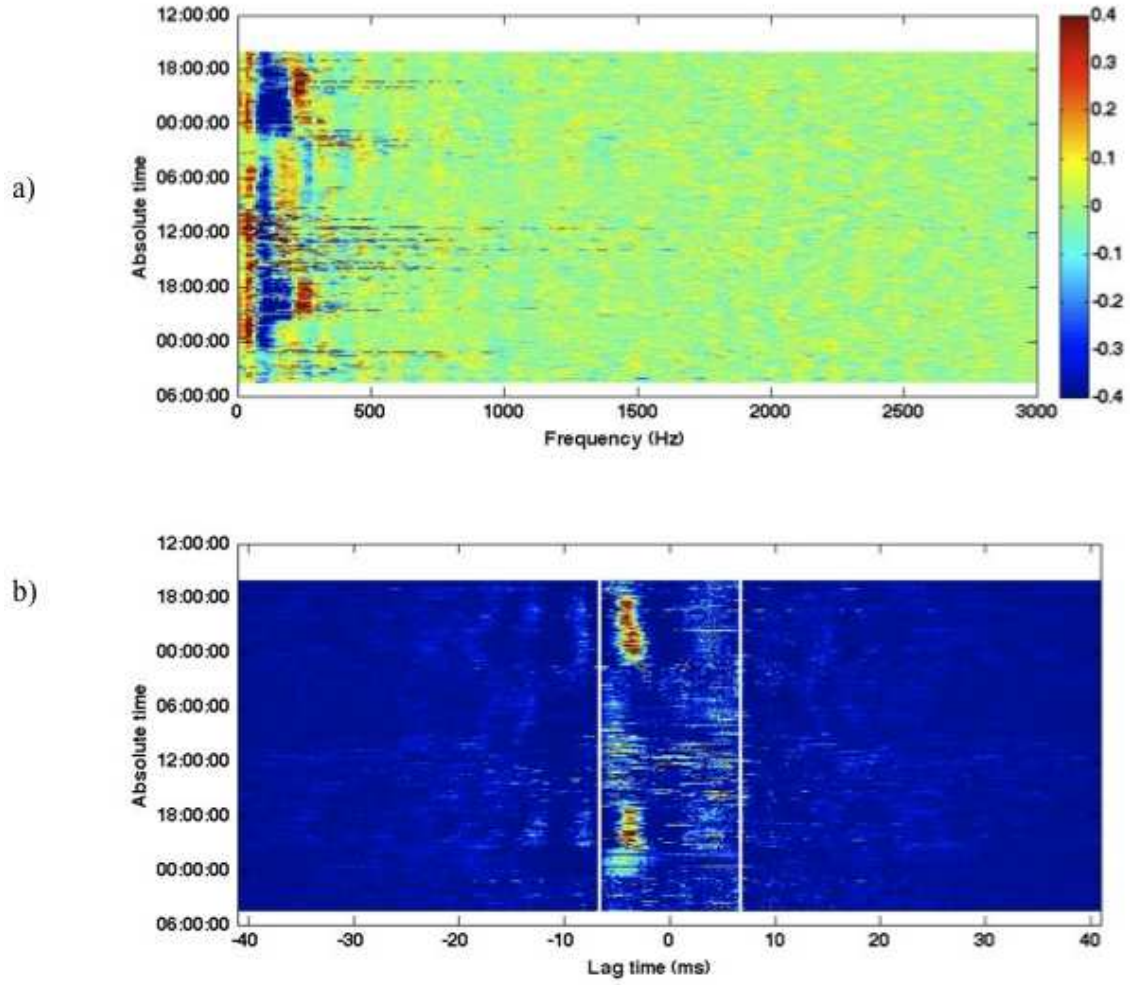

Figure 3-12: Long-term evolution of 30 min estimates per hour for (a) Frequency-domain EC and (b) Time-domain EC, computed at Units 2 and 3 at PP, between 16:00:00 on March 1st and 04:00 on March 3rd. Clock offset and clock drift parameters are the same as in Fig. 3-11. The theoretical time lags corresponding to a 10 m separation (±6.7 ms) are marked with vertical lines in (b).

A second interesting feature of Figure 3-12(a) is that during daylight hours, transient events (presumably boats and whales) generate numerous spikes in coherence between 400 and 1000 Hz as highly directional, transient signals dominate the recordings for a few minutes at a time. Indeed, both the frequency and time domain plots of Figure 3-12 provide indications of such events.

Finally, the time-domain plot in Figure 3-12(b) shows evidence of surface reflected multipath arrivals outside the central ± 6.7 ms region of the plot. These multipath peaks oscillate in lag time as 12 hour cycles, corresponding to tidal changes in the lagoon, which change the local water depth and thus the relative arrival times of surface-reflected multipath.

Figure 3-13 presents a similar representation of Figure 3-12, except that here the cross-coherence of the sign of the equalized noise (SC) is shown, both in the frequency and the time domains. All of the features discussed in Figures 3-12(a) and 3-12(b) are still visible, and the time domain SC shows the double-peaked structure of Eq. (2) much more cleanly.

a)

b)

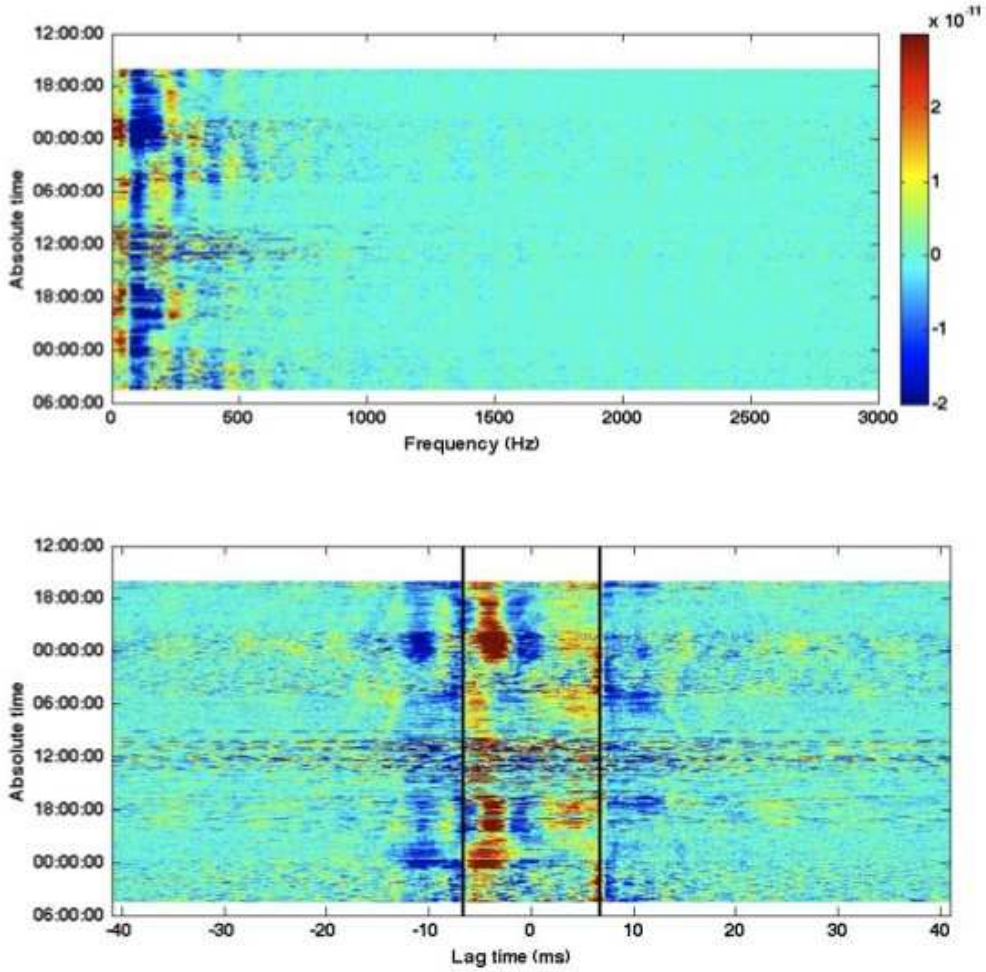

Figure 3-12: Same as Fig. 3-12, but for (a) frequency-domain SC and (b) time domain SC.

Figures3-14 and 3-15(a) plot the EC and SC in both the frequency and time domains for one particular 30 min time-window, beginning at $T_{win,1}$ of 04:00 on March 2nd. This time period was specifically selected because no dominant directional noise source exists. A similar pattern arises 24 hrs later [Figure 3-15(b)], and it is possible to estimate the clock drift using the technique described in Section IV.C. In this figure the initial ambient noise clock drift estimate of 0.2834 s per day has been employed, as well as the clock offset of 2.0631 s derived from the boat events. Figure 3-15(c) shows an estimate of NCF_{total}, which displays two clear peaks close to the timings predicted by Eq. (4), that correspond to a 10 m array spacing (marked by blue lines). Note that the lag between the two peaks in Figure 3-15(c) corresponds to a 9.11 m spacing instead of exactly 10 m. This result is not surprising, in that the deployment may not be a straight line on the lagoon floor.

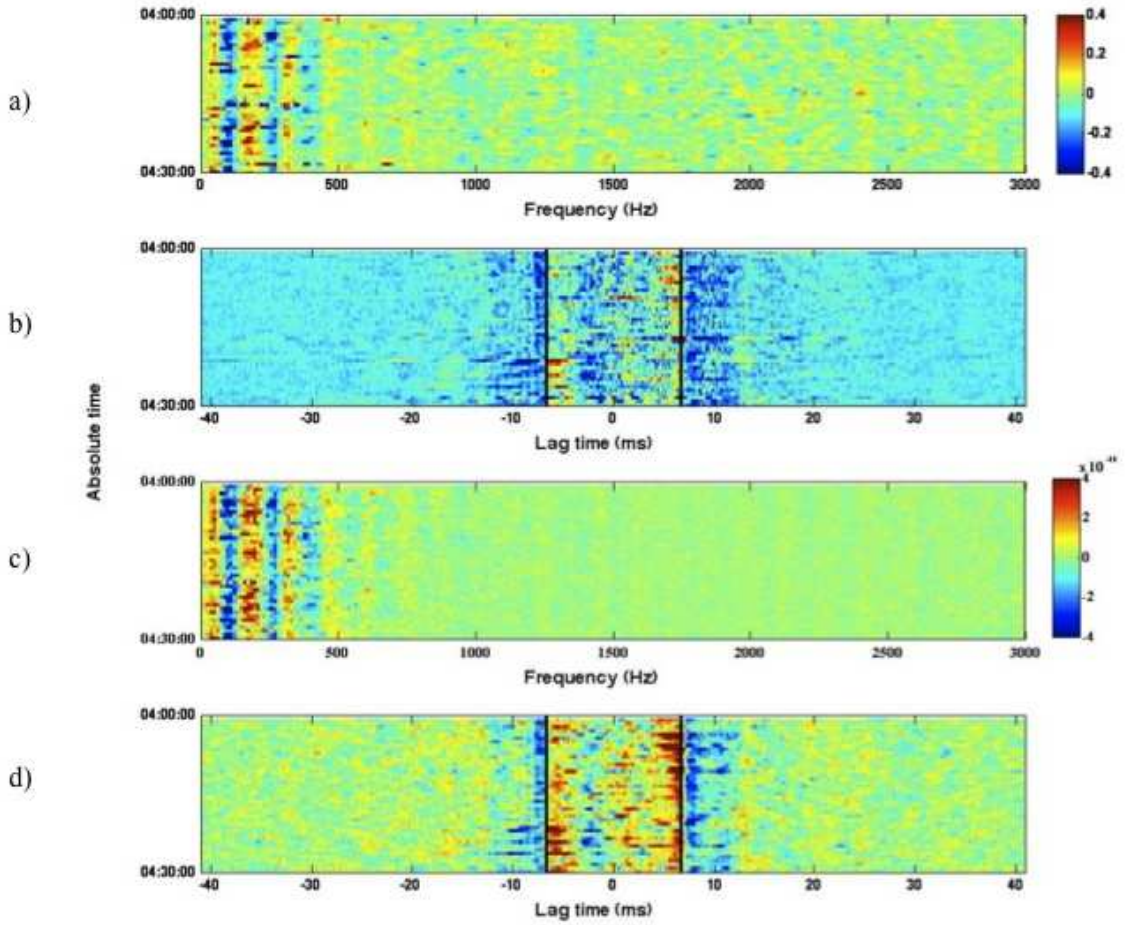

Figure 3-14: 30 min computations of (a) frequency-domain EC; (b) time-domain EC; (c) frequency-domain SC; (d) and time-domain SC. All figures have $T_{win,1}$ of 04:00 on March 2nd. Each horizontal line in the images is generated by averaging 500 snapshots (0.0819 s long) of data at 75% overlap, using a total of 40.96 s of data for each horizontal line. The theoretical time lags corresponding to a 10 m separation (±6.7 ms) are marked with vertical lines in (b) and (d).

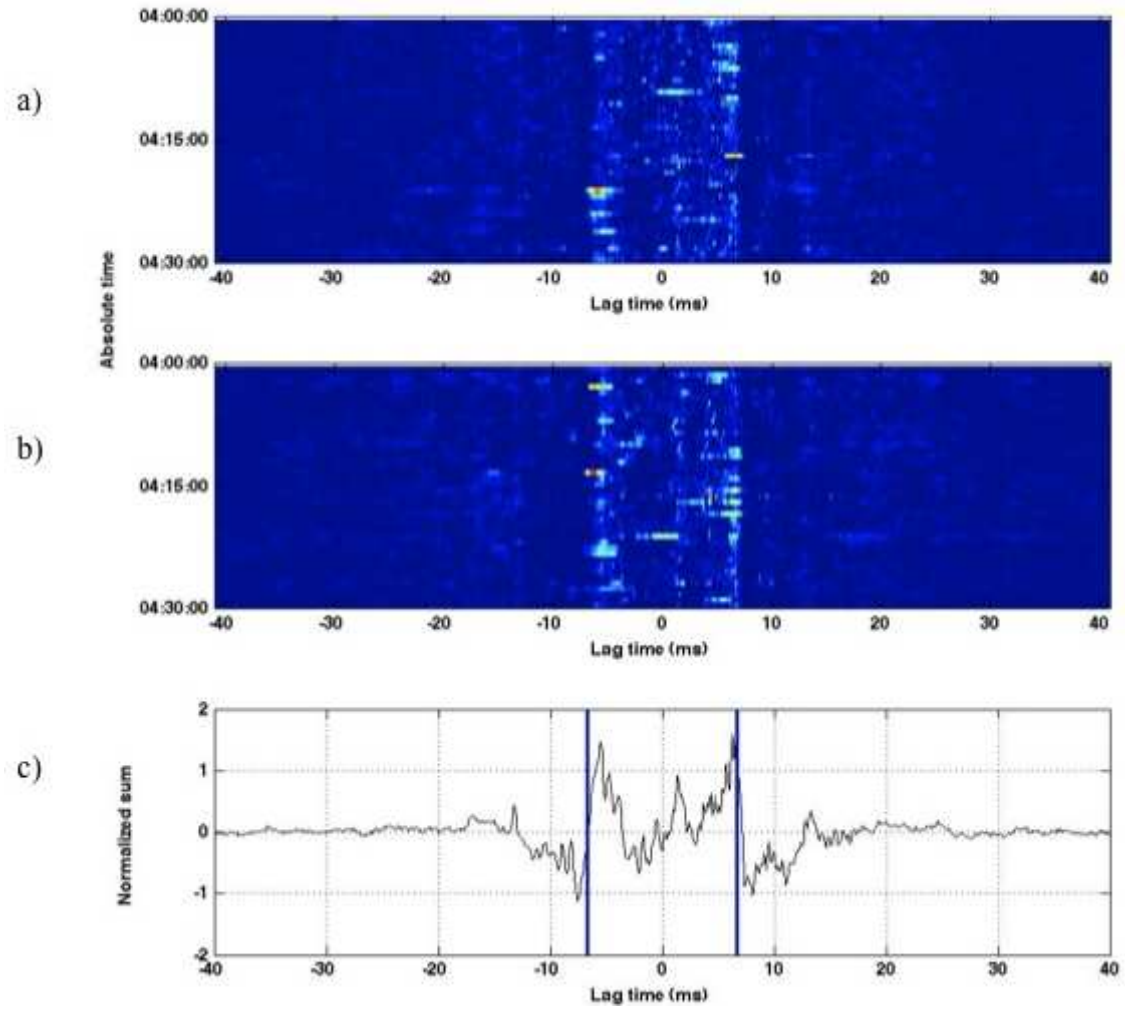

Figure 3-15: 30 min EC computations in the time-domain as a function of time and correlation lag, using computation parameters identical to Fig. 3-14: (a)at a selected $T_{win,1}$ of 04:00 on March 2nd; (b)at a selected $T_{win,2}$ of 04:00 on March 3rd; (c) NCF_{total} function resulting from the vertical sum of (a) and (b).The theoretical time lags corresponding to a 10 m separation (±6.7 ms) are marked with vertical lines in (c).

In order to fine-tune the clock drift estimate $d\tau_d/dt$, the summation of two 30-min EC estimates is repeated, while slightly shifting the second EC estimate horizontally in time delay, as described in Section IV.C. Figure 3-16 plots the peak value A of the resulting NCF_{total} functions as a function of drift shift, where a drift shift

of ‘0’ on the x-axis represents the 0.2834 s per day clock drift originally obtained from the slope of a 5 hr long NCF estimate. The function *A* reaches a maximum at a drift shift of 0 ms per day; therefore, both ambient noise results (the 5 hr long computation and the summation of two 30 min NCF estimates) agree with each other. That clock drift result is 13.4 ms per day off from the boat transit clock drift estimate (Table 3-1). The secondary peaks at ±13 ms per day arise from aligning the peak from the positive lag with the peak from the negative lag.

In principle the clock drift (but not clock offset) can be estimated from situations where Eq. (4) is not a good fit to the data, a situation that arises at 20:00 [Figures 3-17 and 3-18]. At this time of the night, we believe croaker fish chorusing dominates the acoustic environment and is preferentially distributed towards deeper waters of the lower lagoon. Therefore, the peak locations do not match the predictions of Eq. (4), as seen in Figure 3-17(c). However, by summing across two 30-min EC estimates computed 24 hrs apart (at 20:00 on March 1st and 2nd) and measuring the maximum value of NCF_{total} as a function of drift estimate (Figure 3-18), the initial estimate of clock drift from ambient noise once again agrees with the long-term NCF slope estimate (Table 3-1). This result indicates that the azimuthal distribution of vocal croaker fish has remained stable over 24 hours. However, in general, using directional distributions of biological noise to time-align sensors in this fashion seems a risky proposition.

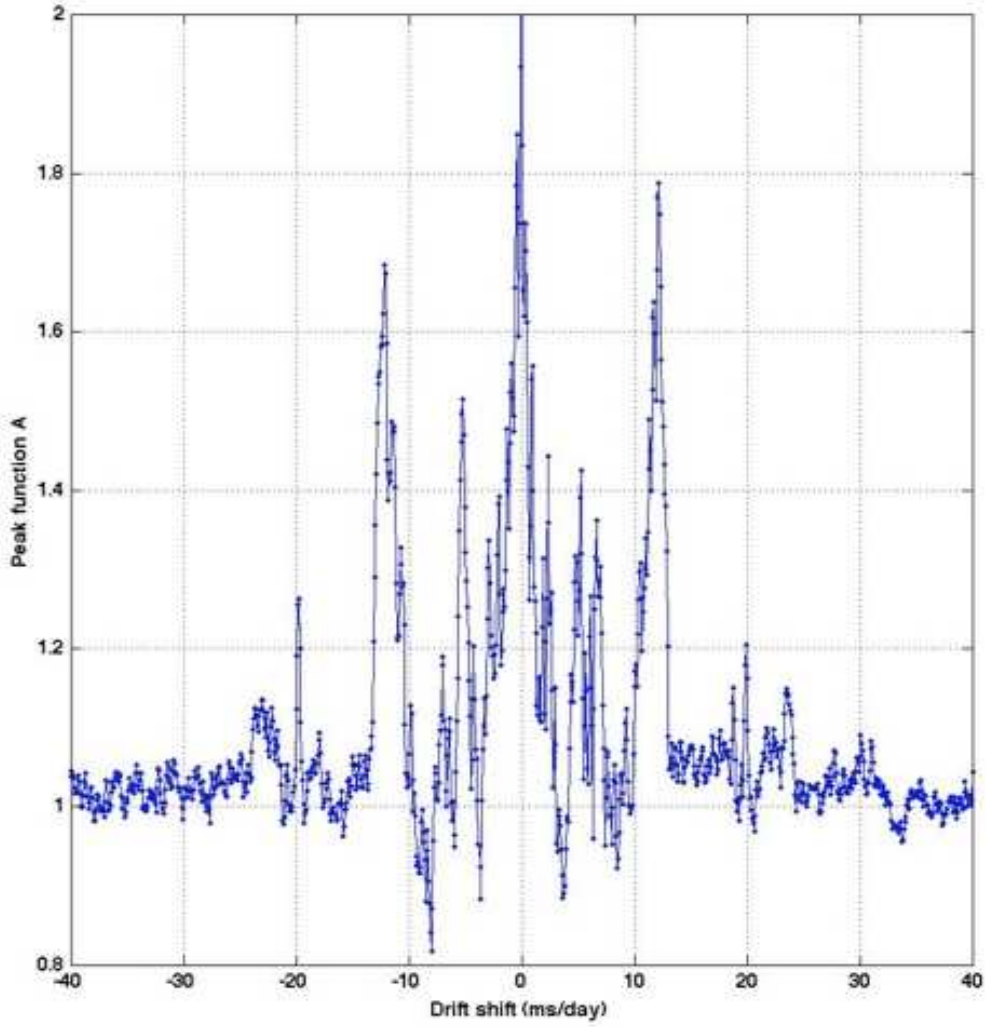

Figure 3-16: Peak amplitude $A(d\tau_d/dt)$ of NCF_{total} functions computed using EC estimates at 04:00 on March 2nd and 3rd, as a function of drift shift in ms per day. A drift shift of 0 represents a 0.2834 s per day drift estimated from boat transit data.

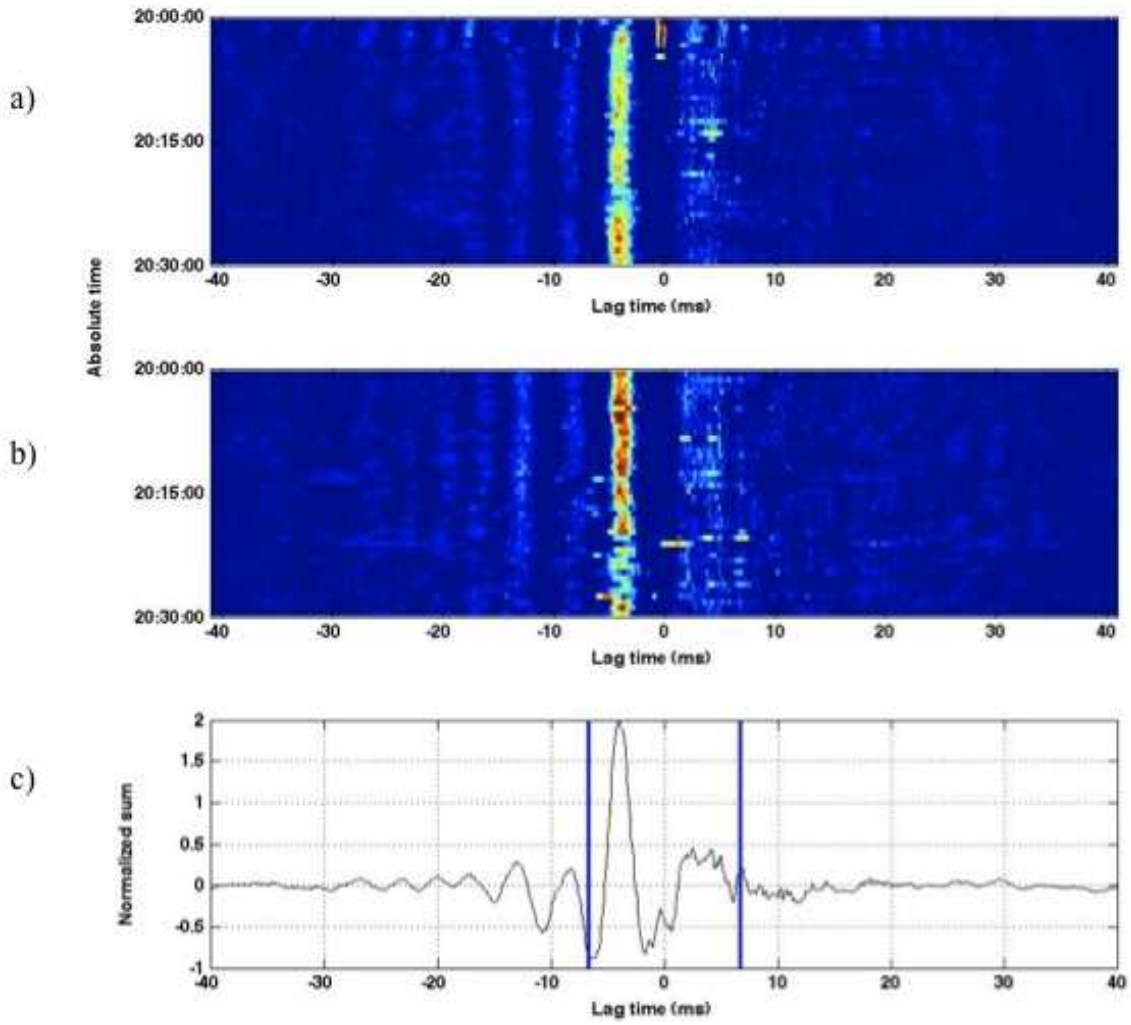

Figure 3-17: Same as Figure 3-15, but at (a)a selected $T_{win,1}$ of 20:00 on March 1st; (b) a selected$T_{win,2}$ of 20:00 on March 2nd; (c) NCF_{total} function as the vertical sum of (a) and (b). The theoretical time lags corresponding to a 10 m separation (±6.7 ms) are marked with vertical lines in (c).

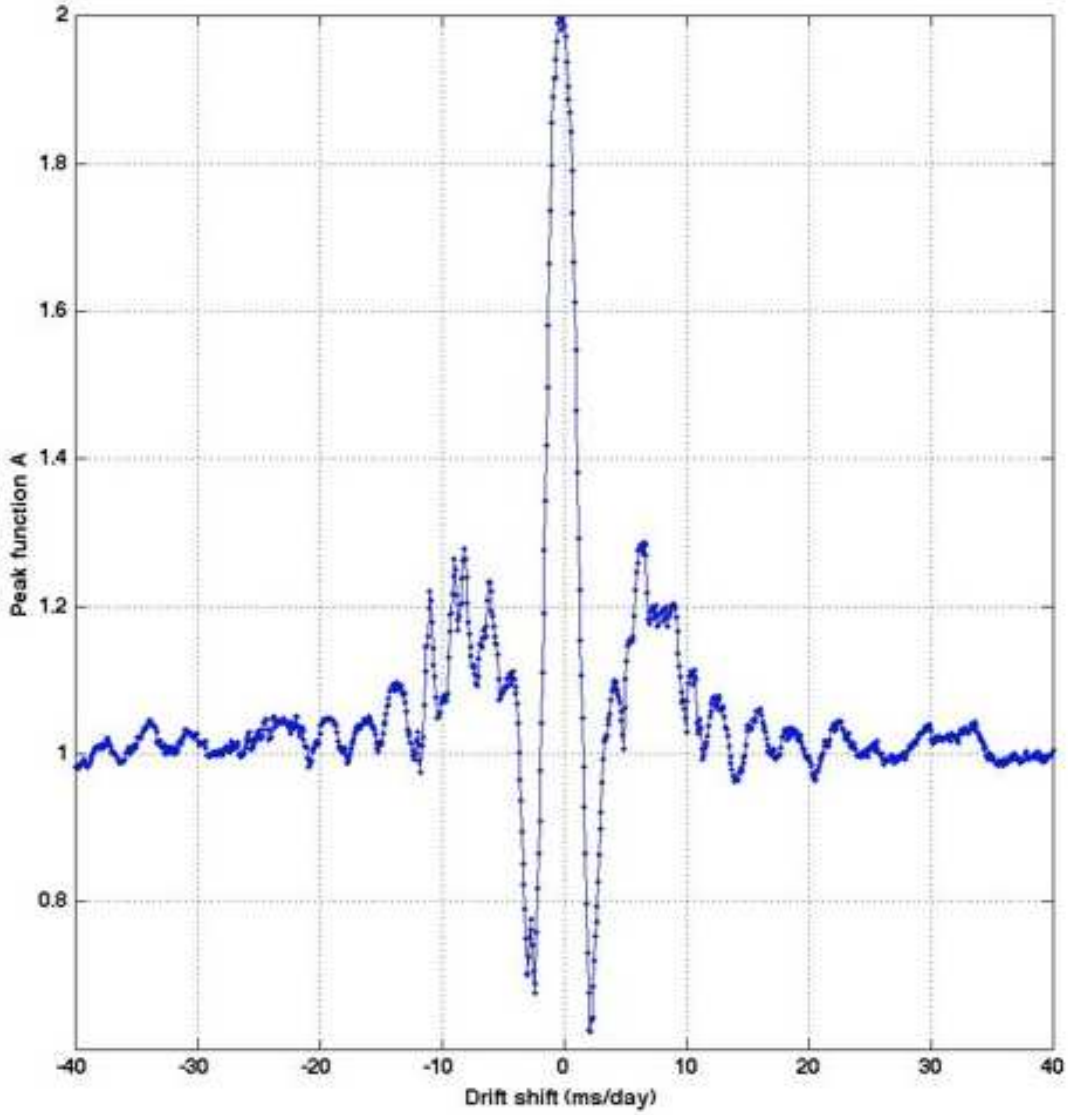

Figure 3-18: Same as Figure 3-16 but using EC estimates at 20:00 on March 1st and 2nd.

C. Estimation of clock offset τ_0 and clock drift $d\tau_d/dt$ at PP (20 m separation)

Figures 3-19 through 3-27 present results similar in format to those presented in the previous section, but applied to the case of two sensors 20 m apart at the Punta Piedra location. Figures 3-19 and 3-20 show the results of using boat transits to

estimate clock offset τ_0 and clock drift $d\tau_d/dt$, whereas Figures 3-21 through 3-27 depict the computations exploiting the background ambient noise.

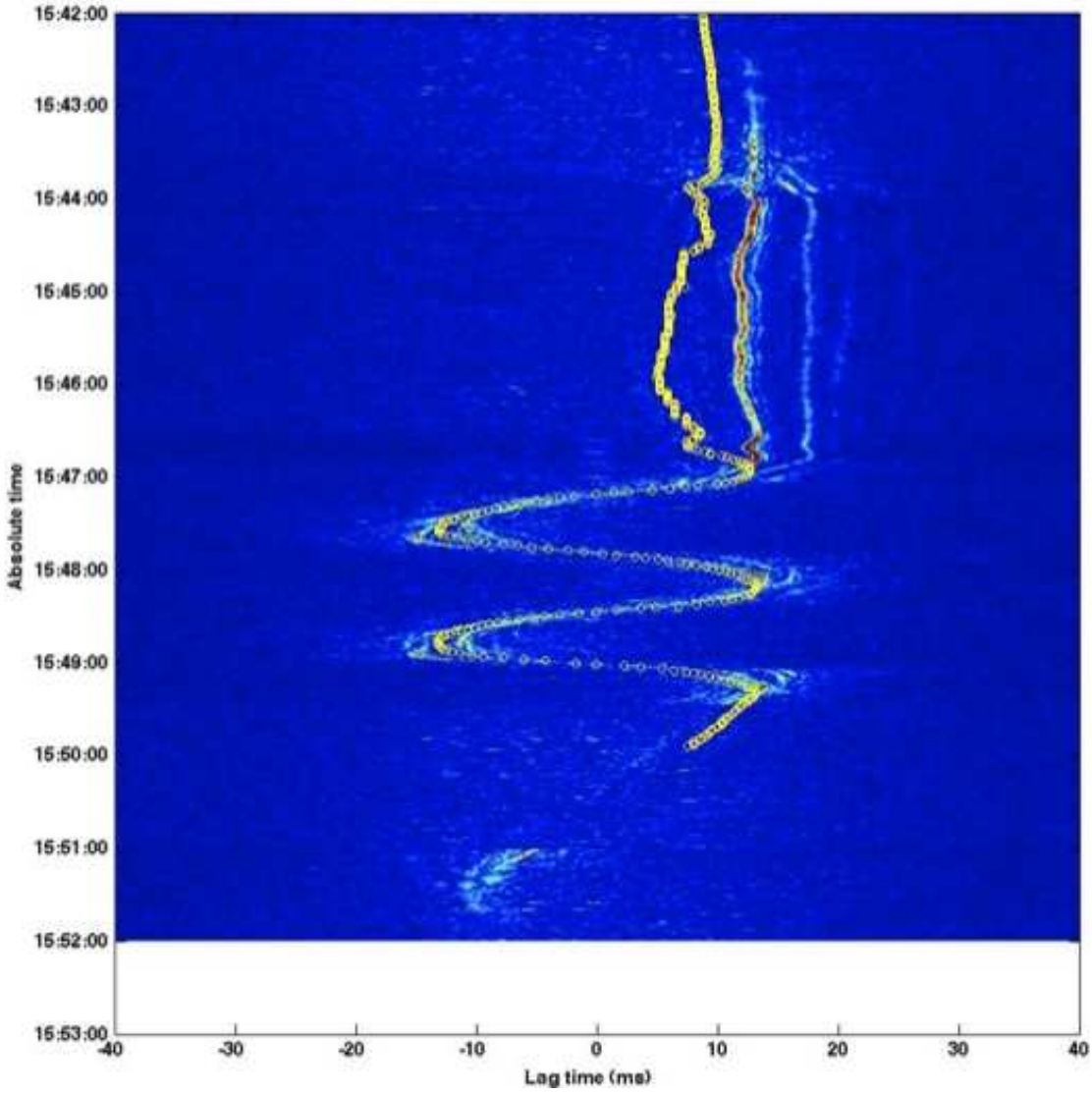

Figure 3-19: The time domain EC between two instruments 20 m apart at PP (Units 2 and 1), overlain with time delays estimated from GPS track of boat circle (yellow dots) on March 1st, 2010 between 15:42:00 and 15:52:00, assuming a clock drift of 0.70 s per day and an offset of 5.74143 s. The EC is generated by averaging 4 snapshots (0.0819 s long) of data at 75% overlap for each estimate.

Initially, the time series of Unit 2 was manually aligned by 1 s with respect to Unit 1. Computing the cross-correlation of a transient event produced a τ_{TE} of 0.2235 s between the two sensors, and the boat circling signature from March 1st at 15:42:00 (Figure 3-19) yielded a τ_{BC} of 0.0176 s, for a total clock offset τ_0 of 1.2411 s on March 1st at 15:46:33. On March 2nd between 10:39:00 and 10:51:00, the research boat transited by PP, cutting the engine and drifting in the vicinity for a period of 3 minutes, approximately between 15:43:30 and 15:46:00 (Figure 3-20). This second event, 19 hrs after the March 1st circle, was used to estimate a clock drift $d\tau_d/dt$ of -0.43 s per day.

The initial clock drift estimate between Units 1 and 2 was estimated from the lagoon's ambient noise in the same fashion as in Section V.B., by computing a 5 hour-long set of EC estimates using 40.96 seconds of data per estimate (or 500 averages of 1024 point FFTs, overlapped 75%). The results shown in Figure 3-21 use the clock offset value previously derived from boat noise (τ_0 of 1.2411 s). By measuring the rate of the drifting peaks in Figure 3-21, a relative clock drift of -0.4294 s per day was established.

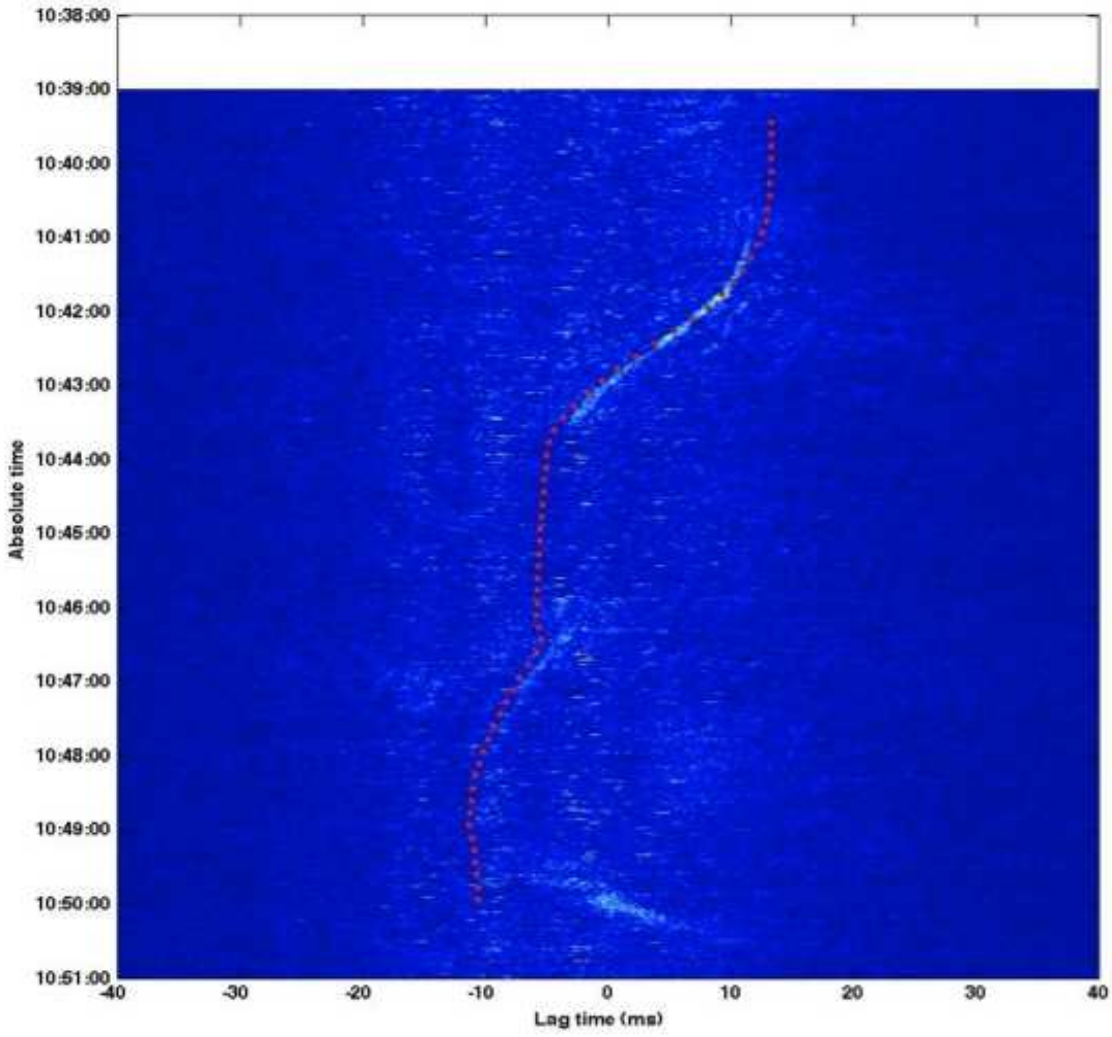

Figure 3-20: The time domain EC between two instruments 20 m apart at PP (Units 2 and 1), overlaid with time delays estimated from the GPS track of a boat transit (red dots) on March 2nd, 2010 between 10:39:00 and 10:51:00. The same clock offset and clock drift is used as in Figure 3-19. The EC is generated by averaging 4 snapshots (0.0819 s long) of data at 75% overlap for each estimate.

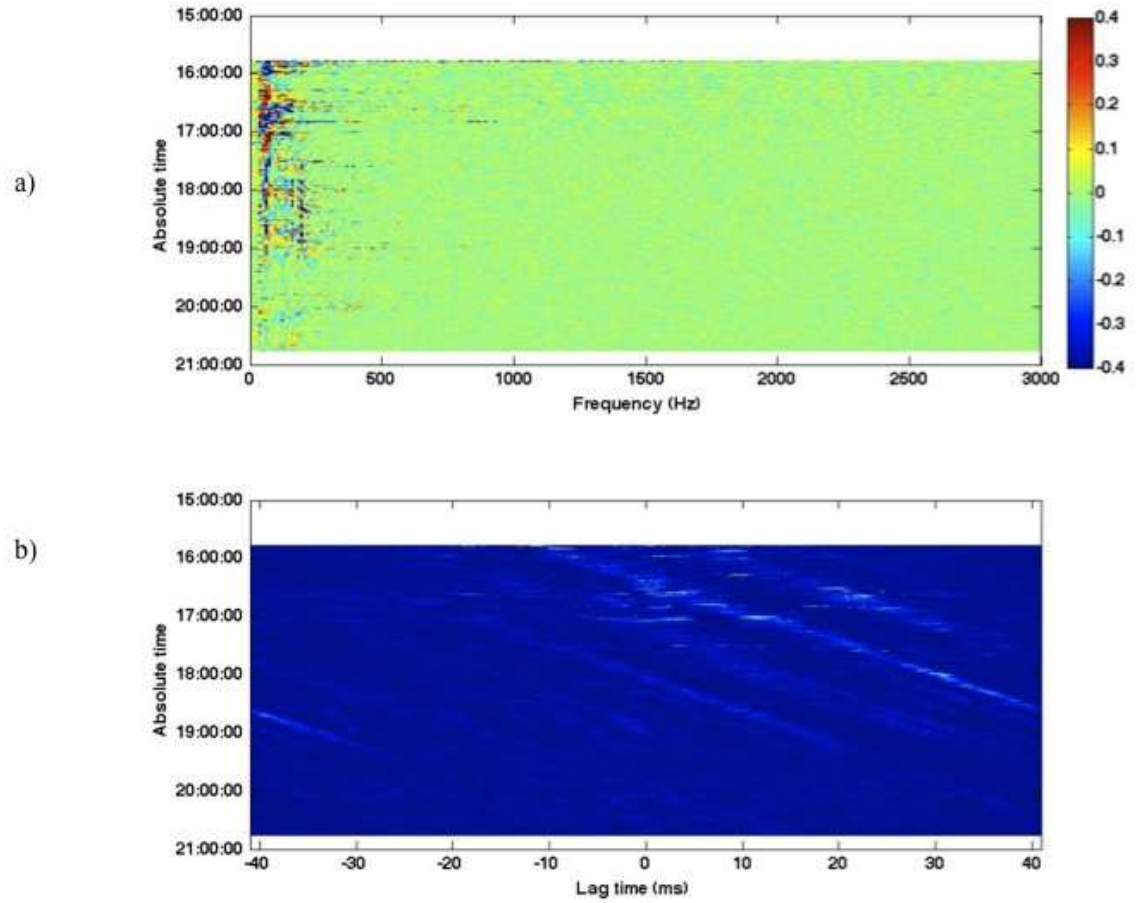

Figure 3-21: Long-term estimation of NCF between Units 2 and 1 at PP, between 15:46:00 and 20:46:00 on March 1st, 2010 using a clock offset of 2.0631 s and no clock drift: (a) frequency-domain EC; (b) time-domain EC as a function of lag time.

Using identical snapshots of data, 30 min-long estimates of EC were computed for each hour through the complete duration of the raw data file. Figure 3-22 stacks them into a long-term record in the frequency domain, while Figure 3-23 shows the associated time-domain representation. From the relationship *2L/c* and an assumed sound speed *c* of 1500 m/s, a predicted separation *L* of 20 m produces theoretical twin

peaks at ± 13.4 ms, which are indicated in the form of white, vertical bars in Figure 3-23.

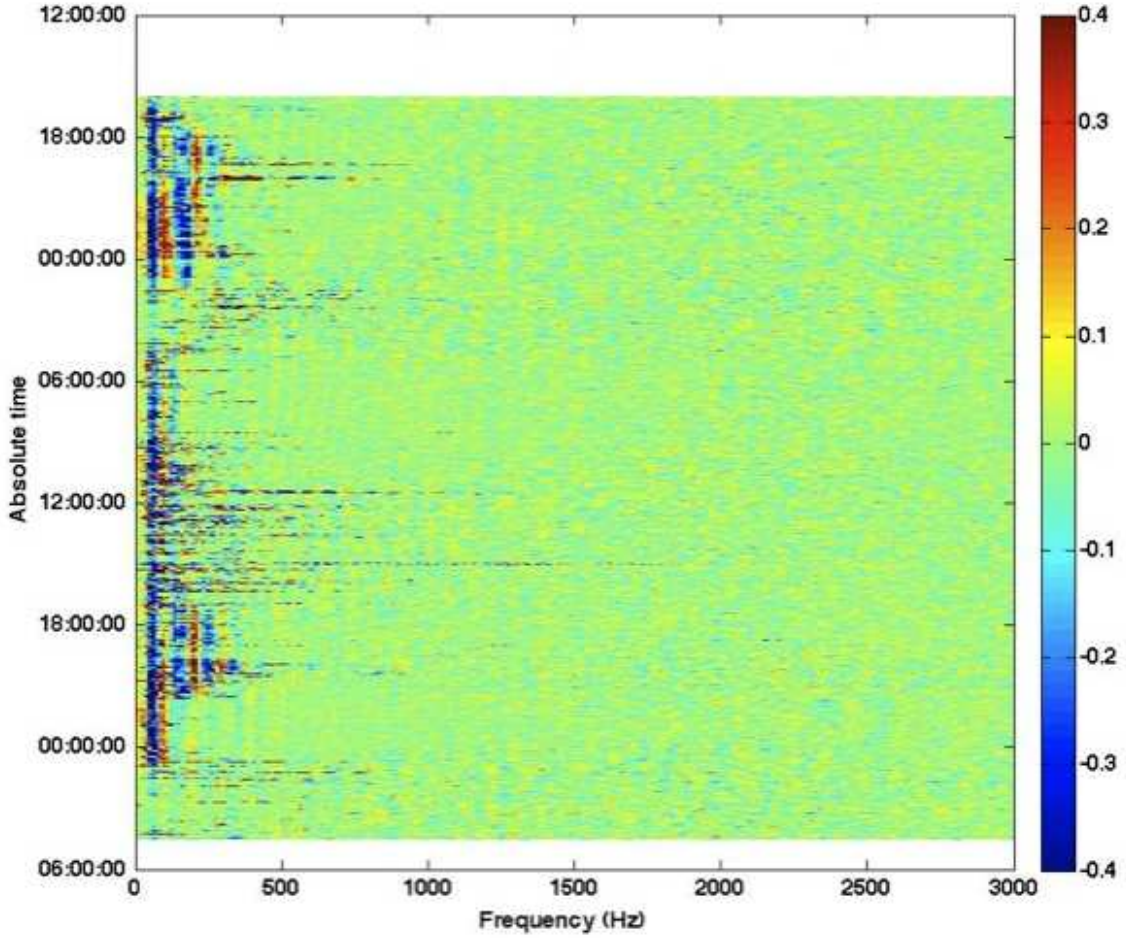

Figure 3-22: Long-term frequency-domain EC composed of 30 min estimates per hour over 37 hours, computed at Units 2 and 1 at PP, between 16:00:00 on March 1st and 04:00 on March 3rd. The EC is generated using a clock offset $\tau 0$ of 1.2411 s and clock drift of -0.4294 s per day.

From the long-term coherence plot (Figure 3-22) it is evident that only frequencies up to about 500 Hz are now contributing to the formation of a double peak

structure in the NCF (vs. 1.4 kHz at 10 m separation). Still, as was the case at 10 m separation, the greatest contributions seem to arise from frequencies below 250 Hz.

Diel variability is present again in the ambient noise temporal structure of the lagoon, with the noise field coherence becoming especially strengthened between 18:00 (local sunset) and midnight in the 50 to 250 Hz range (Figure 3-22). These evening bouts of directional activity are associated with peaks at a lag of -10 s in Figure 3-23, which represent a source co-located at the same 48.6° angle from the array's endfire direction towards the southern portion of the lagoon, as was observed in Section V.B. As was the case at 10 m separation, quick spikes of coherence from directional, transient sources are visible in Figure 3-22, especially during daylight hours, likely related to boat activity. Figure 23 also displays the same 12-hr cyclical fluctuations as Figure 3-12, indicating the effect of tides in the multipath arrival structure.

Figure 3-24 plots two examples of 30 min computations of EC at 04:00 on March 2nd [Figure 3-24(a)] and March 3rd [Figure 3-24(b)], the time periods with the cleanest relationship to Eq. (4). Figure 3-24(c) displays the resulting NCF_{total} function. While the peaks are less evident than at 10 m separation, two peaks that define the endfire noise contributions are clearly visible. The time lag between the peaks indicates that in reality, the relative separation between the two instruments on the ocean floor is 17 m, instead of the 20 m distance measured on the rope.

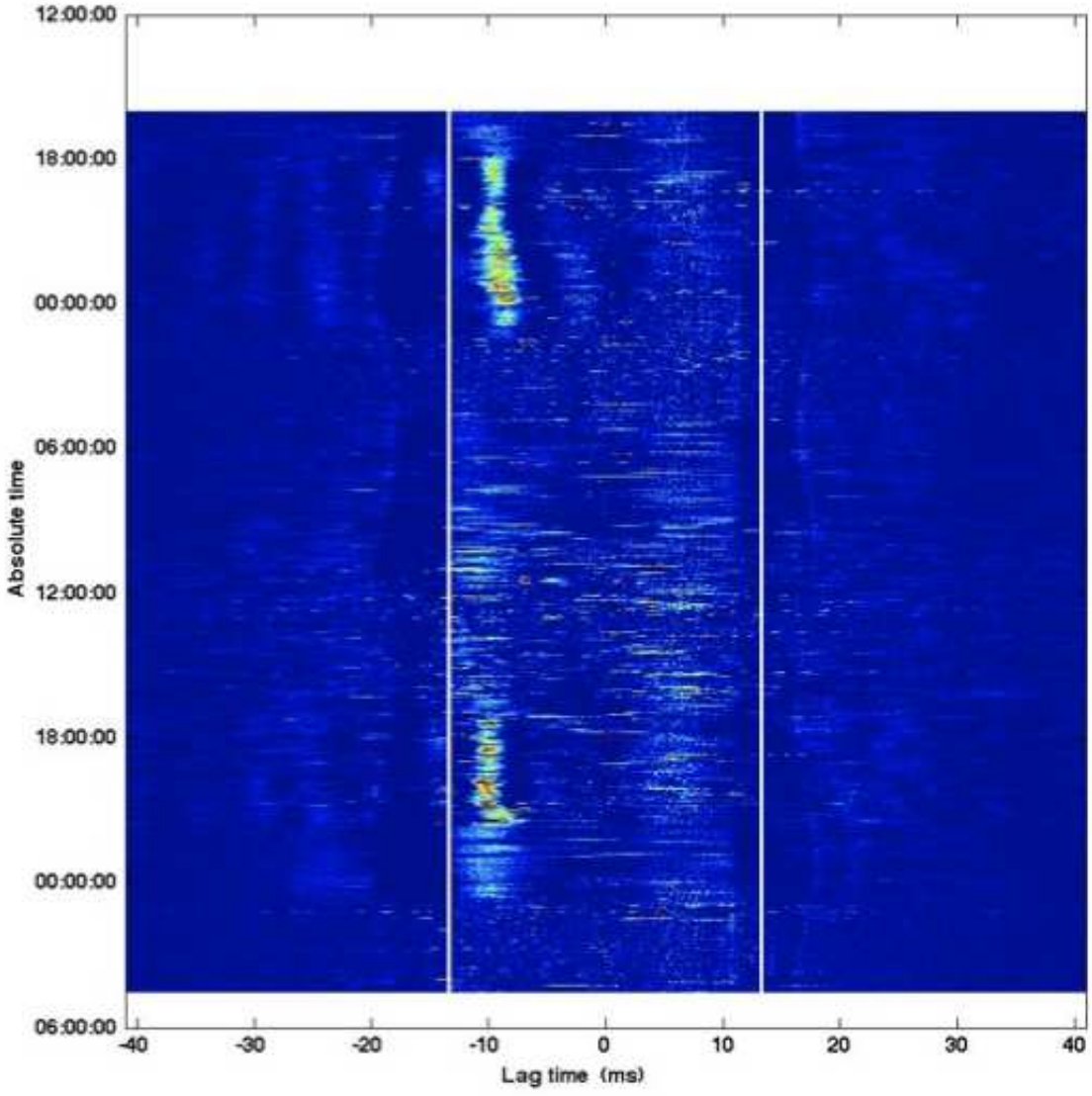

Figure 3-23: The time-domain EC representation of Fig. 3-22. The theoretical time lags corresponding to a 20 m separation (±13.4 ms) are marked with vertical lines.

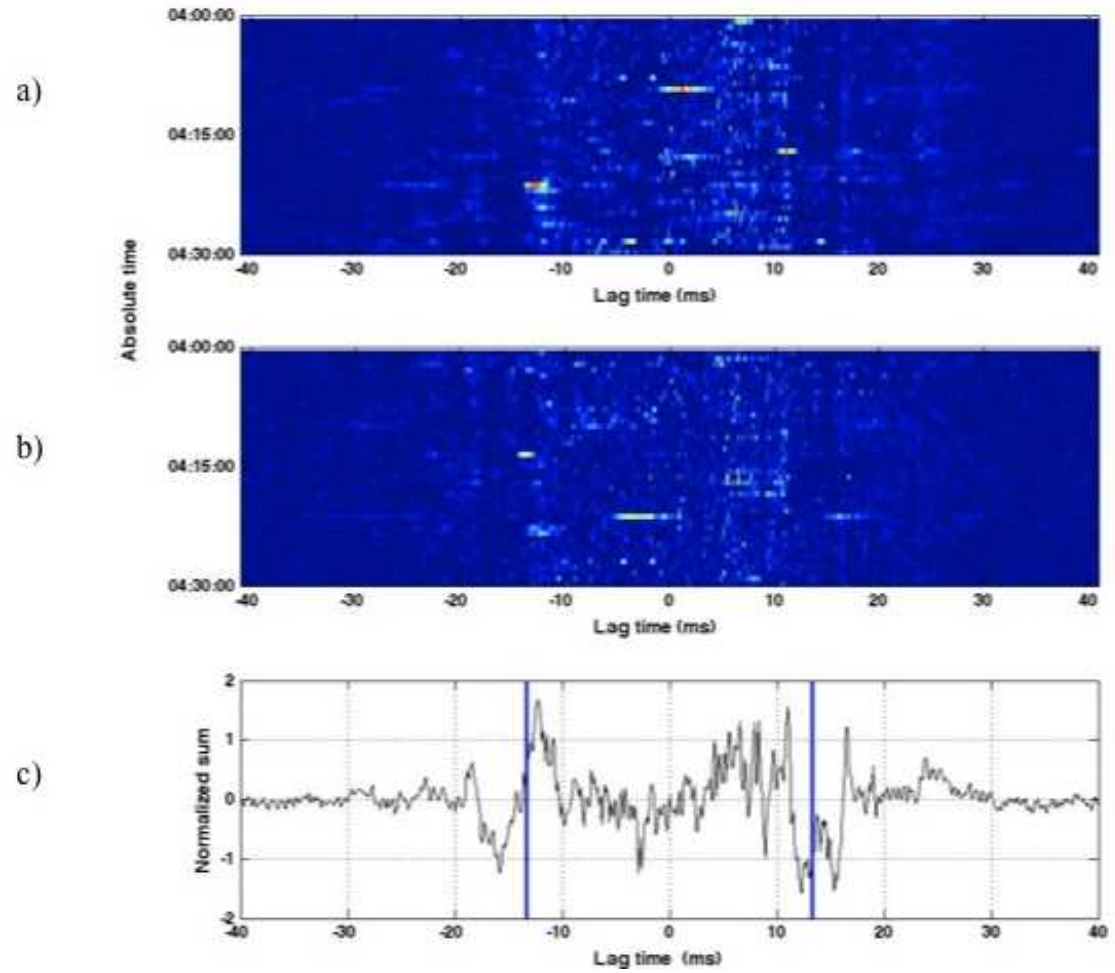

Figure 3-24: 30 min-long EC computations in the time-domain as a function of absolute time and correlation lag, generated by averaging 500 snapshots (0.0819 s long) of data at 75% overlap, for a total of 40.96 s of data for each estimate: (a)at a selected $T_{win,1}$ of 04:00 on March 2nd; (b)at a selected $T_{win,2}$ of 04:00 on March 3rd; (c) NCF_{total} function resulting from the vertical sum of (a) and (b) across lags, over time. The theoretical time lags corresponding to a 20 m separation (±13.4 ms) are marked with vertical lines in (c).

Due to the noisy structure of the NCF, the peak amplitude function $A(d\tau_d/dt)$ (Figure 3-25) fluctuates greatly, and the maximum is not as obvious as in the previous 10 m case. Two candidate peaks are present at 0 ms per day and at 4 ms per day,

signifying that the optimal clock drift $d\tau_d/dt$ could lie between the estimated -0.4294 and -0.4290 s per day (Table 3-1). The peak visible at -18.6 ms per day arises when aligning the negative peak in Figure 3-24(a) with the positive peak in Figure 3-24(b); therefore that peak can be ignored as a real clock drift candidate.

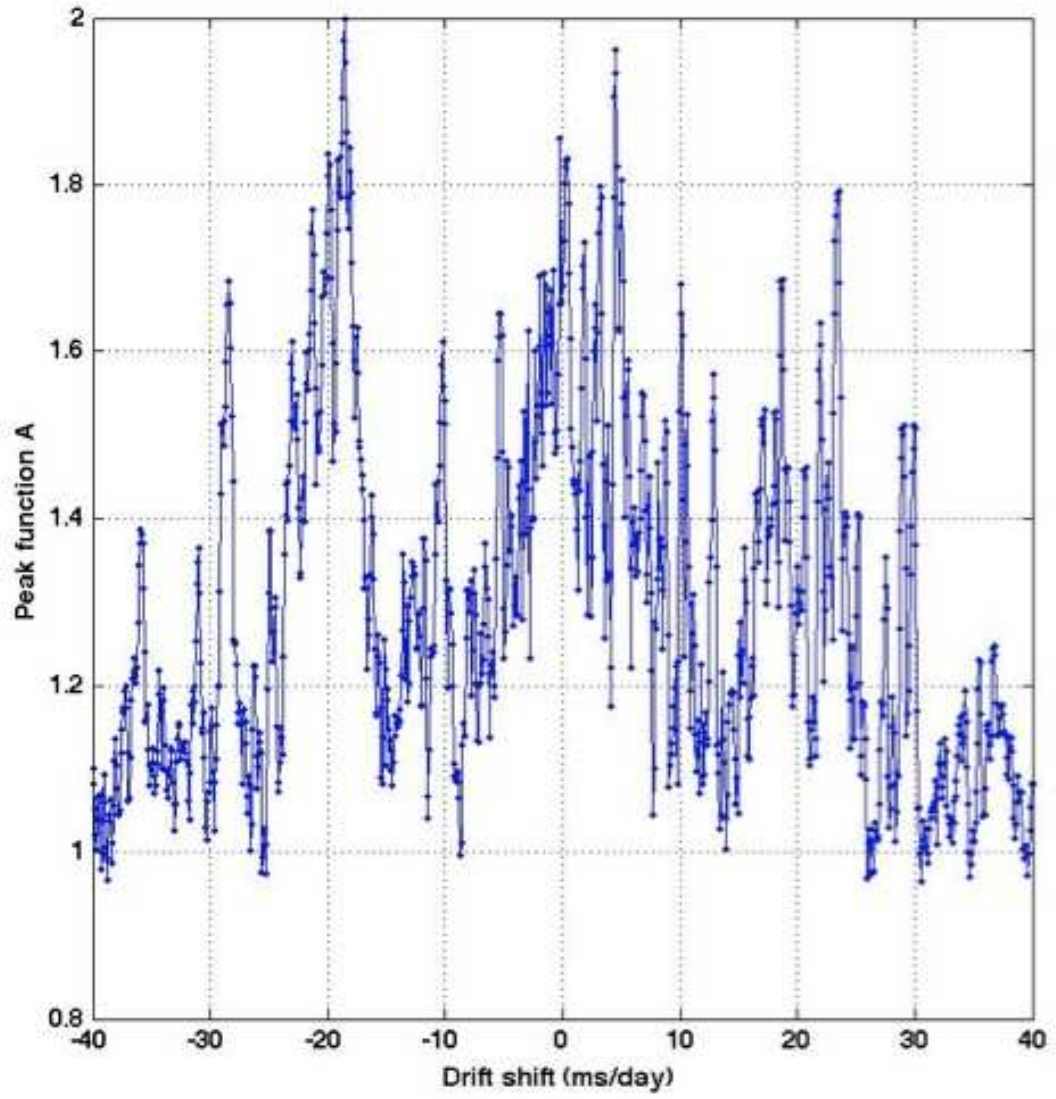

Figure 3-25: Same format as Fig. 3-16, but derived from instruments separated by 20 m.

If the fine-scale drift estimation is applied to a time period when the background noise is highly directional, for example 21:00 (Figure 3-26), the peak function *A* does peak at a drift shift of zero, indicating that the relative clock drift estimated from the drift rate of the long-term NCF is consistent with the drift estimate extracted from the summation of two short (30 min) EC computations. This value is different by only 0.6 ms per day from the estimate using motorboat events (Figure 3-27).

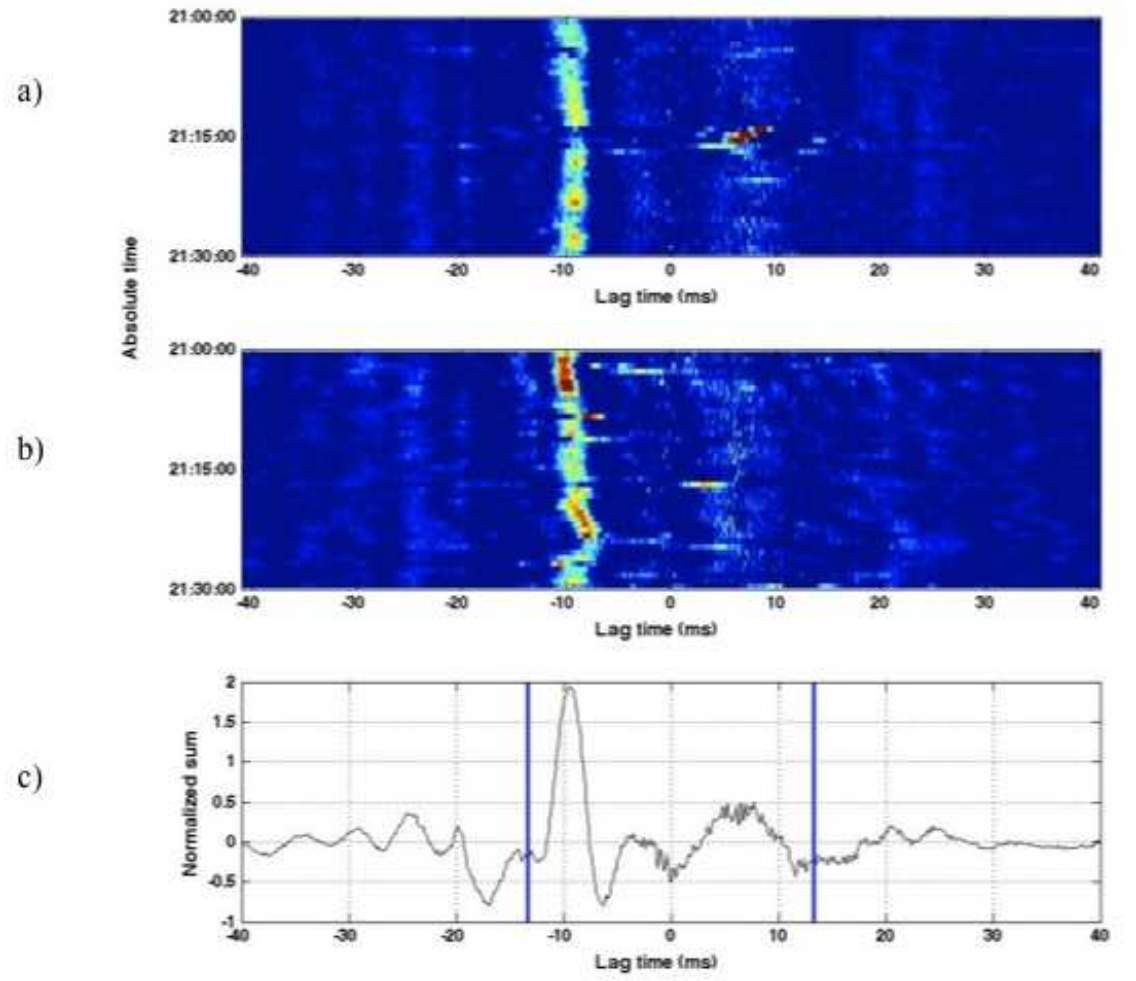

Figure 3-26: Same format as Fig. 3-24, but with different time periods used: (a) at a selected $T_{win,1}$ of 21:00 on March 1st; (b)at a selected $T_{win,2}$ of 21:00 on March 2nd; (c) NCF_{total} function resulting from the vertical sum of (a) and (b) across lags over time. The theoretical time lags corresponding to a 20 m separation (±13.4 ms) are marked with vertical lines in (c).

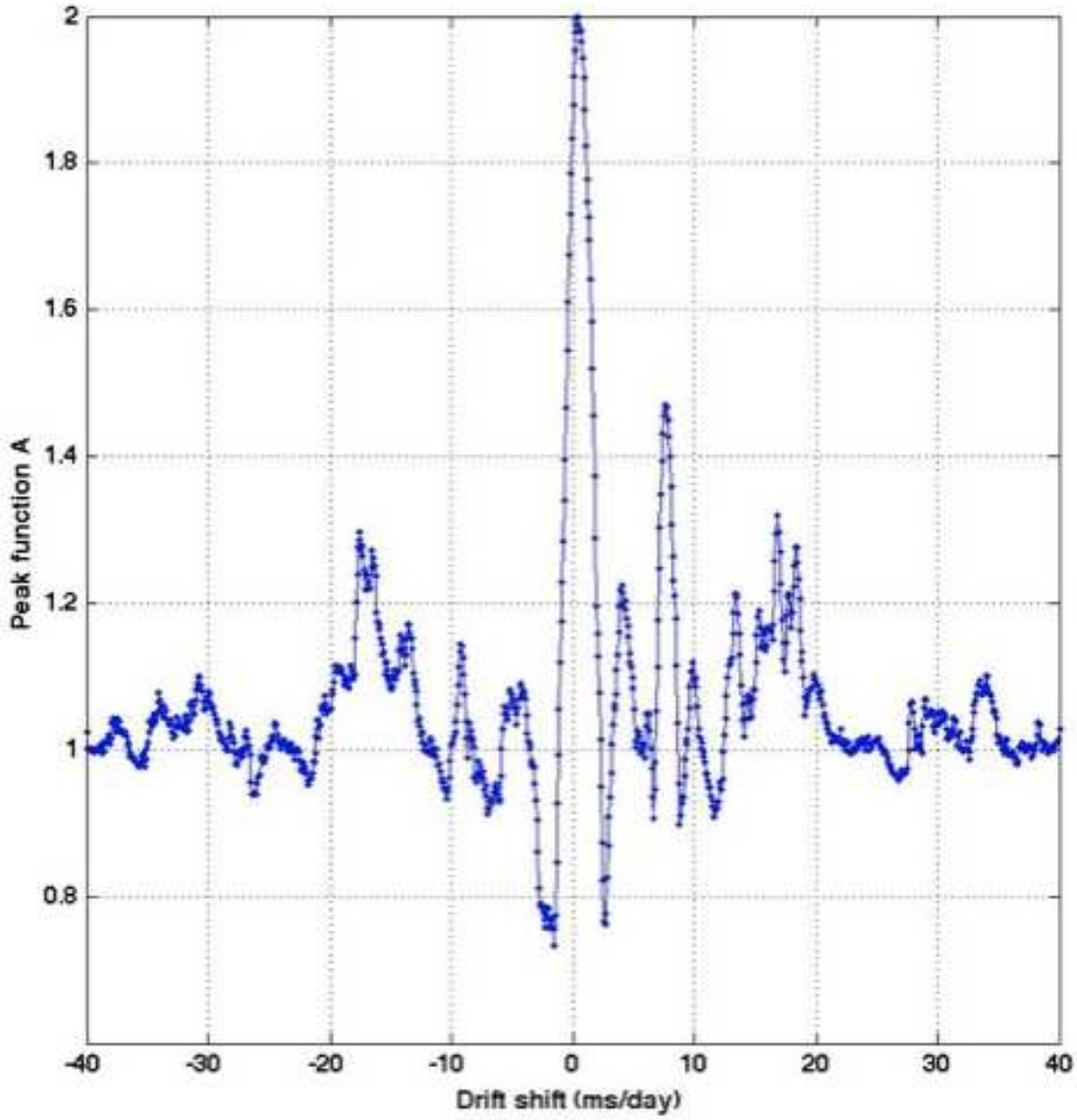

Figure 3-27: Same format as Figure 3-25, but using EC estimates at 21:00 on March 1st and 2nd.

D. Summary of results

Table 3-1: Comparison of time-synchronization results for elements at 10 m and 20 m separation using two methods: a controlled source (boat noise) or diffuse ambient noise.

		10 m separation	20 m separation
Using Boat Event	**Clock offset (τ_0)**	2.0631 s	1.2411 s
	Clock drift ($d\tau_d/dt$)	0.27 s/day	-0.43 s/day
Using Ambient Noise	**Clock offset (τ_0)**	2.0631 s	1.2411 s
	Clock drift ($d\tau_d/dt$)	0.2834 s/day	-0.4294 s/day
	Peak $A(d\tau_d/dt)$(diffuse)	0 s/day	0-0.0004 s/day
	Peak $A(d\tau_d/dt)$(directional)	0 s/day	0 s/day
Difference in clock drift between boat and ambient noise	**$\Delta d\tau_d/dt$**	13.4 ms/day	6 – 2 ms/day

VI. DISCUSSION

A. Ambient noise structure in Laguna San Ignacio

The data spectrograms suggest that at nighttime biological sources dominate the acoustic landscape in LSI (Figure 3-5). This observation agrees with conclusions obtained 25 years ago at the same site (Dalheim, 1984). A particular cluster of directional acoustic sources, located at 48.6° relative to the array's endfire direction, towards the southern (ocean-facing) end of the lagoon, was found to become active for a period of approximately six hours, starting at sunset. Such chorusing activity seems to be present on a diel cycle over two consecutive days. The repetitive nature of this

noise pattern and its spatial consistency, along with the fact that all boat activity on the lagoon ceases at sunset, suggests a non-human, biological origin, presumably croaker fish. It is known that croaker fish exhibit chorusing behaviors around the early evening, which could explain the strong spatial coherence around those times of the day (D'Spain, 2006) (Figures 3-12 and 3-22). It was croaker chorusing that provided an azimuthally-uniform source for TDGF estimates in much previous work on underwater ambient noise TDGF inversion (Sabra, 2005). Unfortunately, whereas croaker data yielded excellent TDGF estimates in earlier studies, in the data set discussed here the high directionality of this (presumed) croaker chorusing destroys the expected two-peak structure. These time periods are thus rendered unusable for the estimation of TDGF, clock offset or element spacing, although Figures 3-18 and 3-27 demonstrate that the relative clock drift can still be estimated.

A long-term inspection of ambient noise spatial coherence shows transient spikes (Figure 3-12 and 3-22) that match times when heavy boat traffic is present in the lagoon, between 10:00 and 16:00. Though not as common, such spikes sometimes occur at night and could be related to quick bouts of whales vocalizing in close proximity to the array. Mapping the frequency-domain spatial coherence over longer time scales could provide a convenient way to obtain insights about nocturnal patterns in gray whale vocal activity.

Due to the large changes in the ambient noise structure that occur throughout the day, it is not surprising that the quality of the double-peak structure predicted by Eq. (4) changes throughout the day as well. It was empirically determined that the

period between 01:00 and 05:00 yielded the best TDGF estimate. Over the duration of one single data file (40 hrs) this trend was repeated over two consecutive days. Longer-term inspections of this data set could be investigated further to determine if this cyclical pattern holds over periods of multiple days or weeks. In addition, the spatial distribution of the directional sources (group of croaker fish) could also be monitored over longer times to determine whether the directionality shifts over the course of a month.

However, even at times that yield the best TDGF estimate (Figures 3-15 and 3-24), the true element spacing does not perfectly match the measured distance along the array rope, which indicates that despite efforts to keep the horizontal deployment line perfectly straight, the combination of strong tides and currents distort the rope.

B. Comparison between 10 m and 20 m element separation

The sharpness of the TDGF direct-path peaks in the NCF is determined by the frequency bandwidth contributing to the spatial coherence, which can be seen in detail in the frequency domain EC plots (Figures 3-12 and 3-22). At 10 m separation, frequencies up to 1400 Hz present some degree of coherence (Figures 3-11, 3-12, 3-13 and 3-14) whereas at 20 m separation, the coherence is only evident up to about 500 Hz (Figure 3-22). The bandwidth loss between 500-1400 Hz that occurs when extending the separation from 10 m to 20 m highlights the large transmission loss encountered in this complex shallow water environment.

Even with this high-frequency loss the distinctive double-peak structure can still be detected in the time-domain EC images corresponding to both 10 m and 20 m configurations (Figures 3-12, 3-13 and 3-23), so most of the information to create them must stem from the lower frequencies. The noise spectrum between 20-250 Hz in particular presents the strongest spatial coherence at almost all times of day. Wind driven ambient noise is likely a dominant mechanism at those frequencies during the daytime, although diel biological sources can dominate for several hours during the night. Frequencies above 500 Hz contribute little in resolving the timing peaks; thus higher-frequency sources like snapping shrimp are not the main driver of the spatial coherence.

C. Comparison between transient source and ambient noise synchronization

Extracting a TDGF estimate from two different types of sound sources requires appropriate averaging timescales. When utilizing a directional, transient event like circling boats, a small number of snapshots of data (four) were found to be ideal for capturing quick changes in the source-receiver path. Conversely, using the lagoon's ambient noise requires about 100 times more averaging snapshots (500) to build a strong enough coherence from which double peaks can be extracted.

A two-step approach to computing the clock offset from boat noise (manual alignment of time series, followed by cross correlation of transient and NCF of boat events) was successful at both 10 m and 20 m separation. This clock offset estimate was used as an initial basis for the long-term computations of ambient noise time

synchronization. Therefore, it could be argued that the ambient noise timing estimates are not truly independent of the boat-derived estimates. However, the ambient noise techniques would have still been possible without prior knowledge of clock offset, since a sufficiently large N_{fft} window was applied to allow detection of a horizontal shift in the peak structure of up to ± L/c. After applying the clock offset estimate from the boat data to the ambient noise computations, no further corrections were necessary, hence noise from boat circles also presented an adequate source for estimating clock offset and the clock drift between the sensors was close to linear with time.

Clock drift estimates computed via long-term ambient noise calculations produced approximations that were only 13.4 ms per day and 0.6 ms per day (at 10 and 20 m, respectively) off from those derived using two boat events more than 12 hours apart (Table 3-1).

In the case of 10 m separation, the ambient noise clock drift estimation from the long-term slope of the double peaks produced an estimate of 0.2835 s per day, which is 13.4 ms per day off from the boat noise drift estimate (0.27 s per day). This result was consistent with an even longer-term measurement that found a zero drift shift in the peak A function, whether diffuse ambient noise (Figure 16) or directional noise (Figure 3-18) was used (Table 3-1). At 20 m separation, the clock drift estimates from boat noise and long-term ambient noise are off by 0.6 ms per day. It was more difficult to distinguish the exact peak in the A function using diffuse ambient noise (Figure 3-25), therefore only defining a range between two candidate peaks (0 to 4 ms

per day) was possible (Table 3-1). However taking advantage of a directional noise source that remains spatially fixed over the course of two days (Figure 3-27), the clock drift between the two 20 m-separated sensors was shown to match the 5 hr NCF prediction and was consistent with the boat-derived estimates.

VII. CONCLUSION

Ambient noise in Laguna San Ignacio, Baja California, Mexico, was recorded for 30 days in 2010 in 8-12 m deep water. The spectral content of and source mechanisms behind the ambient noise at this location remain consistent with those reported 25 years previously by Dahlheim *et al*.

Autonomous elements of a horizontal array, with elements separated by 10 m and 20 m, were synchronized to within 4 ms per day, using standard methods (a directional boat noise source) and more recent noise cross-correlation methods. The standard method exploited a controlled acoustic source at known locations, in this case a boat outfitted with GPS circling around the array at a radius of about 100 m. The second method exploited the lagoon's ambient noise to create a noise correlation function (NCF), from which a double-peak structure can be extracted. From Eq. (4) and plots like Figure 15, the element spacing, initial clock offset, and clock drift were determined. The NCF was processed several different ways, by pre-whitening the noise spectrum, calculating its derivative with respect to time and retaining the sign of the raw time series only. The equalized noise covariance $EC_{ab}(\omega)$ and its signed

counterpart $SC_{ab}(\omega)$ were selected as the best overall tools for resolving a clear double-peak structure at array separations of a few tens of meters. Clock offsets and drifts measured via these two methods are consistent with predictions produced from transient boat sounds.

VIII. ACKNOWLEDGEMENTS

Chapter 3, in part is currently being prepared for submission for publication of the material. Guerra, Melania; Thode, Aaron M. The dissertation author was the primary investigator and author of this material.

This work was supported by the Laguna San Ignacio Ecosystem Science Project (LSIESP) and The Ocean Foundation. We wish to thank Steven Swartz and Jorge Urban for incorporating this acoustic research into the work permits issued to the LSIESP. We are thankful to Rob Glatts for his assistance preparing the hardware in the lab. Delphine Mathias (SIO/UCSD), Diana Ponce (UCSD), Dawn Grebner (SIO/UCSD) and Anaid Urban (UNAM) assisted with the fieldwork. We would also like to thank Stephanie Fried and Shane Walker (SIO) for advice on processing ambient noise cross-correlation data. We are grateful to my Ph.D. committee members William Kuperman, Ann E. Bowles, Jay Barlow, Truong Nguyen and Sarah Mesnick for valuable and thoughtful comments on the manuscript. The authors would like to thank the boat drivers and all personnel at Kuyima Ecoturismo in Laguna San Ignacio for providing accommodations during the fieldwork, for their generous help lending us

anchors and for their skilled boat services that allowed for this data collection to take place.

IX. REFERENCES

Au, W. W. L., and Banks, K. (**1998**). "The acoustics of the snapping shrimp (*Synalpheus parneomeris)* in Kaneohe Bay," J Acoust Soc Am **103**, 41-47.

Brooks, L. A., and Gerstoft, P. (**2009**). "Green's function approximation from cross-correlations of 20-100 Hz noise during a tropical storm," J Acoust Soc Am **125**, 723-734.

Cato, D. H. (**1998**). "Simple methods of estimating source levels and locations of marine animal sounds," J Acoust Soc Am **104**, 1667-1678.

Clark, C. W., Ellison, W. T., Southall, B. L., Hatch, L., Van Parijs, S. M., Frankel,A., and Ponirakis, D. (**2009**). "Acoustic masking in marine ecosystems: intuitions, analysis, and implication," Marine Ecology Progress Series **395**, 201-222.

Cox, H. (**1973**). "Spatial correlation in arbitrary noise fields with application to ambient sea noise," J Acoust Soc Am **54**, 1289-1301.

Cron, B. F., and Sherman, C. H. (**1962**). "Spatial-correlation functions for various noise models," J Acoust Soc Am **34**, 1732-1736.

D'Spain, G. L., and Batchelor, H. H. (**2006**). "Observations of biological choruses in the Southern California Bight: A chorus at mid frequencies," J Acoust Soc Am **120**, 1942-1955.

Dahlheim, M. E., Fisher, H. D., and Schempp, J. D. (**1984**). *Sound production by the*

gray whale and ambient noise levels in Laguna San Ignacio, Baja California Sur, Mexico. In: Jones, M.L., Swartz, S.L. and Leatherwood, S. (eds), *The gray whale (Eschrichtius robustus)*, p 511-541. Academic Press, Orlando, FL, 600p.

Fried, S. E., Kuperman, W. A., Sabra, K. G., and Roux, P. (**2008**). "Extracting the local Green's function on a horizontal array from ambient ocean noise," J Acoust Soc Am **124**, 183-188.

Greene, C. R. (**1987**). "Characteristics of oil industry dredge and drilling sounds in the Beaufort Sea," J Acoust Soc Am **82**, 1315-1324.

Greene, C. R., McLennan, M. W., Norman, R. G., McDonald, T. L., Jakubczak, R. S., and Richardson, W. J. (**2004**). "Directional frequency and recording (DIFAR) sensors in seafloor recorders to locate calling bowhead whales during their fall migration," J Acoust Soc Am **116**, 799-813.

Hodgkiss, W. S., Gerstoft, P., and Murray, J. J. (**2003**). "Array shape estimation from sources of opportunity," Oceans 2003 MTS/IEEE: Celebrating the Past...Teaming toward the Future, 582-585.

Jones, M. L., Swartz, S. L., and Leatherwood, S. (**1984**). *The gray whale (Eschrichtius robustus)*. Academic Press, London, i-xxiv, 1-600.

Knudsen, V. O., Alford, R. S., and Emling, J. W. (**1948**). "Underwater ambient noise," Journal of Marine Research **7**, 410-429.

Lobkis, O. I., and Weaver, R. L. (**2001**). "On the emergence of the Green's function in the correlations of a diffuse field," J Acoust Soc Am **110**, 3011-3017.

Nosal, E. M., and Frazer, L. N. (**2007**). "Modified pairwise spectrogram processing for localization of unknown broadband sources," IEEE J. Ocean. Eng. **32**, 721-728.

Roux, P., Kuperman, W. A., and Grp, N. (**2004**). "Extracting coherent wave fronts

from acoustic ambient noise in the ocean," J Acoust Soc Am **116**, 1995-2003.

Roux, P., Sabra, K. G., Kuperman, W. A., and Roux, A. (**2005**). "Ambient noise cross correlation in free space: Theoretical approach," J Acoust Soc Am **117**, 79-84.

Sabra, K. G., Roux, P., and Kuperman, W. A. (**2005a**). "Arrival-time structure of the time-averaged ambient noise cross-correlation function in an oceanic waveguide," J Acoust Soc Am **117**, 164-174.

Sabra, K. G., Roux, P., and Kuperman, W. A. (**2005b**). "Emergence rate of the time domain Green's function from the ambient noise cross-correlation function," J Acoust Soc Am **118**, 3524-3531.

Sabra, K. G., Roux, P., Thode, A. M., D'Spain, G. L., Hodgkiss, W. S., and Kuperman, W. A. (**2005c**). "Using ocean ambient noise for array self-localization and self-synchronization," IEEE J. Ocean. Eng. **30**, 338-347.

Shapiro, N. M., and Campillo, M. (**2004**). "Emergence of broadband Rayleigh waves from correlations of the ambient seismic noise," Geophysical Research Letters **31**, L07614.

Sonntag, R., Ellison, W. T., Clark, C. W., Corbit, D. R., and Krogman, B. D. (**1986**). "A description of a tracking algorithm and its application to bowhead whale acoustic location data collected during the spring migration near Point Barrow, Alaska 1984-85," International Whaling Commission Report of the Commission **36**, 299-310.

Thode, A. M., D'Spain, G. L., and Kuperman, W. A. (**2000**). "Matched-field processing, geoacoustic inversion, and source signature recovery of blue whale vocalizations," J Acoust Soc Am **107**, 1286-1300.

Thode, A. M., Gerstoft, P., Burgess, W. C., Sabra, K. G., Guerra, M., Stokes, M. D., Noad, M., and Cato, D. H. (**2006**). "A portable matched-field processing system using passive acoustic time synchronization," IEEE J. Ocean. Eng.

31, 696-710.

Tiemann, C. O., and Porter, M. B. (**2003**). "Automated model-based localization of sperm whale clicks," Oceans 2003 MTS/IEEE: Celebrating the Past...Teaming toward the Future, 821-827.

Urban R, J., Rojas-Bracho, L., Perez-Cortes, H., Gomez-Gallardo, A., Swartz, S. L., Ludwig, S., and Brownell, R. L., Jr. (**2003**). "A review of gray whales (*Eschrichtius robustus*) on their wintering grounds in Mexican waters,"Journal of Cetacean Research and Management **5**, 281-295.

Weaver, R. L., and Lobkis, O. I. (**2004**). "Diffuse fields in open systems and the emergence of the Green's function," J Acoust Soc Am **116**, 2731-2734.

Wiggins, S. (**2003**). "Autonomous acoustic recording packages (ARPs) for long-term monitoring of whale sounds," Marine Technology Society Journal **37**, 13-22.

Winant, C. D., and de Velasco, G. G. (**2003**). "Tidal dynamics and residual circulation in a well-mixed inverse estuary," Journal of Physical Oceanography **33**, 1365-1379.

CHAPTER 4:

Summary of the Dissertation

I. SUMMARY OF THE DISSERTATION

This dissertation has presented additional insights to the growing body of work concerning how ambient noise (including its anthropogenic components) influences marine mammal passive acoustic monitoring (PAM). Specifically, Chapter 2 of this dissertation investigated the impact of seismic airgun surveys on the diffuse ambient noise spectrum in shallow Arctic waters, which in turn impacts the effectiveness of PAM efforts. Chapter 3 examined how certain features of the diffuse ambient noise background could be exploited as a time-synchronization tool for PAM technologies.

With those final goals in mind, both shallow-water field sites studied in this thesis involved the seasonal presence of large groupings of baleen whales, along with human activities that also produce sound. These anthropogenic sources contribute to, and occasionally even dominate, the local underwater acoustic scene. Although the temporal, spatial and spectral features of the ambient noise background differ significantly between the Alaskan North Slope and the Baja peninsula, this work has demonstrated that acoustic noise can be, colloquially speaking, “both a blessing and a curse,” to marine mammal PAM research: on the one hand, ambient noise can obscure the ability to effectively apply PAM methods as a mitigation tool (Chapter 2). On the other hand, even diffuse ambient noise embeds information that provides a convenient way to time-synchronize lighter and cheaper independent recorders into array form, potentially expanding the capabilities of reliable PAM systems (Chapter 3).

These conclusions still overlook many aspects about impact of anthropogenic noise on the animals' acoustic ecology, which, as stated initially, constitutes the ultimate motivation for much marine mammal PAM research. Nevertheless, with these results as a starting point, this chapter examines the potential repercussions, as well as recommends complementary directions for future work.

II. IMPLICATIONS OF DISSERTATION RESULTS

In light of the findings from the previous two chapters, I here derive their potential implications to how PAM research is conducted, how the resulting PAM science is interpreted, and how regulatory policies are implemented for mitigation.

Using the methodology developed in Chapter 2, it is now possible to establish the quantified contribution of reverberation arising from industrial impulsive sources to the overall underwater ambient noise budget. This work fills in the gap from previous research that had evaluated this question for continuous sources (Hatch *et al.*, 2008). The results presented here have already helped raise awareness in the bioacoustics community about the important role reverberation can play when developing and standardizing noise level metrics for impulsive noise. Moreover, Chapter 2 raises questions regarding the efficacy of PAM to adequately monitor vocally-active marine mammals in close ranges to a seismic source vessel. Given the large budgets that oil and gas companies dedicate to remaining compliant with federally-imposed marine mammal mitigation practices (Weir and Dolman, 2007), the design of PAM survey protocols should incorporate considerations about the potential

impact from reverberation at various ranges from the source. In general, this evidence reinforces the notion that PAM data should be treated only as a conservative estimate of incidental takes from sound exposure, not as a conclusive assessment.

This reverberation work did not directly explore what the associated repercussion of reduced communication space would be on the acoustic ecology of the surrounding marine life (Clark *et al.*, 2009). However, if PAM recorders were to be considered a proxy for sound exposure to individual animals, the great temporal and spatial variability in metrics like the minimum level metric (MLM) and the reverberation metric (RM) contribute to mounting evidence (Ellison *et al.*, 2012) that rebuffs the current regulatory strategy of utilizing a single, maximum value as a reliable assessment of potential long-term impacts. This supplementary proof also supports the recent shift towards more comprehensive and context-based evaluation frameworks such as in Ellison *et. al.* (2012).

Even as the interpretation of acoustic data becomes more challenging, the actual deployment of these systems may become ever easier. As stated in Chapter 3, arrays built out of autonomous acoustic recorders present many advantages over the traditional, bulky, cabled kind, for example: reduced cost, freedom of configuration and more manageable deployments. The time-synchronization technique presented here may make arrays of independent acoustic sensors more attractive to researchers in the marine bioacoustics community wanting to work with variable array configurations, facilitating and potentially expanding the use of such PAM systems. This surge in access to cheaper acoustic instrumentation may especially benefit small

and relatively new acoustic monitoring projects (like LSIESP), which likely rely on limited resources and cannot finance large vessels to deploy substantial cabling. This promising technology could also boost interest in acoustic monitoring at universities and research institutions in developing countries (like UABCS), driving them to establish local acoustic monitoring efforts, where students could apply their practical research skills, while experiencing a more integrated scientific education.

III. RECOMMENDATIONS FOR FUTURE WORK

Given economic pressures world-wide, the two industries that drive the shallow-water acoustic sources described here, oil and gas exploration (Chapter 2) and whale-watching tourism (Chapter 3), will certainly only increase in the forthcoming decades (Heitmeyer *et al.,* 2003). Thus the work begun here will undoubtedly continue into the future. Based on my hands-on experience in the field, and the analytical methodologies I developed in Chapters 2 and 3, I offer the following suggestions for improving and implementing future research on both topics.

Since the acoustic monitoring effort that produced the Beaufort Sea data used in Chapter 2 has been ongoing since 2006 (Ireland*et al.*, 2009), it would be interesting to extend the reverberation analysis to the open water seasons of other years before and after 2008, in order to evaluate true long-term trends of the Arctic acoustic environment and the lasting effects of the seismic survey contribution on it. In particular, it would be telling to test the linear regression model correlating wind speed and noise levels (in the form of the MLM) on a year with little-to-no local seismic

survey presence, when the acoustic scene was as close to pre-industrial conditions as possible, providing a continuous, multi-week record of the naturally-occurring background noise levels during summer months. (For example, the summer of 2011 was a season of little local seismic activity on the Alaskan North Slope, and preliminary results indicate that it was possible to detect faint signatures of very distant seismic shots to the north-west of the Beaufort Sea [Thode *et al.*, in prep.]). Validating the correlation between wind speed and noise in the absence of seismic sources nearby would reinforce the conclusions that the reverberation metric truly represents an exclusive estimate of the anthropogenic contribution.

More attention should also be paid to the evolution of the last impulse shot before a shut-down procedure (or the last shot before turning the vessel around). Performing a high temporal resolution (i.e. second by second) analysis of this "final" SEL would provide a means for deriving a “reverberation constant” (Schroeder, 1965), a term used in room acoustics to describe the decay in time of the energy of a disturbance until reaching background levels (as a function of distance to the source). Those background levels however, would still contain an anthropogenic component from the source vessel propeller, an aspect not considered in Chapter 2. Here, all of the non-wind contribution to noise was treated as remnant energy from the seismic pulse, when in reality it is likely that at least the immediate seismic vessel itself is generating a portion of that noise. In view of imminent increases in commercial shipping traffic through the Arctic (Corbett *et al*., 2010; Wilson *et al*., 2004), it would seem imperative to improve the methodology to address this issue. One way to tackle

this question would be to again, focus exclusively on periods of time when the seismic airgun array is off but the vessel is nearby, for example while turning around between shooting parallel seismic lines. Eventually other factors ignored in this analysis could be decomposed out of the overall noise budget (Nystuen *et al.*, 2010).

A third suggestion for proposed work based on Chapter 2 involves the stage of calculating the MLM and RM metrics. This analysis contemplated a relationship between the integration parameter ΔT_i (and thus the FFT length*)* and the estimated integration time corresponding to the bowhead whale's hearing, which was inferred from the duration of its most typical call. This species selection reflects the considerable regulatory awareness and large associated resources dedicated in the Alaskan North Slope region to bowhead whale research. However, the resulting metric may not be applicable or ecologically significant to the rest of baleen Arctic whales. Therefore, I would recommend to eventually expand this calculation to other marine mammals, including odontocentes and pinnipeds, by using integration factors that relate to their own particular acoustic perception. Additionally, for all of these species, instead of relying on vocalization duration as an indirect index of hearing integration, this metric could be eventually re-computed to echo advances in our understanding of the functional physiology of marine mammal hearing (Houser *et al.*, 2001; Ketten, 2012; Nachtigall, 2008; Parks *et al.*, 2007) as they become available.

Ultimately, looking forward, the private sector and policy makers should consider standardizing metrics like the MLM and RM into a reporting norm. Beyond that, it could be valuable to invest in turning these metrics into predictive tools that

could adequately estimate levels of noise contributed by seismic surveys through reverberation generated from proposed activities. Together with existing modeling tools like the Acoustic Integration Model (AIM, Frankel *et al.*, 2002), which can estimate point exposure from simulated acoustic footprints in range and depth, these metrics could eventually provide an important step in evaluating the impact from activities within a region in high-temporal resolution, under the framework of the PCAD model (Wartzok and Tyack, 2008) and help aid in the design of parallel PAM studies to ensure that their efficacy is optimal for mitigation purposes.

Another topic in Chapter 3 that was left unexplored is the use of an automated event detector to eliminate episodes (e.g. close-range whale calls) that disrupt the method's underlying assumption that the ambient noise field between the sensors is azimuthally-symmetric. During the early stages of the thesis research, initial attempts were made to build a gray whale detector based on the "energy integration" feature of the software ISHAMEL (Mellinger, 2002). At the time, the goal was to achieve high levels of detector performance. In accomplishing that, this methodology proved ineffective, because of the high-variability in the parameters of gray whale calls. However, in the context of removing highly directional transient sounds, this limited level of performance may be sufficient to improve the emergence of a clearer NCF or reduce the averaged time required for its emergence.

A second, natural extension to the work in Chapter 3 would be the application of multiple, time-synchronized arrays (by means of ambient noise) to the 2-D localization of an acoustic source, for example, a gray whale. The existence of time-

synchronized arrays permits a variety of techniques to allow the estimation of a source's bearing. For this project, I suggest calculating source direction from time of arrival differences (TOAD) by cross-correlation of signals corresponding to a pair of sensors (Altes, 1980; Clark and Ellison, 2000; Clark *et al.*, 1986). Similarly to the boat signatures extracted in Chapter 3, inspection of the data has already confirmed that whale calls were recorded on more than one station around Punta Piedra, confirming that this particular acoustic channel supports sound propagation at these frequencies for up to 2 km range.

A gray whale localization application would match the research goals currently carried out by the Laguna San Ignacio Ecosystem Science Project (LSIESP), as it could potentially allow matching between a whale's acoustic activity and its photographic identification or behavioral state. Furthermore, the demonstration of a localization technique at LSI would allow maps to be constructed of call type distribution in the lagoon as a function of time, opening the door for an eventual statistical analysis of correspondence between vocalization repertoire and demographic groups. Furthermore, at an enclosed location like LSI, where a protocol for regular visual censuses is already implemented (by LSIESP), vocally tracking and identifying individuals could potentially lead to the matching of acoustic signatures and individuals.

Finally, given the historical dataset of visual surveys collected by LSIESP/UABCS, once localization is accomplished, the relationship between those census results and our acoustic recordings should be further explored in the context of

population estimates. An initial study at this location (Ponce *et al.*, 2012) has demonstrated that there is potential for the S1-type call rates to correspond non-linearly with visual counts.

Overall, as illustrated by the studies in this dissertation, research into the impact of noise on marine life still tends to focus on the effects of specific and isolated noise sources (commercial shipping, seismic survey, SONAR, etc.) on individuals of a particular species, exclusively located within a determined area during a finite period of time. However, there remains a significant gap in understanding the chronic, cumulative impact of the overall increase in marine noise levels from multiple, diverse sources. Recently, various multi-disciplinary working group efforts have begun undertaking this complex question and are slowly elaborating new frameworks and tools for the assessment of cumulative effects of underwater noise on marine life (Erbe and King, 2009; Streever *et al.*, 2012). Still, more basic research is needed to gain an improved understanding on the impact of a general increase in noise levels across the marine environment, not just the specific impact of a particular development activity. Given the ranges over which sound can propagate underwater, activities within one location may have an impact many miles from the source and beyond national boundaries, and therefore its regulation may require an international approach. Both field sites presented in this dissertation (Baja California and Alaska) lie within only a few hundred kilometers of major international borders, and the marine mammal species investigated here migrate along corridors that span multiple countries. Thus, I believe that the case studies in this dissertation not only establish near-term results that

can immediately benefit the scientific bioacoustics community, but are representative of the long-term direction of the field of bioacoustic ambient noise studies.

IV. REFERENCES

Altes, R. A. (**1980**). "Detection, estimation, and classification with spectrograms," J. Acoust. Soc. Am., **67**, 1232-1246.

Clark, C., Ellison, W., and Beeman, K. (**1986**). "Acoustic Tracking of Migrating Bowhead Whales," Oceans 86, IEEE Oceanic Eng. Soc., 341-346.

Clark, C. W., Ellison, W., Southall, B., Hatch, L., Van Parijs, S., Frankel, A., and Ponirakis, D. (**2009**). "Acoustic masking in marine ecosystems: intuitions, analysis, and implication," Mar. Ecol. Prog. Ser., **395**, 201–222.

Clark, C. W., and Ellison, W. T. (**2000**). "Calibration and comparison of the acoustic location methods used during the spring migration of the bowhead whale, Balaena mysticetus, off Pt Barrow, Alaska, 1984-1993," J. Acoust. Soc. Am., **107**, 3509–3517.

Corbett, J. J., Lack, D. A., Winebrake, J. J., Harder, S., Silberman, J. A., and Gold, M. (**2010**). "Arctic shipping emissions inventories and future scenarios," Atmos. Chem. Phys., **10**, 9689–9704.

Ellison, W. T., Southall, B. L., Clark, C. W., and Frankel, A. S. (**2012**). "A new context-based approach to assess marine mammal behavioral responses to anthropogenic sounds," Conserv. Biol., **26**, 21–28.

Erbe, C., and King, A. R. (**2009**). "Modeling cumulative sound exposure around marine seismic surveys," J. Acoust. Soc. Am., **125**, 2443–2451.

Frankel, A. S., Ellison, W. T., and Buchanan, J. (**2002**). "Application of the Acoustic Integration Model (AIM) to predict and minimize environmental impacts," Oceans 02 MTS/IEEE, **3**,1438-1443.

Hatch, L., Clark, C., Merrick, R., Van Parijs, S., Ponirakis, D., Schwehr, K., Thompson, M., *et al*. (**2008**). "Characterizing the relative contributions of large vessels to total ocean noise fields: a case study using the Gerry E Studds Stellwagen Bank National Marine Sanctuary," Environ. Manage., **44**, 735–752.

Heitmeyer, R. M., Wales, S. C., and Pflug, L. A. (**2003**). "Shipping noise predictions: Capabilities and limitations," Mar. Technol. Soc. J., **37**, 54–65.

Houser, D. S., Helweg, D. A., and Moore, P. W. B. (**2001**). "A bandpass filter-bank model of auditory sensitivity in the humpback whale," Aquat. Mamm., **27**, 82–91.

Ireland, D. S., Funk, D. W., Rodrigues, R., and Koski, W. R. (**2009**). "Joint Monitoring Program in the Chukchi and Beaufort Seas, open water season, 2006-2007." in LGL Alaska Report P971-2 (LGL Ltd., Environmental Research

Associates, King City, Ont., JASCO Research Ltd., Victoria, BC, and Greeneridge Sciences, Inc., Santa Barbara, CA, for Shell Offshore, Inc. Anchorage, AK, ConocoPhillips Alaska, Inc., Anchorage, AK, and the National Marine Fisheries Service, Anchorage, AK.).

Ketten, D. R. (**2012**). "Marine mammal auditory system noise impacts: evidence and incidence," Eff. Noise Aquat. Life, Vol. 2, pp. 207–12.

Mellinger, D.K. **(2002)**. "Ishmael 1.0 User's Guide. ISHMAEL: Integrated System for Holistic Multi-channel Acoustic Exploration and Localization," NOAA Tech. Memo. OAR PMEL-120, NTIS: PB2002-105264, NOAA/Pacific Marine Environmental Laboratory, Seattle, WA, 26 pp.

Nachtigall, P. (**2008**). "Using auditory evoked potentials to measure marine mammal hearing," J. Acoust. Soc. Am., **124**, 2465.

Nystuen, J. A., Moore, S. E., and Stabeno, P. J. (**2010**). "A sound budget for the southeastern Bering Sea: measuring wind, rainfall, shipping, and other sources of underwater sound," J. Acoust. Soc. Am., **128**, 58–65.

Parks, S. E., Ketten, D. R., O'Malley, J. T., and Arruda, J. (**2007**). "Anatomical predictions of hearing in the North Atlantic right whale," Anat. Rec., **290**, 734–744.

Ponce, D., Thode, A. M., Guerra, M., Urbán R, J., and Swartz, S. (**2012**). "Relationship between visual counts and call detection rates of gray whales

(*Eschrichtius robustus*) in Laguna San Ignacio, Mexico," J. Acoust. Soc. Am., **131**, 2700–2713.

Schroeder, M. R. (**1965**). "New Method of Measuring Reverberation Time," J. Acoust. Soc. Am., **37**, 409-412.

Streever, Bill, William T. Ellison, Adam S. Frankel, Roberto Racca, Robyn Angliss, Christopher Clark, Erica Fleishman et al. **(2012)**. "Early Progress and Challenges in Assessing Aggregate Sound Exposure and Associated Effects on Marine Mammals." In International Conference on Health, Safety and Environment in Oil and Gas Exploration and Production.

Wartzok, D., and Tyack, P. L. (**2008**). "Elaboration of the NRC Population Consequences of Acoustic Disturbance (PCAD) model," Bioacoustics., **17**, 286-288.

Weir, C. R., and Dolman, S. J. (**2007**). "Comparative Review of the Regional Marine Mammal Mitigation Guidelines Implemented During Industrial Seismic Surveys, and Guidance Towards a Worldwide Standard," J. Int. Wildl. Law Policy, **10**, 1–27.

Wilson, K. J., Falkingham, J., Melling, H., and Abreu, R. De (**2004**). "Shipping in the Canadian Arctic: other possible climate change scenarios," IGARSS 2004, IEEE Int. Geosci. Remote Sens. Symp., **3**, 1853–1856.